POLITECNICO
MILANO 1863

SCUOLA DI INGEGNERIA INDUSTRIALE
E DELL'INFORMAZIONE

Laurea Magistrale in Ingegneria Meccanica

SIMULATION OF THE DYNAMIC BEHAVIOR OF A SELF-DRIVEN ELECTRIC VEHICLE

Supervisor
Prof. MASSIMILIANO GOBBI

Master's thesis by
FEDERICO FRERA

ID code 841840

Academic Year 2016/2017

Federico Frera: Master Thesis in Mechanical Engineering, Politecnico di Milano.
October 2017.

Politecnico di Milano:
www.polimi.it

School of Industrial and Information Engineering:
www.ingindinf.polimi.it

Acknowledgement

I would first like to thank Professor Massimiliano Gobbi of the Mechanical department at Politecnico di Milano for the trust that he gave to me and the possibility to develop my Master Thesis work abroad. I am grateful to my supervisor Professor Francisco José Valero Chuliá of the Mechanical Department at Universidad Politécnica de Valéncia, he was always available to help me whenever I ran into a trouble spot or had a question about my job. I am also grateful to many people who shared with me their time during the development of this work, my office colleagues, my mates and my friends.
Nevertheless, without appearing banal, I must express my very profound gratitude to my parents Pierangelo and Antonella, my sisters Francesca and Elena and all my relatives for providing me with unfailing support and continuous encouragement throughout my years of study, this accomplishment would not have been possible without them, Thank you.

Milano, October 2017 F. F.

Contents

Introduction **1**

1 Vehicle Dynamics **5**
1.1 Introduction . . . 5
1.2 Axis system . . . 6
1.2.1 Earth fixed axis system . . . 7
1.2.2 Vehicle axis system . . . 7
1.2.3 Variable definition . . . 7
1.3 Tires . . . 8
1.3.1 Slip angle . . . 10
1.3.2 Camber Thrust . . . 11
1.3.3 Adherence condition of tyre . . . 12
1.4 Fiala's Theory . . . 13
1.5 Forces acting on the vehicle . . . 19
1.5.1 Longitudinal forces . . . 20
1.6 Lateral dynamic model . . . 24
1.6.1 Steady state models . . . 24
1.6.2 High speed cornering . . . 26
1.6.3 Neutral, understeer and oversteer car . . . 30
1.6.4 Neutral steel . . . 30
1.6.5 Understeer . . . 30
1.6.6 Oversteer . . . 30
1.6.7 Gradient comparison . . . 31

2 Vehicle Model **33**
2.1 Introduction . . . 33
2.2 Software's . . . 33
2.2.1 MSC Software . . . 33
2.2.2 ADAMS . . . 34
2.2.3 ADAMS/View . . . 34
2.2.4 SolidWorks . . . 34
2.2.5 MATLAB . . . 35
2.3 Data . . . 36
2.4 Data measurement . . . 37
2.5 Center of gravity . . . 38
2.6 Suspension geometry . . . 40
2.6.1 Front suspension . . . 40

2.6.2 Rear suspension . . . 41
2.6.3 Vehicle roll axis . . . 42
2.7 Modelling of suspensions . . . 43
2.7.1 Rear suspension . . . 43
2.7.2 Front suspension . . . 44
2.8 Dampers . . . 45
2.9 3D modelling . . . 46
2.9.1 Body . . . 46
2.9.2 Rear suspension . . . 47
2.9.3 Front suspension and direction system . . . 48
2.9.4 Final assembly . . . 50
2.10 ADAMS/View . . . 51
2.10.1 File import . . . 51
2.10.2 Model Assembly . . . 52
2.10.3 Wheels and ground . . . 56
2.10.4 Stable position setting . . . 57
2.10.5 Tire cornering stiffness . . . 59

3 Direct dynamics simulations 63
3.1 Introduction . . . 63
3.2 Forces and motions . . . 63
3.2.1 Traction and braking . . . 63
3.2.2 Steering . . . 63
3.3 Measures . . . 64
3.4 General test conditions . . . 64
3.5 Straight line test . . . 65
3.6 Skid past tests . . . 67
3.6.1 Introduction . . . 67
3.6.2 Left turn, constant radius . . . 67
3.6.3 Left turn, constant speed . . . 74
3.7 Moose test . . . 78
3.7.1 Introduction . . . 78
3.7.2 Test procedure . . . 78
3.7.3 Test results . . . 80

4 Inverse dynamics model 85
4.1 Introduction . . . 85
4.2 Trajectory model . . . 85
4.2.1 Vehicle model . . . 87
4.2.2 Vehicle kinematics . . . 87

5 Inverse dynamics results 91
5.1 Introduction . . . 91
5.2 Results . . . 91
5.2.1 Straight line trajectory . . . 92
5.3 Circular trajectory . . . 94
5.4 Moose test . . . 97

6 Conclusions **103**
6.1 Introduction . . . 103
6.2 Conclusions . . . 103
6.3 Future work . . . 104

A Matlab scripts **105**
A.1 Adams imported data . . . 105
A.2 Dampers graph . . . 109
A.3 Center of gravity calibration . . . 109
A.4 Inverse dynamic . . . 111
A.5 Inverse dynamic equation solver function . . . 120
A.6 Moose test program . . . 120
A.7 Leaf spring calculation . . . 129

List of Figures

1 Vehicle model [16] 2

1.1 The driver vehicle ground system 6
1.2 SAE axis 7
1.3 SAE tyre axis system 8
1.4 Slip angle 10
1.5 Slip angle graph 10
1.6 Camber thrust 11
1.7 Camber lateral force [25] 12
1.8 Circle diagram [21] 12
1.9 Tire model [1] 14
1.10 Tire deflection model 14
1.11 Rim deflection model 15
1.12 Contact pressure distribution 16
1.13 Lateral force to side slip angle 18
1.14 Self aligning torque to side slip angle 19
1.15 Pneumatic trail 19
1.16 Forces acting on the vehicle 20
1.17 Forces acting on the wheel 23
1.18 Cornering of a bicycle model 25
1.19 Curving geometry 26
1.20 High speed cornering 27
1.21 Steering angle as function of speed [21] 31

2.1 RBCAR vehicle [26] 36
2.2 Vehicle center of gravity 38
2.3 Axes loads on a slope 39
2.4 Front suspension 40
2.5 Front suspension side-view 41
2.6 Front roll center 41
2.7 Rear leaf spring and axle 42
2.8 Rear roll center 42
2.9 Distance roll axis center of gravity 43
2.10 Rear suspension scheme 43
2.11 Front suspension scheme 44
2.12 Force vs. velocity 46
2.13 Chassis front view 47
2.14 Chassis rear view 47

2.15 Rear suspension . . . 48
2.16 Rear suspension and wheels . . . 48
2.17 Front suspension . . . 49
2.18 Front suspension and wheels . . . 49
2.19 Front suspension and wheels . . . 50
2.20 Virtual model in Solidworks front view . . . 50
2.21 Virtual model in Solidworks side view . . . 51
2.22 Assembled vehicle in ADAMS . . . 52
2.23 Front-side markers . . . 52
2.24 Damper assembly . . . 53
2.25 Wheel connection . . . 53
2.26 Upper arm . . . 54
2.27 Front leaf connection . . . 54
2.28 Direction system . . . 55
2.29 Rear suspension . . . 55
2.30 Front and rear suspension . . . 56
2.31 Wheels and ground . . . 56
2.32 Center of gravity height . . . 57
2.33 Vertical wheel load . . . 58
2.34 Stable configuration . . . 59
2.35 Circular path . . . 60
2.36 Front wheels street angle . . . 60
2.37 Straight line lateral forces . . . 61

3.1 Straight line speed . . . 65
3.2 Straight line path . . . 66
3.3 Lateral forces . . . 66
3.4 Circular path r=40m v=8,88 m/s . . . 68
3.5 Wheels steering angle r=40m v=8,88 m/s . . . 69
3.6 Speed profile . . . 69
3.7 Overall vehicle speed r=40m v=8,88 m/s . . . 69
3.8 Vertical Forces r=40m v=8,88 m/s . . . 70
3.9 Slip angle r=40 m v=8,88 m/s . . . 70
3.10 Lateral forces r=40 m v=8,88 m/s . . . 71
3.11 Test condition r=40 m v=5,28 m/s . . . 72
3.12 Test condition r=40 m v=5,28 m/s . . . 72
3.13 Test condition r=40 m v=5,28 m/s . . . 73
3.14 Test condition r=40 m v=2,22 m/s . . . 73
3.15 Test condition r=40 m v=2,22 m/s . . . 74
3.16 Test condition r=40 m v=2,22 m/s . . . 74
3.17 Test condition r=10 m v=5 m/s . . . 75
3.18 Test condition r=10 m v=5 m/s . . . 75
3.19 Test condition r=10 m v=5 m/s . . . 75
3.20 Test condition r=8 m v=5 m/s . . . 76
3.21 Test condition r=8 m v=5 m/s . . . 76
3.22 Test condition r=8 m v=5 m/s . . . 77
3.23 Test condition r=7 m v=5 m/s . . . 77

3.24 Test condition r=7 m v=5 m/s . . . 78
3.25 Test condition r=7 m v=5 m/s . . . 78
3.26 Moose test path . . . 79
3.27 Moose test direction . . . 80
3.28 Moose test vehicle trajectory . . . 81
3.29 Vehicle speed delta . . . 81
3.30 Velocity and acceleration profile . . . 82
3.31 Moose test vertical tire forces . . . 83
3.32 Sideslip angle . . . 83
3.33 Lateral tire forces . . . 84

4.1 Bicycle model . . . 87
4.2 Kinematics and side slip angles . . . 89

5.1 Vehicle trajectory . . . 92
5.2 Steering and Vehicle slip angle . . . 93
5.3 Tire slip angles . . . 93
5.4 Lateral forces . . . 94
5.5 R=40m V=32 km/h trajectory . . . 94
5.6 R=40m V=32km/h Delta . . . 95
5.7 R=40m V=32km/h Inverse rear sideslip . . . 95
5.8 R=40m V=32 km/h Inverse front sideslip . . . 95
5.9 R=40m V=32km/h Front axle lateral force . . . 96
5.10 R=40m V=32km/h Rear axle lateral force . . . 96
5.11 Moose test trajectory . . . 97
5.12 Longitudinal and lateral velocity . . . 98
5.13 Longitudinal and lateral acceleration . . . 99
5.14 Rear axle side slip angle . . . 99
5.15 Vehicle side slip angle . . . 100
5.16 Front side slip angle . . . 100
5.17 Front axle lateral force . . . 101
5.18 Rear axle slip angle . . . 101
5.19 Steer angle . . . 102

List of Tables

2.1 Mechanical data 37
2.2 Control data 37
2.3 Vehicle mass and wheelbase 38
2.4 Measured axle load 38
2.5 Measured axle loads and slope properties 39
2.6 Center of mass position. 40
2.7 Rear leaf spring properties 44
2.8 Rear spring stiffness 44
2.9 Front leaf spring properties 45
2.10 Front spring stiffness 45
2.11 Damping coefficients 45
2.12 Slip angle test data 59

3.1 Road friction coefficients 65
3.2 Moose test track dimensions 79

5.1 Vehicle data 92

Abstract

Automatic driving cars are very close to being sell in the market, the driver is not necessary anymore. An autonomous vehicle helps to have a better efficiency and allows a minimization of the number of crashes.

From the engineering point of view, this is a tough challenge, universities and car manufacturers work intensively on the developing of autonomous cars.

This thesis work provides a vehicle model able to predict its dynamic behaviour by using a virtual prototype instead of a real one, helping the programmer to check the goodness of a script, able to generate optimal trajectories for the car.

The work also touches the study of an inverse dynamic problem, in which, hypothetical trajectories are produced and tested obtaining forces and slip angles generated in the tires during the motion of the vehicle.

Keywords: Electric vehicle; vehicle dynamics; ADAS car; trajectories; motion analysis.

I veicoli a guida autonoma sono ormai prossimi all'inserimento sul mercato; il conduttore non è più necessario. Un veicolo autonomo aiuta ad avere una maggiore efficienza e permette una minimizzazione del numero di incidenti.

Dal punto di vista ingegneristico questa è una sfida complicata, pertanto università e produttori di automobili stanno collaborando ed investendo risorse nello sviluppo di veicoli a guida autonoma.

Questa tesi fornisce un modello di veicolo il cui comportamento dinamico può essere predetto tramite l'utilizzo di un prototipo virtuale che permette ad un programmatore di validare la qualità delle traiettorie generate da un algoritmo in grado di controllare il veicolo stesso.

Il lavoro tratta altresì lo studio di un problema di dinamica inversa in cui traiettorie ipotetiche vengono generate e provate ottenendo forze ed angoli di deriva formatesi durante il moto del veicolo.

Keywords: Veicolo elettrico; dinamica del veicolo; veicolo ADAS; traiettorie; analisi del moto.

Introduction

Scope of the thesis

This Master Thesis is written within the Mechanical engineering Master program at the Politecnico di Milano. The thesis is part of a project which is financed by the European Community and it focuses on the creation of a dynamic model of a self-driven electric vehicle that is under investigation at Universidad Politécnica de Valéncia a by "ai2"[4], Institute of Automatic and Industrial Informatics for the software improvement and study, in collaboration with the Mechanical department for the vehicle dynamic behaviour.

Nowadays, the autonomous car is being studied and constructed with the objective to be accessible and safe in the near future for every person. The car needs to be able to exactly perform the trajectory imposed by the driver which is no longer a human but it is a computer. The trajectory generated by the software needs to be correctly reproduced by the vehicle. To do that it is necessary to know how a car behaves and performs under a given trajectory, in which many parameters have to be taken into accounts such as the inertial characteristic, the power delivered by the engine and the tire behaviour. These studies are performed in tracks with expensive tests, difficulties to fast change parameters and components and finally, lack of space to perform the tests without risk of collision with person or objects. Due to these reasons, many test procedures are preferred to be done by means of a virtual model, as close as possible to the reality, thus saving money for expensive tests, avoiding unnecessary risks and useless wastes of time.

State of the art

The vehicle's dynamic behaviour knowledge is an important topic for the safety and for the efficiency of a vehicle. Being aware of the vehicle response it is necessary to establish trajectories. A human driver or mostly an automatic control is responsible for the vehicle direction. Automatic systems can be categorized as driver assistance systems, like lane-keeping assistance or cruise control which are able to maintain a given velocity or make a correction on the driver steering. Nowadays, the objective is to arrive until the complete autonomous vehicle [24]. A self-driven vehicle needs a control unit, able to take into account the vehicle dynamics and its boundaries determined by the physical limitation, such as maximum angle of steer, adherence and power delivered by the engine or brakes [10].

There are some algorithms in literature which make an attempt to implement a

code, able to predict the vehicle behaviour [6]. A proper model should be useful to compare the trajectories calculated by the algorithm with the actual car behaviour.

Due to the lack of space and the cost of real tests, a model permits to save time and money. Many models are developed into ADAMS to perform vehicle analysis. The level of accuracy depends on what the engineer is looking for during the analysis.

The thesis [22] as instance, has as objective to simulate with a good accuracy the vehicle dynamics of a Formula SAE car [12].

Another full vehicle model, developed to test performances, is represented by the article proposed by Donghyun Kim, Sungho Hwang, and Hyunsoo Kim [16], in whose aim is the evaluation of the behaviour improvement, given by the compensation of the error coming from the sideslip angle and from the yaw rate of an hybrid vehicle (HEV). The compensation is given by controlling the rear wheel torque provided by an electric engine. The actuation is provided by a fuzzy-rule-based control algorithm. Figure (1) shows the car model for the desired simulation.

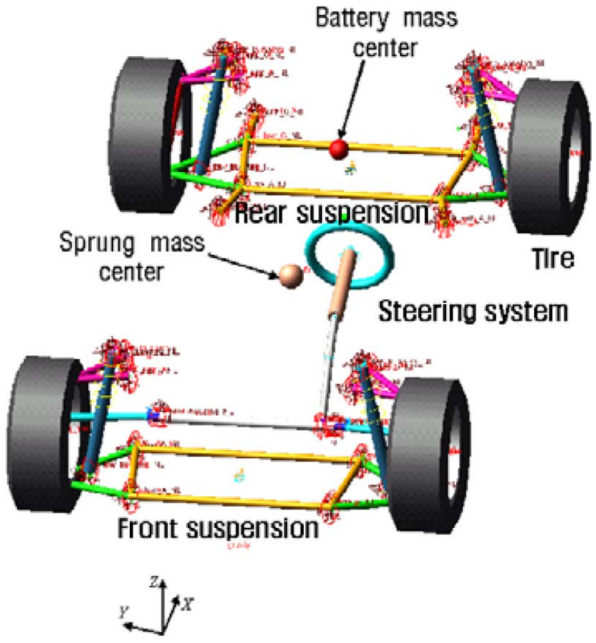

Figure 1: Vehicle model [16]

In the article proposed by Prof.Taehyun Shim [28], is a matter of interest to evaluate the number of DOF which are necessary to make an accurate analysis of a vehicle. Many models are present in literature; this last essay, after a brief introduction of the existing models, makes a focus on the differences between the 8 DOF vehicle model with a 14 DOF one. Finally, in the last part of the article makes an analysis of the possible limitations of the 14 DOF model with a current vehicle.

Objective

The thesis work faced with the creation of a virtual model able to reproduce the vehicle behaviour as close as possible to the reality.
Many algorithms are being written by colleagues in order to be able to predict as much as possible the vehicle behaviour and to be as fast as possible to be processed since they are making computation in real time of the best trajectory to perform to avoid obstacle for example and to raise a given position in a reasonable way.
Many trajectories generated by the software are unfeasible in the reality, for example, the steering angle imposed could be too high, the car slip could be excessive, the limit of adherence could be excess etc. All these parameters have to be taken into account by the software.
In the second part of the thesis, a really simple algorithm has been written, relying on the so called "Bicycle model" to understand which is the limitation of such a simple design. The data obtained for this inverse dynamics are then compared to the virtual model, which is the reference for the real behaviour of the car.
As known from the theory, as far the velocity, the lateral acceleration increases and curvature radius decreases, the model is not able to correctly reproduce anymore the reality.

Method

In order to have a general vision about vehicle dynamics, a chapter has been dedicated to review and explain concepts which are present in literature and essential to create a model. Concepts about vehicle dynamics used in this work have been analysed to better understand how the car has been modelled.
There are many theories and models present in literature, it is difficult to explain briefly each one. The focus has been done only on those models that have been necessary to model the vehicle and are useful to understand the reason of given choices or the reason of determinate behaviours.

A reference system is necessary to describe the vehicle behaviour, there are several standards which define the car reference system. For this particular case, it was chosen the standard proposed by the Society of Automotive Engineers (SAE) [27].

After the literature review, it has been explained how the vehicle modelling has been done.
The work can be divided into three main areas:

- The initial part of the job consists of the acquisition of the necessary data collection to build a real reproduction of the actual model.
  In this step, every part has been measured and drafted for a further reproduction. The vehicle has been weighted on each axle on a flat surface and on a slope in order to obtain the exact position of the centre of mass.
  As to last, in order to measure with an acceptable approximation the vehicle sideslip, a series of circular tests has been done in the street, measuring the

deviation from the perfect circle that should be done by the vehicle in absence of lateral accelerations.

- The secondary step consists on the modelling of the existing vehicle by creating an appropriate model in ADAMS/View. It is necessary to introduce in the program all the parameters necessary to define the dynamic properties like tire's cornering stiffness, damping properties, inertial properties and springs stiffness.
- The third step consists of the creation of an inverse dynamic problem, able to predict forces, slip angles and steer angle necessary to perform a given trajectory.

In the last chapter, it has been done an analysis of the results, a comparison between the direct and inverse dynamic problem. A critical evaluation of the results has been done to discuss the goodness of the results and to propose further improvement of the study.

Chapter 1

Vehicle Dynamics

1.1 Introduction

The research in vehicle dynamics started about on 1950s [17]. Engineers and researchers have tried to deeply understand the dynamic behaviour of vehicles. They are subjected to a wide range of driving conditions such as moderate drive or emergency manoeuvre.
A good knowledge of the vehicle behaviour helps to improve safety, stability, comfort etc. With the advent of the electronic and the informatics, it has been possible to perform a series of complicated design simulations, every time more close to the reality.

Automotive companies are constantly improving their products, nowadays the trend is the marketing of an autonomous and zero emission vehicle [15]. The autonomous driving requires a really good knowledge of the vehicle dynamics and the trajectories produced by the control unit need to take into account vehicle parameters.

This chapter provides information on the dynamic modelling of the vehicle.
The vehicle axis system used throughout the simulation is in accordance with SAE standard, as described in SAE J670e [8].
The vehicle is usually studied as a rigid body, which has six degrees of freedom during the movement.

A body can only be made to move or change in direction under the action of force, so it is extremely important to evaluate the forces that occur while a vehicle is being driven.

An important role is played by the tires as any change of speed or direction involves forces acting on tires which they are responsible to maintain the vehicle in contact with the ground and maintain the direction by exchanging forces with the ground.

The body and the suspension system as well are extremely important to make

a correct analysis of the dynamic car behaviour.

The resultant force is a composition of tyre, aerodynamic and gravitational components. All these forces are governed by different laws and act in different location and direction with respect to the vehicle chassis.

It is necessary to define the behaviour of a vehicle, usually it is possible to describe it in terms of three characteristics, the performance, handling and ride.

The performance characteristics are referred to the ability of the vehicle to accelerate, to overcome obstacles and to decelerate.
Handling qualities are concerned with the vehicle response after a driver command and to the ability to stabilize external disturbances.
Last, ride characteristics are related to the vibrations of the vehicle excited by the surface irregularities and its effect on the passengers.

The overall behaviour of a vehicle is the result of the interaction between the driver, the vehicle, the environment, as shown in Figure (1.1)[35].

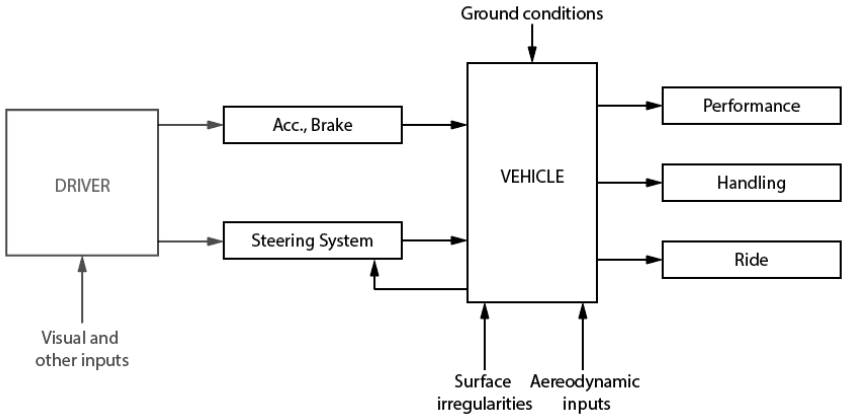

Figure 1.1: The driver vehicle ground system

By considering the Figure (1.1), the overall vehicle dynamics can be divided into longitudinal, vertical and lateral dynamic. Every subsystem is connected each one.

1.2 Axis system

At any given instant of time, a vehicle is subjected to a single force acting at some location and in some direction. This force can be considered an external force or an applied force. It is able to maintain a given velocity or produce an acceleration or deceleration of the vehicle itself.

Therefore, to study the vehicle performance it is necessary to define a system of axes, being able to express all the variables as the acceleration, the velocity and

the position.

1.2.1 Earth fixed axis system

According to $SAEJ670e$ [27] it is defined a fixed reference system attached to the ground, denoted by the capital letter X, Y, Z. The axis X, Y lay in the ground plane and Z is vertical downward. The fixed system location and orientation are arbitrarily determined by the user.

1.2.2 Vehicle axis system

This reference system is fixed on the vehicle, Figure (1.2) represents the convention used by SAE. The origin is positioned in the car's center of gravity, the system is orthogonal and right-handed.

The body movement can be described according to a specific rotation and translation about each axis [21]. The $x - axis$ is horizontal and positive forward in the direction of motion when the vehicle is travelling in a straight-line on a level road. The $x - axis$ lies in the longitudinal plane of symmetry. The $y - axis$ points to the driver's right, is horizontal and 90° to the $x - axis$. The $z - axis$ is perpendicular to the other two, it is vertical and positive downward.

In most studies related to handling and directional control, only the $x - y$ plane of the vehicle is considered. The vertical axis, z, is usually taken into account when studying ride, pitch, roll and stability analysis.

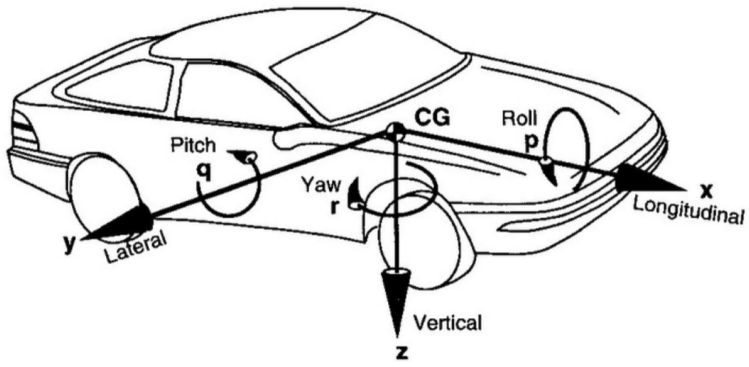

Figure 1.2: SAE axis

1.2.3 Variable definition

The following sub-chapter, lists a series of relevant definitions of variables, useful to describe the vehicle behaviour.

Longitudinal direction: forward moving direction of the vehicle. The forward direction can be seen in two ways, in the first one by looking with respect to the

vehicle body itself, in the other one by looking with respect to a fixed reference point. The second one exposed, is usually used when the location information of the vehicle is required with respect to a starting or ending point.

Lateral direction: sideways moving direction of the vehicle. As described for the longitudinal direction, here as well, there are two ways of looking at the lateral direction, one with respect to the vehicle and one with respect to a fixed reference point.

Roll angle: it is defined as the rotation around the $x - axis$. When the vehicle rolls, the body leans as when cornering [21].

Pitch angle: it is defined as the rotation around the $y - axis$, pitch angle is particularly important when the vehicle is subjected to an acceleration or a deceleration due to braking [21].

Yaw angle: The third angle taken into account is the rotation around the $z - axis$, which is the direction perpendicular to the road with the direction toward the ground [21].

1.3 Tires

All the forces which are able to move and guide the car on a surface with exception of the aerodynamical forces are generated by the tire-road contact.
It is extremely important to be aware of the forces which are acting, to determine how a vehicle turns, brakes and accelerates. The tyre has to fulfil basically three functions which are to support the vertical load of the car, provide longitudinal forces for accelerating or braking and finally to develop lateral forces for cornering [8]. The tyre is a viscoelastic toroid and so, quite a complicated non-linear system.

To define uniquely the forces and moments acting on the tyre, $SAE\ j670$ defines the axis orientation [21].

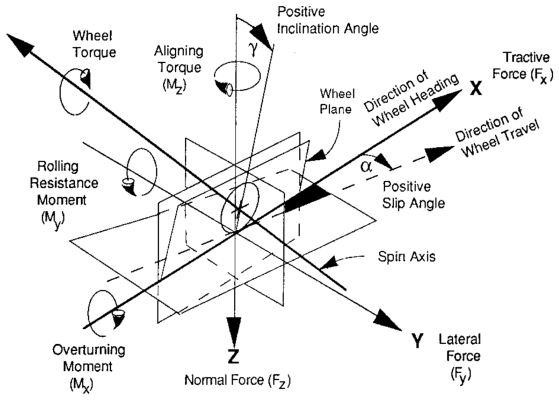

Figure 1.3: SAE tyre axis system

The origin of the axis system is fixed in the centre of the tyre contact, the $x - axis$ is the intersection of the wheel plane and the ground plane with positive direction forward. The $z - axis$ is perpendicular to the ground plane with positive direction entering in the ground. Consequently, the $y - axis$ is on the ground, and its direction is chosen to make the system axis orthogonal and right hand.

With the assumption to locate all the forces at the centre of the contact area, three forces and three moments are acting on the tyre from the ground.

The following list defines forces, moments and angles useful to to describe the wheel behaviour [8].

Longitudinal Force F_x: component of the force acting on the tyre by the road in the plane of the road and parallel to the intersection of the wheel plane with the road plane.

Lateral Force F_y: component of the force acting on the tire by the road in the plane of the road and normal to the intersection of the wheel plane with the road plane.

Normal Force F_z: component of the force acting on the tire by the road which is normal to the plane of the road. The normal force is negative in magnitude.

Overturning Moment M_x: moment acting on the tire by the road in the plane of the road and parallel to the intersection of the wheel plane with the road plane.

Rolling ResistantMoment M_y: moment acting on the tyre by the road in the plane of the road in the plane of the road and normal to the intersection of the wheel plane with the road plane.

Aligning Moment M_z: moment acting on the tire by the road which is normal to the plane of the road.

Slip angle α: angle between the direction of wheel heading and the direction of travel. Positive slip angle corresponds to tire moving to the right as it advances in the forward direction.

Camber angle γ: angle between the wheel plane and the vertical. Positive camber corresponds to the top of the tire leaned outward from the vehicle.

The mechanic of the force generation is not going to be explained in order not to make the topic too long, it is not object of study in this work. Only experimental charts have been taken into account to study the macro behaviour of the tire. Information about tire is obtained in function of the construction geometry, the vertical load, the inflation pressure, the surface friction coefficient and the speed.

1.3.1 Slip angle

When a tire is subjected to a lateral force it will drift to the side because of the formation of an angle between the direction of heading and the direction of travel. the angle formed is called slip angle.

Figure (1.4) represents the schematic deformed path when the tire is subjected to a lateral force and the presence of the slip angle. The contact path will be subjected to a slip region and a contact patch.

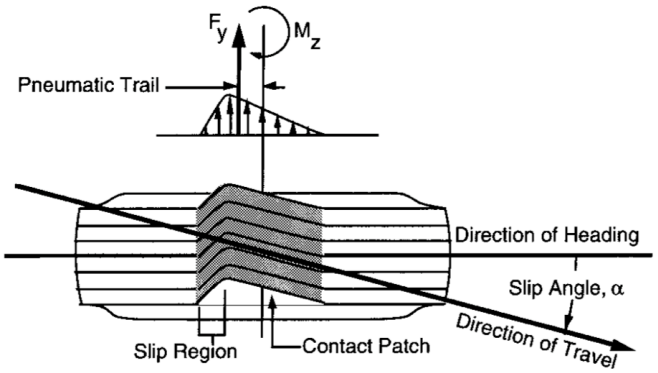

Figure 1.4: Slip angle

The resultant force F_y is not centred in the tire. The SAE convention suggests to apply the F_y in the middle of the contact path, adding an aligning moment M_z which is calculated as the lateral force multiplied F_y by the pneumatic trail.

Considering a steady state load acting on a wheel and performing a test with different slip angles it is possible to create a graph which put into relation the lateral force as a function of a given slip angle.

Figure (1.5), shows a relation between the resultant lateral force F_y with respect to the slip angle α.

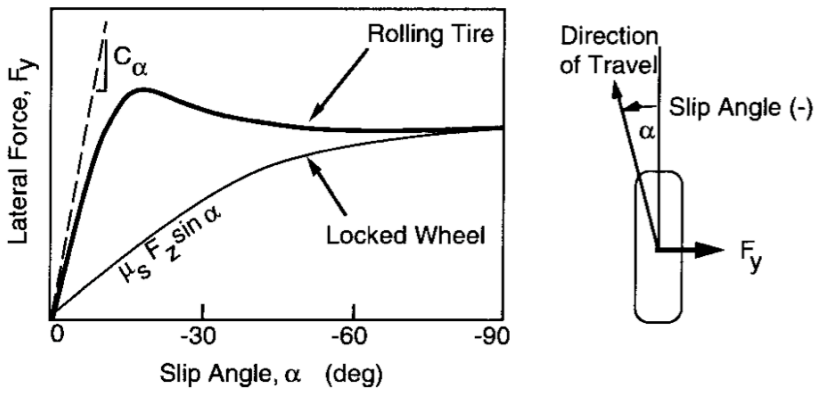

Figure 1.5: Slip angle graph

The relationship between the lateral force as a function of the slip angle presents a non-linear behaviour, with exception of the origin. At the beginning, considering a small value of slip angle, it can be noticed quite a linear trend.

Increasing the slip angle, the lateral force increases to a maximum, after this peak, the force decreases asymptotically to a constant value.

Under the assumption of small levels of lateral acceleration, a linear analysis of the tire can be done. In this area is possible to approximate the tire slip at the zero slope point.
The so called "cornering stiffens" can be defined as follows.

$$C_\alpha = -\frac{\partial F_y}{\partial \alpha}|_{\alpha=0} \tag{1.1}$$

Still referring to the Figure (1.5), it can be noticed that if a positive angle is present, a negative force is produced. To deal with a positive number of C_α, the SAE convention defines C_α with a minus in the formula.

1.3.2 Camber Thrust

Another source of lateral force is given by a non-vertical orientation of the tire with respect to the ground. The angle between the vertical plane and the tilted plane of the wheel is called camber angle.

The lateral force produced by the camber is called "camber thrust". The sign of the camber is defined with respect to a vertical line that passes through the wheel and it is perpendicular to the ground. A positive camber is defined when the wheel leans outward at the top.

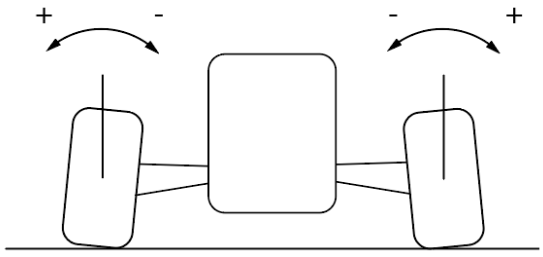

Figure 1.6: Camber thrust

The lateral force produced is always directed in the direction in which the tire is inclined. With the same procedure of the slip angle, it is possible to draw in a graphic the lateral force as a function of the camber angle.

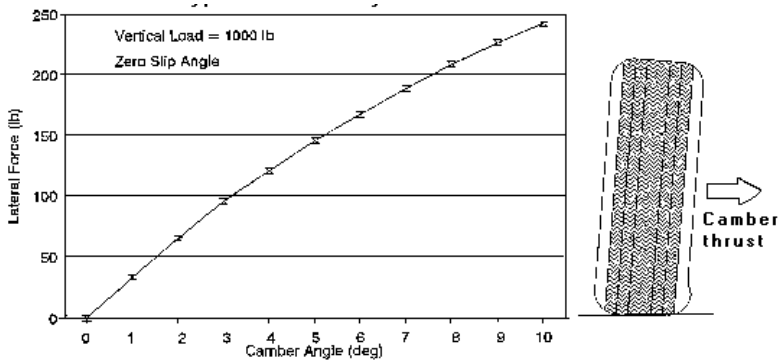

Figure 1.7: Camber lateral force [25]

Calculating the slope at the origin, is possible to calculate the camber stiffness C_γ.

$$C_\gamma = -\frac{\partial F_y}{\partial \gamma}|_{\gamma=0} \tag{1.2}$$

1.3.3 Adherence condition of tyre

The longitudinal and lateral force can be represented into a graphic as a function of the traction (or braking) speed ration and as a function of the slip angle.

The longitudinal and lateral force have an interaction between them. The effect of this interaction is studied into a diagram which is the friction ellipse and the friction circle [21].

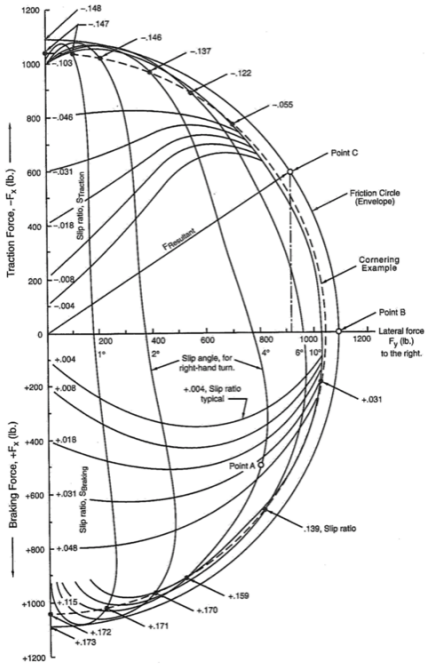

Figure 1.8: Circle diagram [21]

The friction circle represents the force-producing limit of the tire for a set of operating conditions.

Figure (1.8a) shows an example of a circle diagram with different test conditions.

When the tire is going straight, no slip angle and no lateral force are present. As the slip angle increase, a lateral force will appear and the magnitude of the longitudinal force will decrease.

This diagram is extremely important because allows the designer to understand which is the maximum magnitude of the force that the tire can generate under a given operating condition.

By taking into account the Pythagorean theorem it is possible to calculate the maximum force that the tire can supply in a certain condition.

$$F_R^2 = F_x^2 + F_y^2 \tag{1.3}$$

1.4 Fiala's Theory

Many tire models have been developed to mathematically reproduce their behaviour. Depending on the kind of study a simple or more sophisticated model can be chosen. The tire behaviour can be described as well by using empirical formulas, which may not have any physical correlation with the effective behaviour of the tire, such as the Magic Formula [23] and other experimental tests traduced into mathematical form.

Between the existing models, for the specific work, it has been chosen the mathematical model proposed by E.Fiala [1]. The model is widely used nowadays to perform analysis of the lateral forces produced by the side slip of the tires.

In this model, the tire is modelled as shown in the Figure (1.9).
The rim is modelled as a stiff body, B is the pneumatic tube and sidewall that can elastically deform itself in both vertical and lateral directions. C is the equivalent thin tread base joined to the sidewall at both sides. Finally, D is the equivalent to the tread rubber which is not a continuous circular body, but a series of independent spring bodies located around the tire's circumference.

When a lateral force is acting on a wheel, on the ground contact surface, the carcass will be deformed in the lateral direction, the tread base will have a bending deformation in the lateral direction and the rim, since is considered to be stiff, will not be deformed.

Under the assumption that the contact between the tire and the ground has the same deformation at the front and rear of the path, the line which connects the points defined in the centerline of the areas is defined as the $x - axis$. The

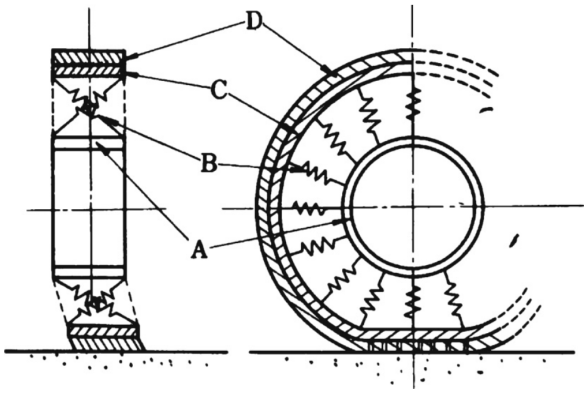

Figure 1.9: Tire model [1]

perpendicular to the $x-axis$ represents the $y-axis$ and it is located at the front endpoint. The $x-axis$ is parallel to the tire rim centerline and also the tread base centerline before deformation. in these axes, the distance along the $x-axis$ from the contact surface from endpoint is x, and the lateral displacement from the $x-axis$ is y, y_1 is the lateral displacement from the $x-axis$ for $0 \leq x \leq l_1$, and y_2, is the lateral displacement from $x-axis$ for $l_1 < x \leq l$. In the region $0 \leq x \leq l_1$ there is no relative slip between the tire and the ground. The region $l_1 < x \leq l$ is where the relative slip is produced. β is the side-slip angle of the tire, l is the contact surface length, and b is the contact surface width [1].

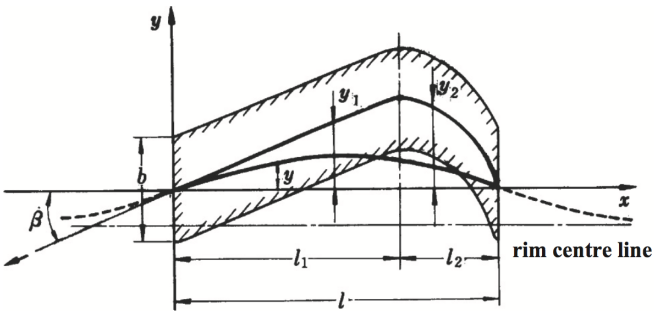

Figure 1.10: Tire deflection model

By taking into account the lateral deformation, y, of the tread base, if it is ideally extended along the tire circumference, as in the Figure (1.11) , it is possible to model the path as a beam with infinite length, in contact with a large number of springs (as B in Figure (1.9)).

The deformation of the beam is considered by taking the lateral force acting on the tire as F, the rim centerline as the $x-axis$, and the line passing through the tire center perpendicular to the $x-axis$ as the $y-axis$. If the force is acting only on the $y-axis$ ($i.e.$, $x=0$), the following equation can be write:

$$EI\frac{d^4y}{dx^4} + ky = w(x) \tag{1.4}$$

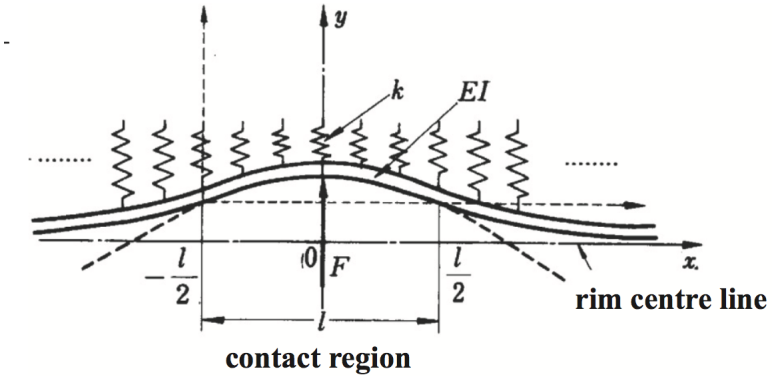

Figure 1.11: Rim deflection model

If $x \neq 0$, then $w(x) = 0$, and if $x = 0$, then $w(x) = F$. E is the Young's modulus of the tread material, I is the geometrical moment of inertia of the tread base, and k is the spring constant per unit length of the spring support. Solving the previous equation, the lateral displacement, y, is given by the following equation as a general solution:

$$y = \frac{\alpha F}{2k} e^{-ax} [\cos ax + \sin ax] \tag{1.5}$$

α can be obtained and the formula is:

$$\alpha = \frac{1}{\sqrt{2}} \left(\frac{k}{EI} \right)^{\frac{1}{4}} \tag{1.6}$$

The tread base displacement within the ground contact region is assumed to be y at $|\alpha x| \ll 1$. It is possible to approximate $\cos ax \approx 1$ and $sin\alpha x = \alpha x$. y can be approximated as a second-order equation of x.

$$y = \frac{\alpha F}{2k} (1 - \alpha^2 x^2) \tag{1.7}$$

Finally, by taking into account that $y = 0$ at $x = 0$ and $x = l$ it is possible to express y as:

$$y = \frac{\alpha^3 l^2 F}{2k} \frac{x}{l} \left(1 - \frac{x}{l} \right) \tag{1.8}$$

The equation is able to express the lateral displacement, y, of the tread in accordance with Figure (1.11)

Taking into account Figure (1.10), for the region $0 \leq x \leq l_1$ there is no relative slip between the tire and the ground. The contact surface deforms relatively in the opposite direction to the tire's lateral travelling direction. The lateral displacement,

y_1, for each point on the contact surface along the longitudinal direction can be written as follows:

$$y_1 = tan\beta x \tag{1.9}$$

A force per unit length in the lateral direction acts upon each point on the contact surface along the longitudinal direction. A shear strain on $(y_1 - y)/d$ occurs between the tread rubber and the tread base.

$$f_1 = K_0(y_1 - y) = K_0 \left[\tan \beta x - \frac{\alpha^3 l^2 F}{2k} \frac{x}{l} \left(1 - \frac{x}{l} \right) \right] \tag{1.10}$$

$$K_0 = G\frac{b}{d} = \frac{E}{2(1+\nu)} \frac{b}{d} \tag{1.11}$$

G is the shear modulus of the tread, and ν is the Poisson Ratio.

Once that f_1 exceed the friction limit between the tread and the ground, a relative slip will occur. The slip region is denoted by $l_1 < x \leq l$ and the shear strain of the tread rubber is $(y_2 - y)/d$. The f_2 is the force responsible for the strain.

By considering the force W as the load acting on a tire, p, the pressure distribution along the $x - direction$ can be represented by a second-order equation, with the maximum at the tire center, as shown in Figure (1.12).

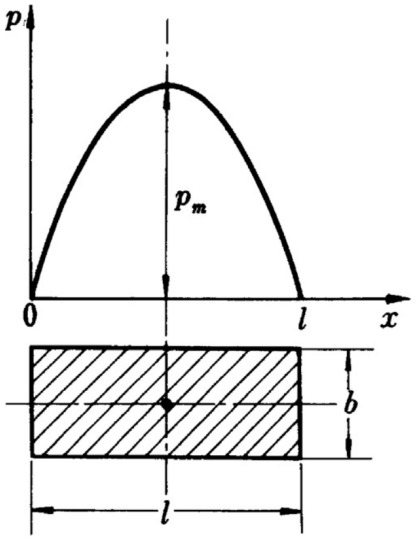

Figure 1.12: Contact pressure distribution

The pressure trend and the maximum peak can be written as:

$$p = 4p_m \frac{x}{l} \left(1 - \frac{x}{l} \right) \tag{1.12}$$

$$p_m = \frac{3W}{2bl} \tag{1.13}$$

f_2 becomes as follows:

$$f_2 = K_0(y_2 - y) = \mu p b = 4\mu p_m b \frac{x}{l}\left(1 - \frac{x}{l}\right) \tag{1.14}$$

μ represents the friction coefficient between the tread rubber and the ground, $l1$ is the value of x that satisfies $f_1 = f_2$.

Since the lateral force acts on each point on the contact surface along the longitudinal direction, it is possible to consider a small increment dx and calculate the total lateral force F acting on the whole contact path.

$$\begin{aligned} F &= \int_0^{l_1} f_1 dx + \int_{l_1}^{l} f_2 dx \\ &= K_0 \int_0^{l_1} \left[\tan\beta x - \frac{\alpha^3 l^2 F}{2k}\frac{x}{l}\left(1 - \frac{x}{l}\right)\right] dx + \int_{l_1}^{l} 4\mu p_m b \frac{x}{l}\left(1 - \frac{x}{l}\right) dx \end{aligned} \tag{1.15}$$

The integral results quite hard to solve, Fiala had approximated F, obtaining a really effective method able to put into relation the tire side-slip angle and the lateral force.

$$F = \frac{K_1 l^2}{2}\tan\beta - \frac{1}{8}\frac{K_1^2 l^3}{\mu p_m b}\tan^2\beta + \frac{1}{96}\frac{K_l^3 l^4}{\mu^2 p_m^2 b^2}\tan^3\beta \tag{1.16}$$

$$K_1 = \frac{K_0}{1 + \frac{\alpha^3 \beta}{12k} K_0} \tag{1.17}$$

Referring another time to Figure (1.10) it is possible to see that the lateral force acting on the path is not symmetric. The asymmetry generates a moment around the vertical axis of the wheel. The torque which is generated is the so called self-aligning torque.

As done for the lateral force, it is possible to take into account a small portion of the path and calculate the moment about the axis. for $0 \leq x \leq l_1$ the moment is expressed as $(x - l/2)f_1 dx$ and for $l < x \leq l_1$ as $(x - l/2)f_2 dx$. By integrating along the path it is possible to express the total moment acting on the tire.

$$\begin{aligned} M &= \int_0^{l_1} \left(x - \frac{l}{2}\right) f_1 dx + \int_{l_1}^{l} \left(x - \frac{l}{2}\right) f_2 dx \\ &= K_0 \int_0^{l_1} \left(x - \frac{1}{2}\right)\left[\tan\beta x - \frac{\alpha^3 l^2 F}{2k}\frac{x}{l}\left(1 - \frac{x}{l}\right)\right] dx + \int_{l_1}^{l} 4\mu p_m b \left(x - \frac{1}{2}\right)\frac{x}{l}\left(1 - \frac{x}{l}\right) dx \end{aligned} \tag{1.18}$$

Another time, the equation is too complicated, Fiala made an approximation as follows:

$$M = \frac{K_l l^3}{12}\tan\beta - \frac{1}{16}\frac{K_l^2 l^4}{\mu p_m b}\tan^2\beta + \frac{1}{64}\frac{K_l^3 l^5}{\mu^2 p_m^2 b^2}\tan^3\beta - \frac{1}{768}\frac{K_l^4 l^6}{\mu^3 p_m^3 b^3}\tan^4\beta \quad (1.19)$$

The expression put into relation the tire slip-angle and the self-alligning torque.

If β is small, it is possible to evaluate the cornering stiffens as:

$$K = \left(\frac{dF}{d\beta}\right)_{\beta=0} = \frac{K_l l^2}{2} \quad (1.20)$$

With the Fiala's model the lateral force, F, is almost proportional to $\tan\beta$ under the assumption of small side-slip angle. At a certain β, the lateral force reaches the saturation and dose not increase further with increase of the side-slip angle.

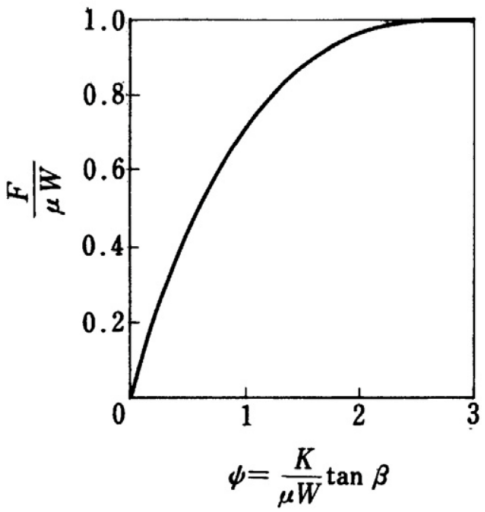

Figure 1.13: Lateral force to side slip angle

In the case of the self-aligning torque, it is proportional to $\tan\beta$ for a small side-slip angle. After a certain β the self-aligning torque reaches a maximum and decreases as β increase more. When β is small $tan\beta \approx \beta$ the self aligning torque can be treated as proportional to β, when this condition is no longer satisfied, the trend has a non linear behavior.

It is possible to make a further simplification of the formula (1.16) under the assumption of low β. It is possible to express the lateral force and the self aligning torque as follows in the equation.

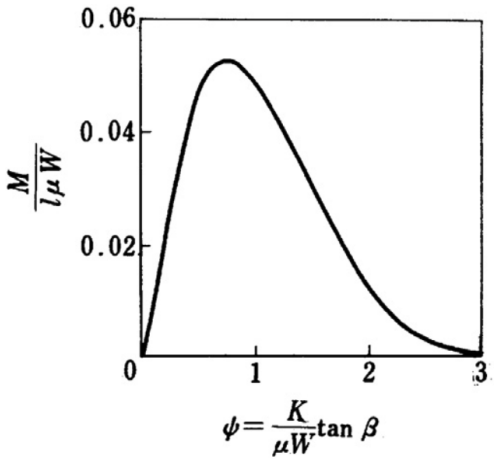

Figure 1.14: Self aligning torque to side slip angle

$$F \approx \frac{K_l l^2}{2}\beta = K\beta \tag{1.21}$$

$$M \approx \frac{K_l l^3}{12}\beta = \xi_n K\beta \tag{1.22}$$

K represents the cornering stiffness while ξ_n represents the so-called pneumatic trail which is expressed as:

$$\xi_n = \frac{M}{F} \tag{1.23}$$

By collecting all the assumption done, it is possible to draw a schematic contact path in accordance with the model:

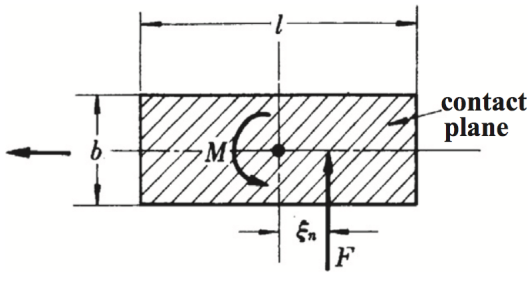

Figure 1.15: Pneumatic trail

1.5 Forces acting on the vehicle

At any instant of time the a vehicle is subjected to a series of forces which varies continuously. Those forces are able to maintain the vehicle at a certain speed or in

a certain curvature. They could be able to create a condition of instability in the vehicle.

Tires, aerodynamic and gravitational forces creates the global force field acting on the vehicle.

The exact knowledge of that forces can lead to a good evaluation and approximation of the car behaviour. Because of the complexity of the problem the object of study can be divided into subsystems which are coupled or not, basing on the complexity of the model.

Usually the forces are divided into longitudinal, lateral and vertical. Resultant forces and moments are usually defined as acting on the vehicle. Normally, as expressed by the normative J670e "Vehicle dynamics terminology" a force acting along the $x - axis$ is positive if it is in the forward direction of the vehicle. The force which represent the load acting on a tire acts in upward direction and so, it is negative according to the reference system previously defined. [8]. When a car is cornering, or subjected to an aerodynamic field, a lateral force will be present as well.

1.5.1 Longitudinal forces

By considering the Newton's Second Law it is possible to describe which forces are acting on the vehicle. Considering the longitudinal direction, the forces acting on the vehicle are caused by different sources which do not act on the center of gravity, thus producing moments.

Considering the Figure (1.16) all the forces acting on a vehicle are shown.

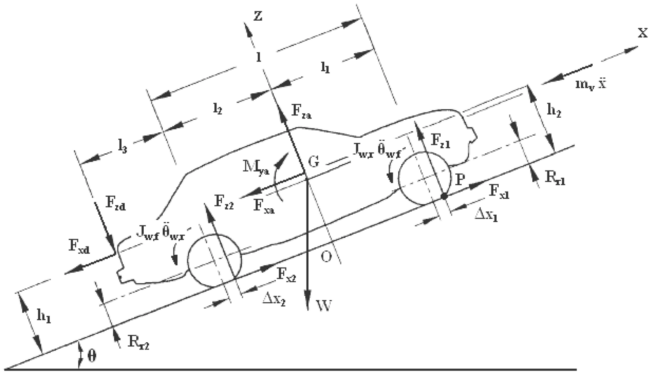

Figure 1.16: Forces acting on the vehicle

It follows the explication of the forces displayed in the picture:

W: weight of the vehicle acting at its center of gravity, G, with a magnitude equal to its mass times the acceleration of gravity. On a grade it may have two components, a longitudinal component which is proportional to the sine of the

slope and parallel to the road, and a vertical component which is proportional to the cosine of the slope and perpendicular to the road surface.

m_v: mass of the vehicle.

J_{w_f} and J_{w_r}: Inertia of the front and rear wheels.

d^2x/dt^2: linear acceleration of the vehicle along the longitudinal axis.

$d^2\vartheta_f/dt^2$ *and* $d^2\vartheta_r/dt^2$: angular accelerations of the vehicle along the spin $z-axis$ at the front and rear wheels.

l: Wheelbase of the vehicle, that means the length between the two spin axes.

l_1 and l_2: center of gravity location, referring to both axles.

l_3: distance between the vertical drawbar load and rear axle.

F_{x_a}, F_{z_a} and M_{y_a}: Aerodynamic forces acting on the body of the vehicle; the former, in x direction, may be represented as acting at a point above the ground indicated by the height, h_2, or by a longitudinal force of the same magnitude in the ground plane with an associate moment equivalent to F_{x_a} times h_2; instead M_{y_a} represents the aerodynamic pitching moment.

h_1 and h_2: lengths between the line of action of the inertia force and the aerodynamic one, respectively.

Δx_1 and Δx_2: Characteristic length between the line of action of the inertia force and the aerodynamic one, respectively.

R_{r_1} and R_{r_2}: Rolling radius of the front and rear wheels, respectively. However, their magnitude is always equal and so, it is fixed as R_r.

F_{x_1} and F_{x_2}: Rolling resistance of the front and rear tires.

F_{z_1} and F_{z_2}: Vertical load of the vehicle at the front and rear tires.

F_{z_d} and F_{z_d}: Drawbar loads. Exactly, they are the longitudinal and vertical forces acting at hitch point when the vehicle is towing a trailer.

To evaluate the normal components of the contact ground-tyre of the vehicle two equations of dynamics equilibrium are required. By considering two wheels for each axle it is possible to write the equilibrium equation about the point P and a global one in forward direction:

$$m_v\ddot{x}h_1 + 2J_{w,f}\dot{\vartheta}_{w,f} + 2J_{w,r}\dot{\vartheta}_{w,r} - 2F_{z2}(l - \triangle x_1 + \triangle x_2) + F_{zd}(l + l_3 + \triangle x_1) + \\ + F_{xd}h_1 + F_{xa}h_2 - F_{za}(l + \triangle x_1) - M_{ya} + W_x h_1 + W_z(l_1 + \triangle x_1) \tag{1.24}$$

It is for simplicity assumed a null contribution of the aerodynamic forces F_{z_a} and M_{y_a}, different from the x direction:

$$F_{z_a} = 0 \tag{1.25}$$

$$M_{y_a} = 0 \tag{1.26}$$

Analogy for both drawbar forces, that is the vehicle running without trailer($F_{x_d} = 0$); therefore, it is assumed that the inertia of the wheels have the same magnitude, like as the characteristic lengths:

$$J_{w,_f} = J_{w,_r} = J_w \tag{1.27}$$

$$\Delta_{x_1} = \Delta_{x_2} = U \tag{1.28}$$

Finally, like working hypothesis the elementary rotation of the wheels at the same axle assumes equal values:

$$\vartheta_{w_f} = \vartheta_{w_r} = \vartheta_w \tag{1.29}$$

Thus, the equation of equilibrium around the point P becomes:

$$m_v\ddot{x}h_1 + 4J_w\ddot{\vartheta_w} - 2F_{z_2}l + F_{x_a}h_2 + W_x h_1 + W_z\,(l_1 + U) = 0 \tag{1.30}$$

Where w_x and w_z represent the components of the vehicle weight that, supposing that the vehicle is moving on a road with a small slope it is possible to write:

$$W_x = W sin\vartheta = m_v g i \tag{1.31}$$

$$W_z = W sin\vartheta = m_v g \tag{1.32}$$

Finally, the equation which is able to provide the rear load transfer on the tire is:

$$F_{z_2} = \frac{1}{2l}\left[m_v\ddot{x}h_1 + 4J_w\ddot{\vartheta_w} + F_{x_a}h_2 + m_v g h_1 i + m_v g(l_1 + U)\right] \tag{1.33}$$

With the same procedure, writing the equilibrium in the vertical direction it is possible to obtain the front load transfer,

$$2F_{z_2} + 2F_{z_1} - F_{z_d} + F_{z_a} - W_z = 0 \tag{1.34}$$

where, for the same considerations about the drawbar and aerodynamic forces,

$$F_{z_1} = \frac{m_v g - 2F_{z_2}}{2} \tag{1.35}$$

The front and rear load is composed by two components, a static load and a dynamic load. Arranging the equations (1.30) and (1.33), the vertical load is obtained as:

$$F_{z_1} = F_{z_1}^S - \frac{1}{2l}\left[m_v \ddot{x} h_1 + 4J_w \ddot{\vartheta_w} + F_{x_a} h_2 + m_v g h_1 i + m_v g U\right] \tag{1.36}$$

$$F_{z_2} = F_{z_2}^S + \frac{1}{2l}\left[m_v \ddot{x} h_1 + 4J_w \ddot{\vartheta_w} + F_{x_a} h_2 + m_v g h_1 i + m_v g U\right] \tag{1.37}$$

Where the terms $F_{z_1}^s$ and $F_{z_2}^s$ represents the front and rear static load respectively and they assume the following form:

$$F_{z_1}^s = m_v g \frac{l_2}{2l} \tag{1.38}$$

$$F_{z_2}^s = m_v g \frac{l_1}{2l} \tag{1.39}$$

Instead, to study the longitudinal components of the contact two more dynamic equation of equilibrium are required. First, considering a single axle and considering the forces acting on the wheel as shown in Figure (1.17).

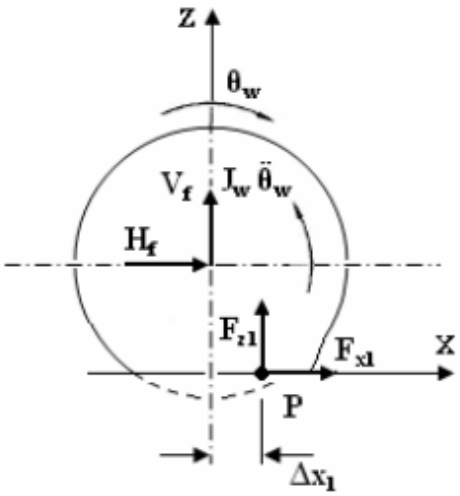

Figure 1.17: Forces acting on the wheel

Writing the equilibrium about the rotation axis of the front wheel,

$$J_w \ddot{\vartheta}_w + F_{z_1} U + F_{x_1} R_r = 0 \tag{1.40}$$

from which is obtained the value of the normal rear force,

$$F_{x_1} = -\frac{J_w \ddot{\vartheta}_w + F_{z_1} U}{R_r} \tag{1.41}$$

And so, the global equilibrium of the vehicle in forward direction gives the following relation,

$$m\ddot{x} - 2F_{x_1} - 2F_{x_2} + F_{x_a} - F_{x_d} + W_x = 0 \tag{1.42}$$

rewriting the formula, the normal front force is obtained:

$$F_{x_2} = \frac{1}{2}\left(m_v \ddot{x} + m_v g i + F_{x_a}\right) + F_{x_1} \tag{1.43}$$

1.6 Lateral dynamic model

There are many degrees of freedom associated with the dynamic of a vehicle. Due to its complexity, it is necessary to create a simplified model which is able to make a good approximation of it. Depending on the kind of study that the engineer is looking for, there are different models which take into account a different number of degrees of freedom. As for instance, it is possible to use a linear two degree of freedoms model, 2 D.O.F.s, a linear 4 D.O.F.s model or a non-linear 4 D.O.F.s model [11].

1.6.1 Steady state models

The easiest model which is able to describe a vehicle is called "Bicycle model" [21]. This model was chosen in this work, in the inverse dynamics analysis because of a series of assumptions previously illustrated.

The vehicle is supposed to be studied with the following hypothesis:

- the vehicle is a rigid body moving on a geometric plane
- the longitudinal and lateral load transfer is neglected
- the body is not subjected to rolling or pitching motions
- the tires have a linear behaviour
- the vehicle speed is constant
- aerodynamic effects are neglected
- the suspension system does not affect the calculation
- the steering angle is small

The series of assumption implies that the model is good under the condition of smooth cornering and for relatively low velocities.

In order to perform a study of a vehicle is necessary to know the tire's cornering stiffness, the position of the center of gravity and the geometric steer angle.

The series of assumption imply that the model is good under the condition of smooth cornering and for relative low velocities.

In order to perform a study of a vehicle is necessary to know the tire's cornering stiffness, the position of the center of gravity and the geometric steer angle.

Figure (1.19) shows a scheme of the vehicle, there are two degrees of freedom which are the v lateral velocity and the r yawing velocity.

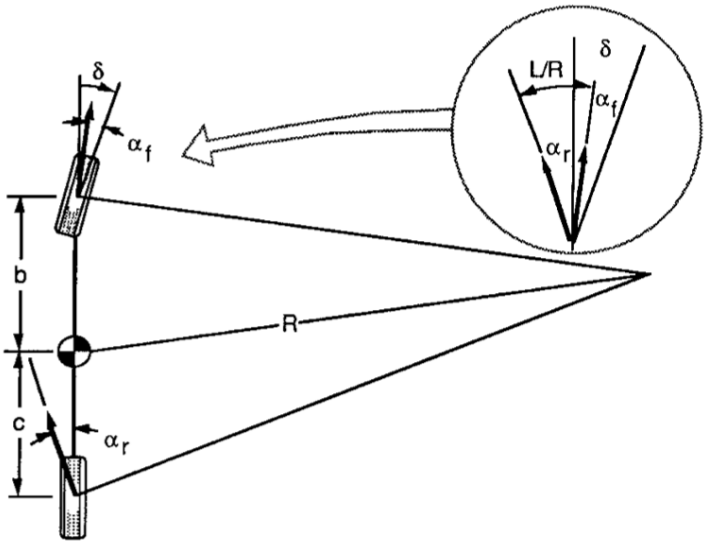

Figure 1.18: Cornering of a bicycle model

The model input is the front wheel steer δ. representing the steering angle of both wheels.

Considering a very low-speed cornering in the steady-state condition, neglecting all the accelerations and taking into account the assumption done for the Bicycle model, the slip angle can be considered as null. If the rear wheel has no slip angle, the center of turn lies on the projection of the rear axle. The perpendicular of the front wheels should pass through the same point, defined as the center of the turn. If the lines don't pass through the same point, the front wheels have some scrub during the turn. Figure (1.19) shows the ideal geometry to have a perfect turn [17].

Assuming small angles, the steer angles are obtained as,

$$\delta_o = \frac{L}{(R + \frac{t}{2})} \tag{1.44}$$

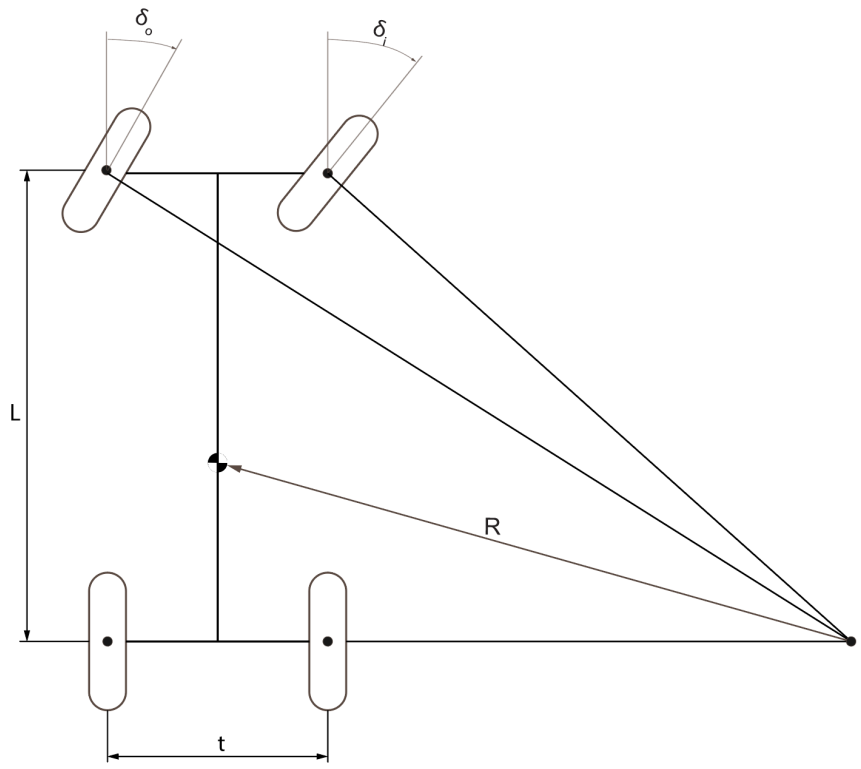

Figure 1.19: Curving geometry

$$\delta_i = \frac{L}{(R - \frac{t}{2})} \tag{1.45}$$

The average angle of the front wheels is called Ackerman Angle:

$$\delta = \frac{L}{R} \tag{1.46}$$

where, l is the vehicle wheelbase and R the radius of curvature.

The concept of Ackerman angle Geometry is usually employed to denote the exact geometry of the front wheels. A correct angle depend on the wheelbase and the angle of turn. An error in the Ackerman Angle can provoke a front tire wear. With a correct geometry the steering torques usually increase with the steer angle increase, giving the driver a natural feel in the feedback through the steering wheel.

1.6.2 High speed cornering

When the vehicle is travelling through a curve at high speed, the equations described above are not valid anymore. Due to the presence of the lateral acceleration, it is present a lateral force in the wheels that can not be neglected. The influence of these lateral forces increases as far the speed of the vehicle increase.

The lateral forces will produce a slip angle in the tires which is the angle between the orientation of the wheel and the orientation of its velocity vector. To define the

lateral force it is important to know the magnitude of the cornering stiffness, which is affected by many factors, as explained in the previous chapters. One of the most important factors is represented by the load applied to the tire. It is possible to define a cornering coefficient which is defined as:

$$CC_\alpha = \frac{C_\alpha}{F_z} \tag{1.47}$$

The steady-state cornering equations are derived from the application of the Newton's Second law. It is taken into account the bicycle model previously described, travelling a big curvature radius, much greater than the wheelbase. Small angles are taken into account, the difference between the inner and outer angle of direction is negligible, it is taken into account a steering angle δ, with a lateral force equal to the sum of the force acting on the inner and outer wheel.
The slip angle is defined as α_F for the front wheel and α_R for the rear wheel. The vehicle's instantaneous center O is represented by the point at which the two lines perpendicular to the velocities of the two wheels are met. Let $L = a + b$ be the

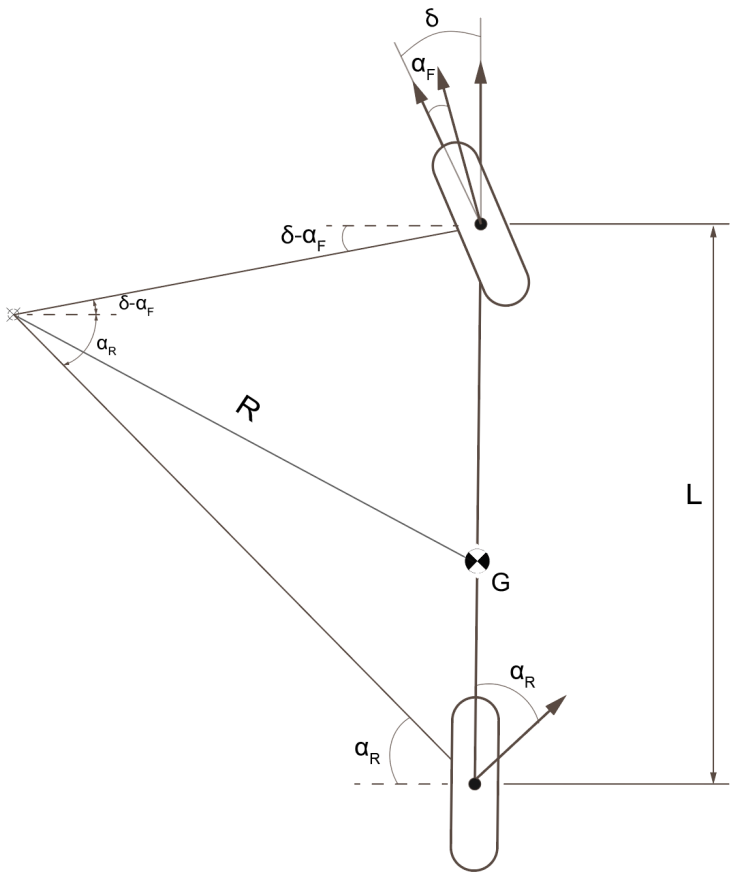

Figure 1.20: High speed cornering

wheelbase. From Figure, the angle formed at center of rotation is. Under the assumption that the road radius is much larger than the wheelbase of the vehicle

$R \gg L$, it possible to obtain

$$\delta - \alpha_f + \alpha_r \approx \frac{L}{R} \tag{1.48}$$

Thus, the steady state steering angle is given by

$$\delta = \frac{L}{R} + \alpha_f - \alpha_r \tag{1.49}$$

The steady state slip angle α_F and α_R are related to road radius. As already said, with the presence of slip angles, lateral forces are generate in the tire-ground contact. The cornering equations are obtained by using the Newton's second law. Always considering the bicycle model, the equilibrium equation is obtained.

$$\sum F_Y = F_{Y_F} + F_{Y_R} = mV^2/R \tag{1.50}$$

where:

- F_{Y_F}= lateral (cornering) force at the front axle
- F_{Y_R}= lateral (cornering) force at the rear axle
- m= mass of the vehicle
- V= forward velocity
- R= radius of the turn

The vehicle needs to be in equilibrium about its center of gravity, the resultant moment produced by the lateral forces needs to be zero.

$$F_{Y_F} a - F_{Y_R} b = 0 \tag{1.51}$$

From the moment equilibrium (1.51), it is obtained:

$$F_{Y_F} = \frac{b}{a} \cdot F_{Y_R} \tag{1.52}$$

Considering the relationship between front ad rear tire forces of equation (1.52) in the force equilibrium equation (1.50), it is obtained:

$$F_{Y_R} = m\frac{a}{L} \cdot \frac{V_x^2}{R} = m_R \cdot \frac{V_x^2}{R} \tag{1.53}$$

where

$$m_R = m\frac{a}{L} \tag{1.54}$$

is the amount of mass loading the rear axle.

With the same procedure of the rear axle, the amount of vehicle mass loading the front axle is defined by the formula,

$$m_F = m\frac{b}{L} \tag{1.55}$$

from which it is possible to obtain the lateral force acting on the front axle

$$F_{Y_F} = m\frac{b}{L} \cdot \frac{V_x^2}{R} = m_F \cdot \frac{V_x^2}{R} \tag{1.56}$$

Under the assumption of small slip angles, the lateral tire forces are directly proportional to its slip angle.

Expressing the cornering stiffness of the front tire as C_{α_F} and for the rear C_{α_R}, the slip angle are:

$$\alpha_f = \frac{F_{Y_F}}{2C\alpha_f} = \frac{m_f}{2C\alpha_f} \cdot \frac{V_x^2}{R}, \quad \alpha_r = \frac{F_{Y_R}}{2C\alpha_r} = \frac{m_r}{2C\alpha_r} \cdot \frac{V_x^2}{R} \tag{1.57}$$

By substituting, it is obtained the equation of the steady state steering angle:

$$\delta = \frac{L}{R} + \alpha_F - \alpha_R = \frac{L}{R} + \left(\frac{m_F}{2C_{\alpha_F}} - \frac{m_R}{2C_{\alpha_R}}\right)\frac{V_x^2}{R} \tag{1.58}$$

Defining the parameter K_v, called understeer gradient,

$$K_v = \left(\frac{m_F}{2C_{\alpha_F}} - \frac{m_R}{2C_{\alpha_R}}\right) \tag{1.59}$$

and writing the lateral acceleration,

$$a_y = V^2/R \tag{1.60}$$

The steering angle can be written in a compact form,

$$\delta = \frac{L}{R} + K_v a_y \tag{1.61}$$

The equation (1.61) is the formula that relates the vehicle velocity and road curvature to the steering angle required for negotiating the circular road.

1.6.3 Neutral, understeer and oversteer car

By taking into account the consideration done in the previous chapter and the bicycle model, it is possible to define the concept of neutral, understeering or oversteering car.

1.6.4 Neutral steel

A neutral steer is represented by a null understeer gradient K_v. This coefficient is null due to the fact that the front slip angle is always equal to rear slip angle.

$$\frac{m_f}{C_f} = \frac{m_r}{C_r} \Rightarrow K_v = 0 \Rightarrow \alpha_f = \alpha_r \tag{1.62}$$

If the vehicle presents a neutral steer behaviour and it is going through a constant radius curve, no change in the steering angle is required as speed is varied. So, the steering angle required to make a turn is equivalent to the Ackerman angle. Physically a neutral steer corresponds to a balance on the vehicle such that the "force" of the lateral acceleration at the center of gravity causes an identical increase in slip angle at both front and rear wheels.

1.6.5 Understeer

In the case of an understeering vehicle, the gradient $K_v > 0$, due to a larger slip angle at the front tires with respect to the rear tires.

$$\frac{m_f}{C_f} > \frac{m_r}{C_r} \Rightarrow K_v > 0 \Rightarrow \alpha_f > \alpha_r \tag{1.63}$$

Due to the difference in the slip angles, in the case of understeer, when considering a constant radius turn, the steering angle will have to be increased with speed in proportion to K_v times the the lateral acceleration. Thus, the direction needs to be increased linearly with the lateral acceleration and with the square of the speed. In the understeering case, the lateral acceleration at the center of gravity causes the front wheels to slip sideways to a greater extent than at the rear wheels. Thus, to maintain the radius of turn, the front wheels must be steered to a greater angle [21].

1.6.6 Oversteer

In the case of an oversteering vehicle, the gradient $K_v < 0$ due to a smaller slip angle at the front tires compared to the rear tires.

$$\frac{m_f}{C_f} < \frac{m_r}{C_r} \Rightarrow K_v < 0 \Rightarrow \alpha_f < \alpha_r \tag{1.64}$$

In the case of oversteer, on a constant radius turn, the steering angle will have to decrease when speed and lateral acceleration increases. In this case, the lateral acceleration at the center of gravity causes the slip angle on the rear of the vehicle

turns the front wheels inward, thus diminishing the radius of the turn. The increase in lateral acceleration that follows causes the rear drift out even further and the process continue unless the steering angle is reduced to maintain the radius of the turn.

1.6.7 Gradient comparison

The steering angle as a function of the vehicle longitudinal speed is shown in Figure (1.21) It is examined the case of neutral steer, oversteer and understeer. [21] With the presence of an understeer, the angle increases with the square of the

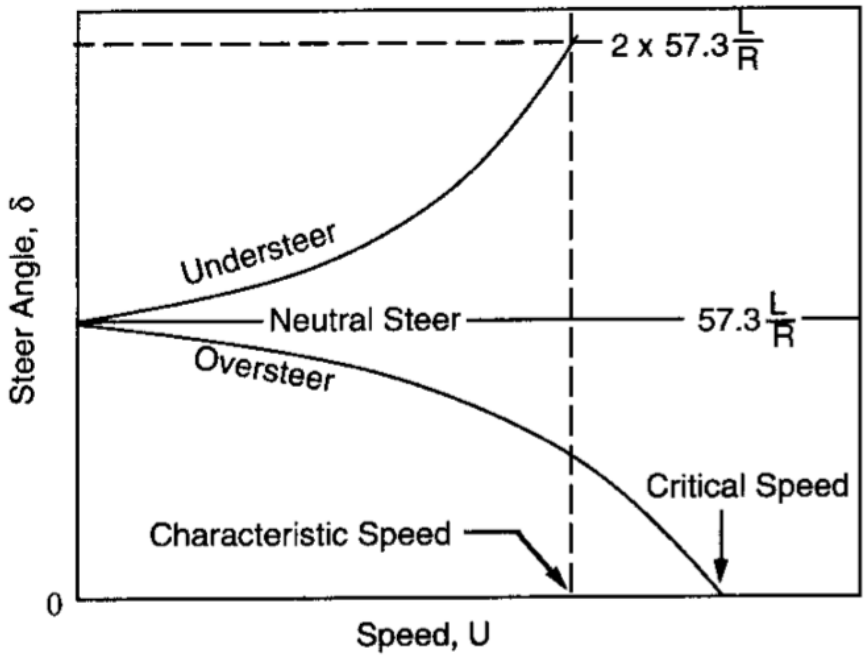

Figure 1.21: Steering angle as function of speed [21]

speed, reaching twice the initial angle at the characteristic speed. In the case of oversteer, the steering angle decreases with the square of the speed and become zero at the critical speed value. It is possible to define for an understeering vehicle a parameter known as the characteristic speed. The characteristic speed is defined as the speed at which the steering angle required to negotiate any turn is twice the Ackerman Angle.

$$K_v a_y = 57,3\frac{L}{R} \tag{1.65}$$

Since a_y is function of the square of the speed, the characteristic speed V_{char} results to be:

It is possible to define for an understeering vehicle a parameter known as the characteristic speed. The characteristic speed is defined as the speed at which the steer angle required to negotiate any turn is twice the Ackerman Angle.

$$K_v a_y = 57.3 \cdot \frac{L}{R} \tag{1.66}$$

Since a_y is a function of speed squared, the characteristic speed is:

$$V_{char} = \sqrt{57,3Lg/K_v} \tag{1.67}$$

Instead, in the case of an oversteering vehicle, a critical speed will exist above which the vehicle will be unstable. The critical speed is given by the expression:

$$V_{crit} = \sqrt{-57,3Lg/K_v} \tag{1.68}$$

In the case of an oversteering vehicle, K_v is negative, so the expression under the square root is positive and has a real value.
It is possible to notice that the critical speed of the vehicle depends on its geometrical properties. A long-wheelbase vehicle presents a higher critical speed compared to a short one.

Chapter 2

Vehicle Model

2.1 Introduction

The chapter shows how the vehicle has been virtually reproduced. In the first part of the chapter, a list of the software's used to do the thesis was analysed, explaining the features of each one and the reason for the choice. It is then explained how the geometric properties and mass of the components was obtained, in order to define the model as close as possible to the reality. Suspension and tire properties are them modelled and defined through proper approximations. Finally, the model was reproduced into ADAMS, the main environment used to analyse the dynamics of the vehicle.

2.2 Software's

2.2.1 MSC Software

MSC Software Corporation is an American company founded in 1963 under the name MacNeal-Schwendler Corporation (MSC). The company developed its first structural analysis software called $SADSAM$ (Structural Analysis by Digital Simulation of Analog Methods) at that time. The company was involved in the aerospace industry to improve finite element analysis technology.

In 1965 MSC was awarded the original contract from NASA to commercialize the finite element analysis (FEA) software known as Nastran (NASA Structural Analysis). MSC produces many of the CAE technologies that are now employed by industry to analyze and predict stress and strain, vibration and dynamics, acoustics, and thermal analysis.

MSC has then developed or acquired many other CAE applications such as Patran, Adams, Marc, Dytran, Fatigue, SimXpert, SimDesigner, SimManager etc.

Nowadays, MSC offers a Simulation Data and Process Management platform that has been deployed in industries including automotive, aerospace, shipbuilding, electronics etc.

These programs are targeted at optimizing product development and enable engineers to validate and optimize their designs using virtual prototypes. Nowadays even real physical prototypes that traditionally have been used in product design sometimes are replaced in favor of computer models and analyses [30].

2.2.2 ADAMS

Adams is one of the most widely used multi-body Dynamics software. The name is the acronym of Automated Dynamic Analysis of Mechanical Systems. The software is equipped with Fortran and C++ numerical Solvers. This program permits to improve the engineering efficiency and helps to reduce the product development costs by creating virtual prototypes instead of real ones. The software permits to evaluate and manage motions, structures, actuation, controls etc., to better optimize product designs for performance, safety, and comfort.

Adams contains real physics and continuously solving equations for dynamics, kinematics, statics and quasi-statics, it is also compatible with other programs which enable import/export of models from CAD programs and perform co-simulations in real time.

The suite contains different programs, for instance, Adams/View, Adams/Chassis, Adams/car and Adams/Mechatronics [30].

2.2.3 ADAMS/View

Adams/View is a widely used Multi-body Dynamics Simulation software made by the software company MSC Software. It is commonly used in the industry and in the universities [30].

It is possible to built and simulate models of any mechanical system that has moving parts. A series of validations of the model against test data can be performed and the model can be refined by using flexible parts, realistic geometries and controls [2].

In Adams/View it is possible to import files from other solid modeling computer-aided design programs since the creation of complex models/parts are too time consuming in the software.

2.2.4 SolidWorks

SolidWorks is a solid modeling computer-aided design (CAD) and computer-aided engineering (CAE) computer program published by Dassault Systèmes [33].

The software is a solid modeler which utilizes a parametric feature-based approach to create models and assemblies. The software is written on Parasolid-kernel.

The parameters are referred to constraints whose values determine the shape or geometry of the model or assembly. They can be numeric parameters (line lengths, circle diameter, ect.) or geometric parameters (tangent, parallel, concentric, horizontal, vertical, etc.).

The creation of a model starts usually from a planar sketch, which consist of a series of lines, arcs, conics and splines. Dimensions and relations are used to define the sketch. It follows the three dimensional creation by using different features.

After the creation of a model is possible to create an assembly or create a view of it. The assembly consist of a series of models which are linked trough different mates.

After the creation of the part/assembly it is possible to export them into a wide series of formats to have a compatibility with other softwares.

2.2.5 MATLAB

MATLAB is a high-performance language for technical computing produced by MathWorks inc. The software is able to integrate computation, visualization, and programming in an environment as easy and accessible as possible, where the problems and solutions are expressed in a familiar and mathematical notation.

The program is typically used for math and computation, algorithm development, modeling, simulation and prototyping, data analysis, exploration, and visualization, scientific and engineering graphics, application development, etc.

The name of the software stands for matrix laboratory. The software is provided with a large number of toolboxes which are useful to solve particular classes of problems [18].

2.3 Data

The studied vehicle is produced and distributed by the company "Robotnik". The car model is "RBCAR" [26].

Figure 2.1: RBCAR vehicle [26]

The car can be drive as fully automatic or in the traditional way with the driver control; it can be used for transport of people and goods or for academic research.

For the last reason, the vehicle is the object of study by the university, it is easy to mount accessories for obstacles avoidance or connect it to external components being able to control the robot in real time, controlling speed angle of direction, etc., or making it drive autonomously.

There is the possibility to mount many sensors like scanning lasers, DGPS kits, etc.

The vehicle is a rear wheel drive, the motion is provided by an electric AC motor, powered by a stack of traditional lead batteries or by an hydrogen fuel cell. The traction is controlled by an incremental encoder and the direction through a power steering with an absolute encoder.

The following mechanical data are provided by the producer Data-sheet [26]:

Table 2.1: Mechanical data

Dimensions	2660 × 1230 × 1720
Weight with batteries	690 Kg
Payload	2 People, 150 Kg on the box
Speed	32 Km/h
Motor	3,3 kW AC 48V
Autonomy	70 Km
Brakes	Hidraulics
Chassis	ABS thermoformed
Max. climbing angle	25 %

Table 2.2: Control data

Controller	Open architecture ROS
Communication	Embedded PC with Linux WiFi 802.11n
Connectivity	Remote

2.4 Data measurement

Every measure and further study are referred to the unloaded vehicle since, for this thesis, there is no interest to study the full load condition. In fact, the objective is to study trajectories to be implemented for the autonomous driving without any person on board.

Some data were already provided by the producer and listed in the table (2.1) and (2.2), but they were not enough to define all the necessary information.

The first real step of the modelling consists of a practical take-over. The vehicle is disassembled and each useful part is measured in detail. The suspension and the direction system has been meticulously measured. The geometry is strongly related to the dynamic behaviour.

A part from the geometrical measures, many parts have been weighed. The measured mass of each part has been compared to the 3D reproduction in order to check the quality of the draw and the density of the material chosen for the virtual model. This is due to the fact that the inertial properties of the vehicle are unknown. The University does not have a machine able to measure the inertial properties, thus all the inertial properties have been obtained by the 3D model developed in Solidworks.

Once completed the measurement of each component, the vehicle has been weighted to measure the center of gravity position. The longitudinal position is found measuring the load acting on the front and rear axle. For the height, it has been necessary to weight the axles on an inclined plane.

2.5 Center of gravity

The measurement of the center of gravity is essential to correctly define the vehicle dynamics. The overall mass is known by the data sheet, the height of the center of gravity and the load on each axle needs to be measured.

Figure (2.2) shows the resultant vertical force in the stationary condition for the front and rear axle. In order to calculate the position of the center of gravity, it is necessary to weight the load acting on the front and rear axle.
The useful data for the calculation of the center of gravity position are listed in table (2.3).

Table 2.3: Vehicle mass and wheelbase

Mass m	[Kg]	690
Wheelbase l	[m]	1,65

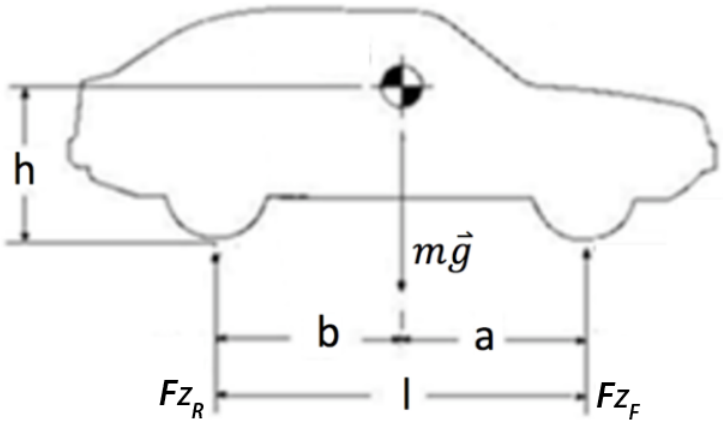

Figure 2.2: Vehicle center of gravity

The measured load on the front and rear axle is listed in table (2.4). The load

Table 2.4: Measured axle load

Rear axle load F_{z_R}	[N]	4512,4
Front axle load F_{z_F}	[N]	2256,4

acting on each wheel is half of the axle load, b is obtained by writing the equilibrium of moments about the rear axle,

$$- F_{Z_F} \cdot l + m \cdot g \cdot b = 0 \tag{2.1}$$

$$b = \frac{F_{Z_F} \cdot l}{m \cdot g} = 0,550\ m \tag{2.2}$$

a is obtained by writing the equilibrium of moments about the front axle,

$$F_{Z_R} \cdot l - m \cdot g \cdot a = 0 \tag{2.3}$$

$$a = \frac{F_{Z_R} \cdot l}{m \cdot g} = 1,1\ m \tag{2.4}$$

To calculate the height of the center of gravity the loads acting on the front and rear axle is measured on an inclined plane, Figure (2.3). The measured load at the

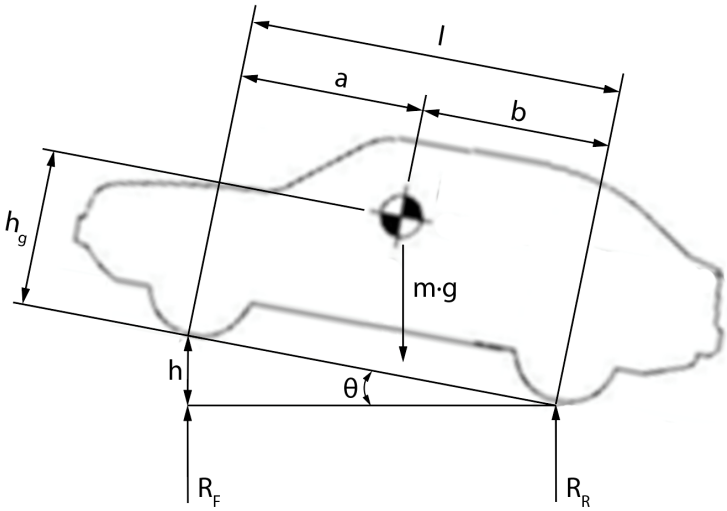

Figure 2.3: Axes loads on a slope

front and at the rear axle is listed in table (2.5).

Table 2.5: Measured axle loads and slope properties

Rear axle load R_R	[N]	4242,3
Front axle load R_F	[N]	2526,6
Step height h	[m]	0,3
Wheelbase l	[m]	1,65
Wheel radius r	[m]	0,235

Measuring the load acting on the front and rear axle the h_g is derived. The angle ϑ is defined as:

$$\vartheta = asin\left(\frac{h}{l}\right) = 0,128\ rad = 7,3339° \tag{2.5}$$

The height h of the center of gravity is obtained with the following formula [21]:

$$h = \left[b - l\left(\frac{R_F}{m \cdot g}\right)\right] * cot\vartheta + r = 0,5\ m \tag{2.6}$$

The center of mass position is calculated and resumed in the table (2.6)

Table 2.6: Center of mass position.

front axle distance a	[m]	1,1
rear axle distance b	[m]	0,55
heigth h	[m]	0,3

2.6 Suspension geometry

In this section, a study of the geometric properties of the front and rear suspension is done, calculating the roll center and the vehicle roll axis, starting from the data obtained during the 3D modelling.

2.6.1 Front suspension

The front suspension is not characterized by a common geometry that can be found in the literature. The structure is formed by an independent superior trapezoidal linkage guided by a leaf spring at the bottom.

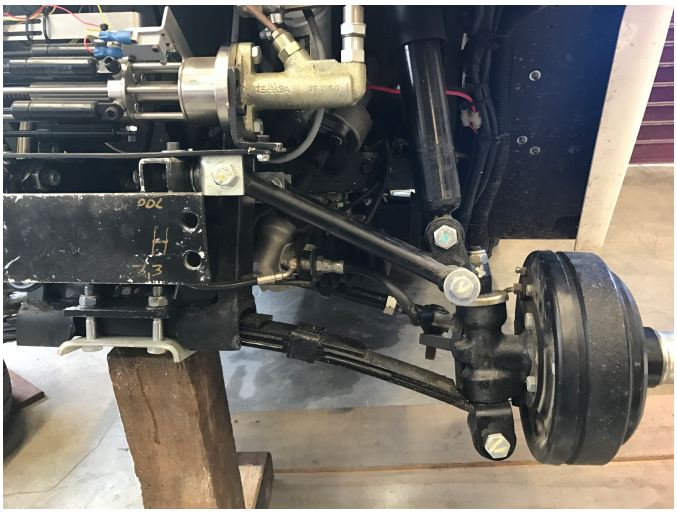

Figure 2.4: Front suspension

The roll center is defined as the point about which the vehicle rolls while cornering. Its location is found using the principles of the instant center of rotation [7].

Extending the lines of the upper linkage and the leaf spring, they intersect in a certain instantaneous center (ICR).

Another line is extended from the ICR to a point in which the tire is in contact with the ground. The point at which this line intersects the vehicle center is called roll center.

Figure 2.5: Front suspension side-view

Calculating with the procedure exposed, using a graphical method, Figure (2.6), the roll center of the front suspension is located at $h_1 = 88\ mm$ from the ground.

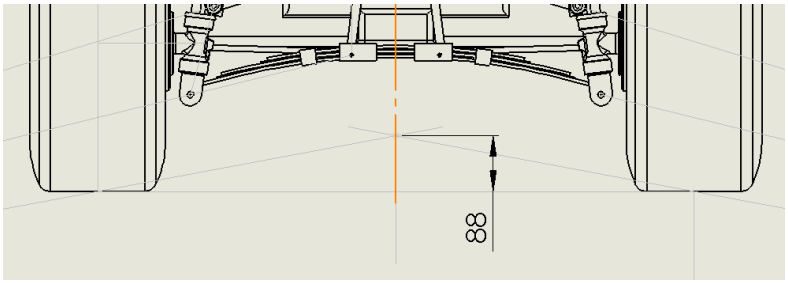

Figure 2.6: Front roll center

2.6.2 Rear suspension

The rear suspension is formed by a traditional rigid axle with longitudinal leaf springs.

The center of roll is obtained by drawing the theoretical line formed between the upper link and the lower link, the vertical line line passing through the axle, where the intersection of the two gives the center of roll [7]. Calculating with a graphical method, the center of roll results to be equal to $h_2 = 392mm$.

(a) **(b)** Slip angle

Figure 2.7: Rear leaf spring and axle

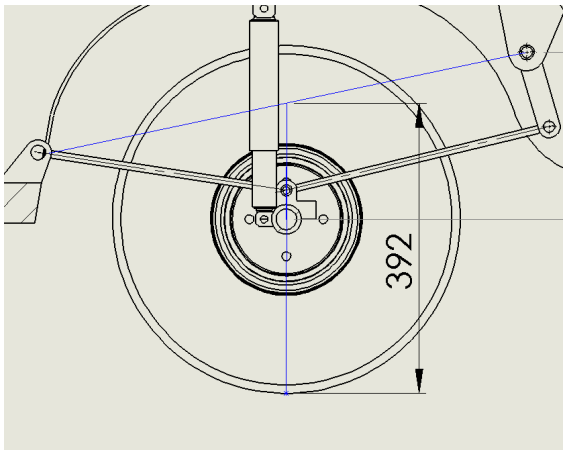

Figure 2.8: Rear roll center

2.6.3 Vehicle roll axis

The vehicle roll axis is defined as the line that joins the front and the rear roll center [7]. The h' distance is the distance from the center of gravity and the roll axis, measured in the vertical direction, as shown in the figure (2.9).

The distance between the center of gravity and the roll axis results equal to $h' = 215\ mm$.

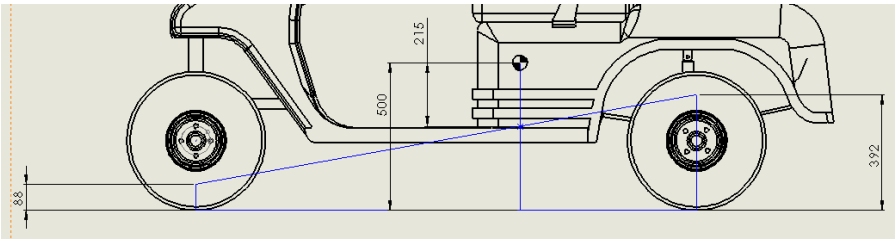

Figure 2.9: Distance roll axis center of gravity

2.7 Modelling of suspensions

To implement the model into ADAMS/view the suspension's leaf springs has been approximated by an equivalent system formed by bars and springs. It would have been possible to use the "Leafspring Toolkit" provided by MSC Software [29], which works with a discrete beam approach.
Since the expensive toolkit was not available for this work in the university, the leaf springs have been well approximated by methods found in the literature.

2.7.1 Rear suspension

The rear leaf spring can be approximated as a system of bar linkages with a vertical spring which has the same stiffness of the real system. As shown in Figure (2.10), the damper results to be located in the same location of the spring.

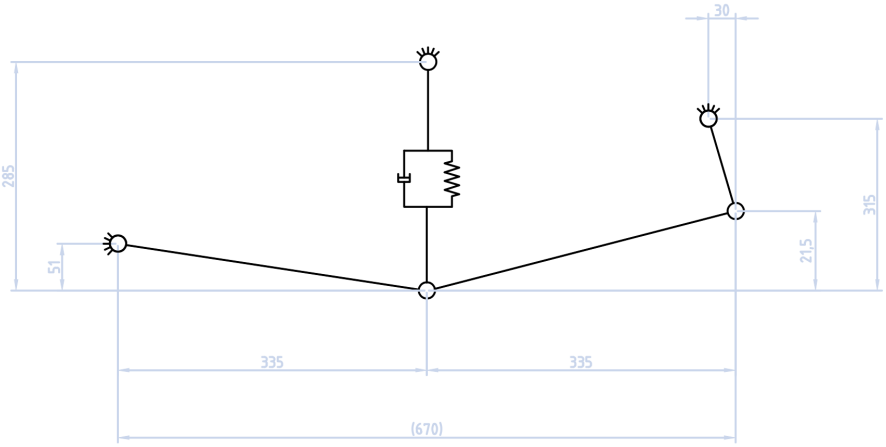

Figure 2.10: Rear suspension scheme

The equivalent stiffness of the leaf spring can be obtained by taking into account the equation (2.7) [5].

$$K = \frac{(2 + n^{'}/n)(E \cdot n \cdot b \cdot h^{'})}{6 \cdot l^3} \tag{2.7}$$

where n' is the number of complete leafs at the extremities, n is the number of leafs, E the Young's modulus, l is the half length of the leaf spring, b the width and h the thickness of each leaf.

The spring property measured are listed in Table (2.7)

Table 2.7: Rear leaf spring properties

Number of leafs		5
Number of complete leafs at the extremity		1
Young's modulus	[N/mm2]	206.000
I	[mm]	335
b	[mm]	40
h	[mm]	5

By computing the data, it is possible to obtain the stiffness of the two springs mounted on the rear suspension of the vehicle.

Table 2.8: Rear spring stiffness

K_{rear}	[N/mm]	50,2278

2.7.2 Front suspension

The front leaf spring is equivalent to a system formed by a pin-pin beam, connected between the chassis and the wheel hub, plus an equivalent spring at the extremity. The Figure (2.11) shows the structure just described. The damper is not shown in the picture since mounted on the upper part of the hub, which is not relevant for the model of the equivalent system.

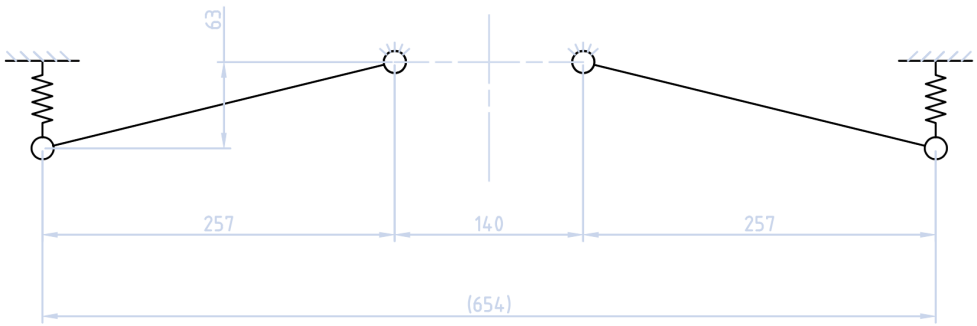

Figure 2.11: Front suspension scheme

As calculated for the rear, it possible to obtain the stiffness at the front with the same formula. The data acquired are listed in Table (2.9), while the resulting stiffness (2.10).

Table 2.9: Front leaf spring properties

Number of leafs	4
Number of complete leafs at the extremity	1
Young's modulus	206'000 N/mm2
I	327 mm
b	33
h	5

Table 2.10: Front spring stiffness

K_{front}	36,3867 N/mm

2.8 Dampers

The four dampers properties have been difficult to obtain because of the lack of tools to evaluate the damping behaviour of each one.

In accordance with the commercial automotive dampers, the damping of rear and front have been set, as the first attempt, as reported in Table (2.11).

Table 2.11: Damping coefficients

Front damping C_F	[Ns/mm]	8,00
Rear damping C_R	[Ns/mm]	15,00

After few simulations, the assumption of a constant value of damping exhibited some problems of instability. To improve the dynamic behaviour it has been set the damping behaviour as a non-linear function, Figure (2.12). The behaviour has been supposed equal for both the pair of front and rear dampers. the insertion of a nonlinear behaviour has shown an improvement of the general performances.

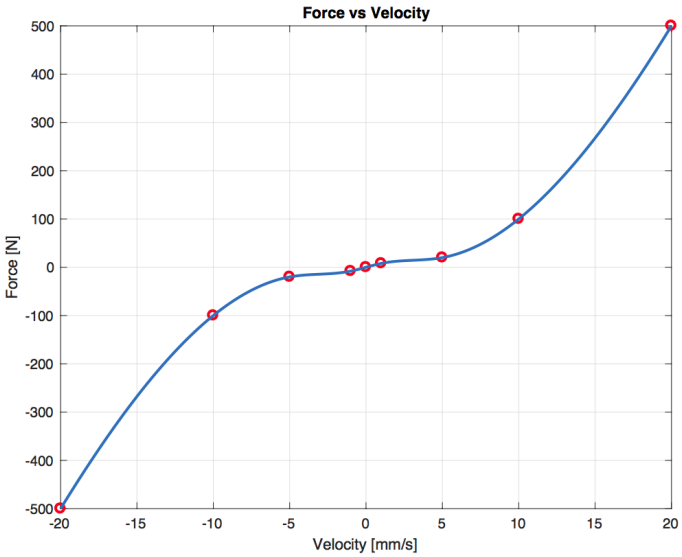

Figure 2.12: Force vs. velocity

2.9 3D modelling

After the evaluation of all the geometric features, load distributions, and the equivalent leaf spring, a faithful 3D representation of the vehicle has been made. The vehicle was modelled into Solidworks, first of all creating all the single parts which have been successively assembled into an assembly.

Once obtained the model, in order to check the goodness of the representation, a series of tests have been done. Comparing the total weight of the assembly in the program, the mass needs to coincide with the actual one, measured with the weight scale and supplied by the datasheet [26]. Next, the longitudinal position of the center of gravity needs to correspond to the calculated one. The height h of the COG has been measured afterwards into ADAMS/View simulating the contact with the ground since the effect of the suspension deformation due to the proper load needs to be taken into account. After having checked all the mass and geometrical features, the inertia of the vehicle has been copied to set the inertial properties into ADAMS.

2.9.1 Body

The body has been modelled as a single part since no relative motion is present between each one. Every component has been divided into different bodies to assign the right properties to each one.

The chassis is formed by ABS Thermoformed while all the other parts are formed by aluminium or steel.

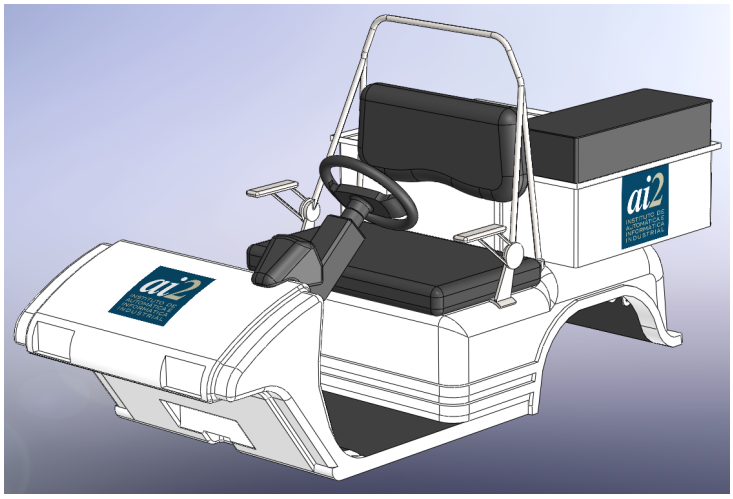

Figure 2.13: Chassis front view

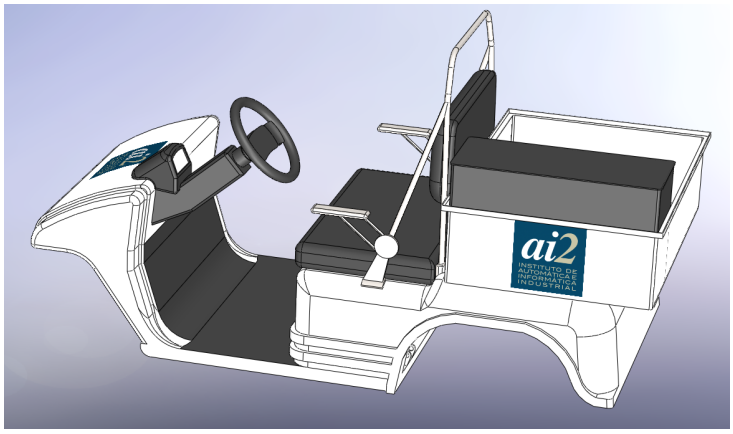

Figure 2.14: Chassis rear view

2.9.2 Rear suspension

The rear suspension has been modelled into parts, successively mounted into the vehicle assembly. The layout is the one equivalent to the linkage exposed before. The spring damper element is composed of a telescopic pipe which does not have any kind of stiffness or damping. It has been designed only to have a better assembly into ADAMS/View by using it to define the sliding joint. Figure (2.15) and (2.16) show the 3D assembly of the suspension with and without wheels.

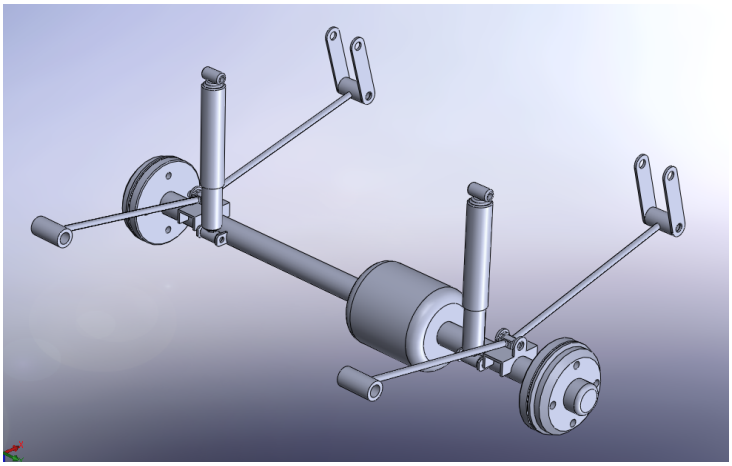

Figure 2.15: Rear suspension

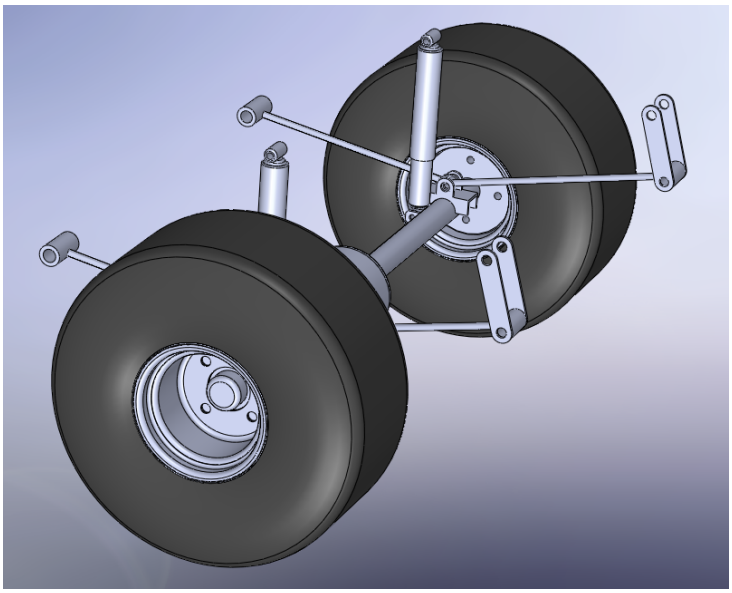

Figure 2.16: Rear suspension and wheels

2.9.3 Front suspension and direction system

As it has been done for the back, the front suspension has been designed into parts which have been successively mounted into the vehicle assembly. The direction system has been modelled as a simple system of bars connected by rotational joints equivalents to the Uniball connection mounted at the edge of the links.

It is important to notice that the vehicle is equipped with two direction systems, the first one is connected to the steer moved by the driver, the second one is the one moved by the automatic system. For the previous considerations, the steering system reproduced and taken into account for the calculation is the second one.

Figures (2.17), (2.18), (2.19), display the assembly of the front suspension with and without wheels.

Figure (2.17) shows the leaf spring which has been designed only for graphical reasons, all the study has been done with the equivalent structure, previously described.

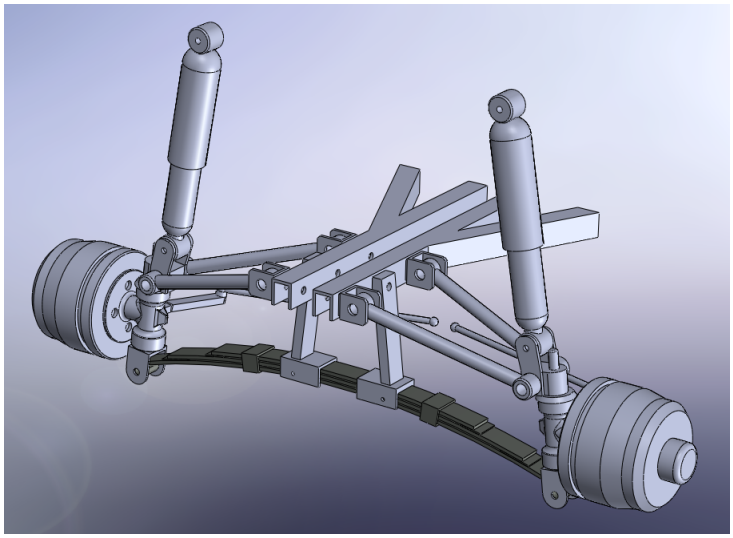

Figure 2.17: Front suspension

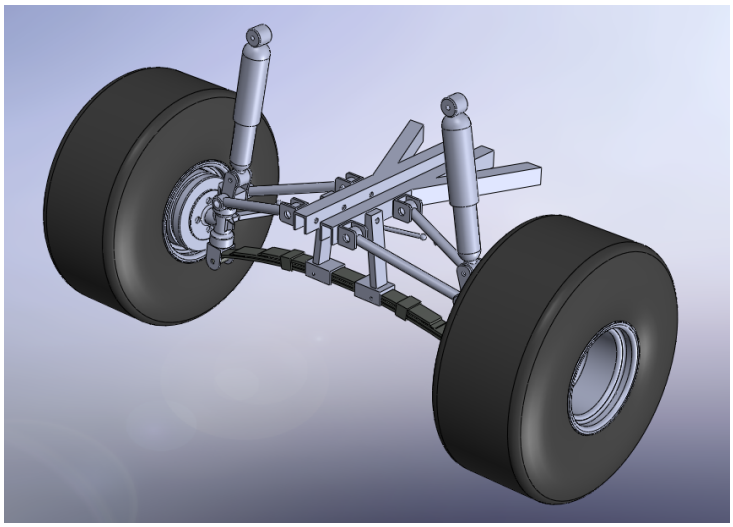

Figure 2.18: Front suspension and wheels

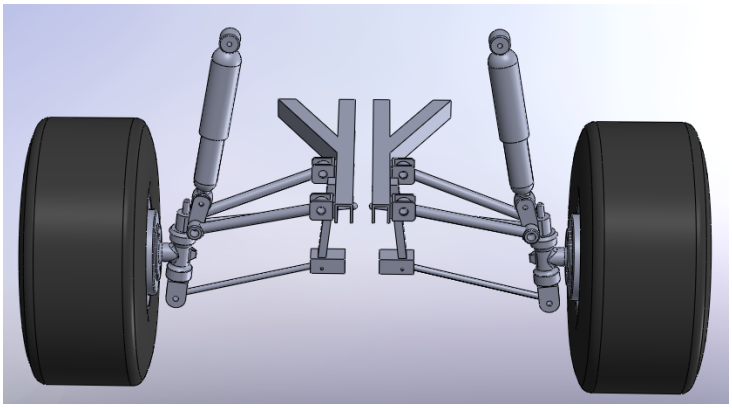

Figure 2.19: Front suspension and wheels

2.9.4 Final assembly

The group of chassis, front suspension, direction system and rear suspension has been mounted into a new assembly representing the whole car. It has been checked the total weight and derived the values of the moment of inertia along the three axes.

After a control of all the measurements repressing the car, the model has been exported from SLDASM into the Parasolid ".x_t" format.

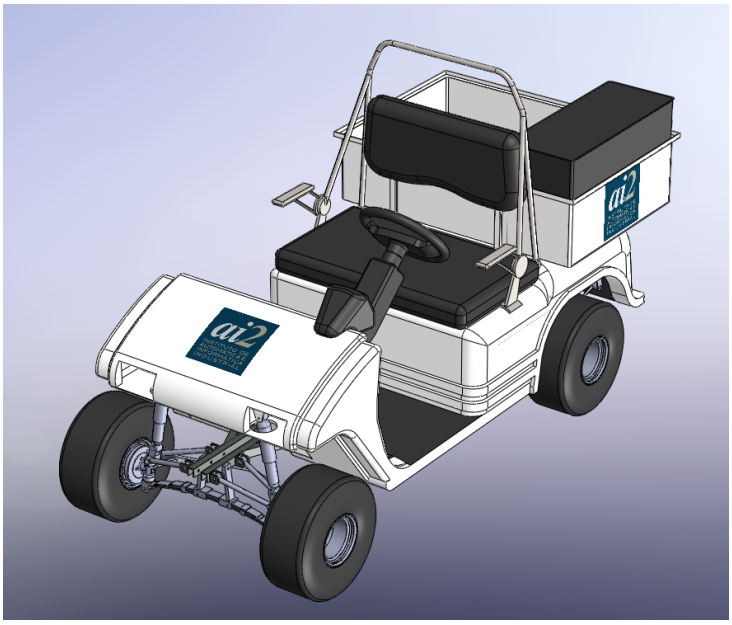

Figure 2.20: Virtual model in Solidworks front view

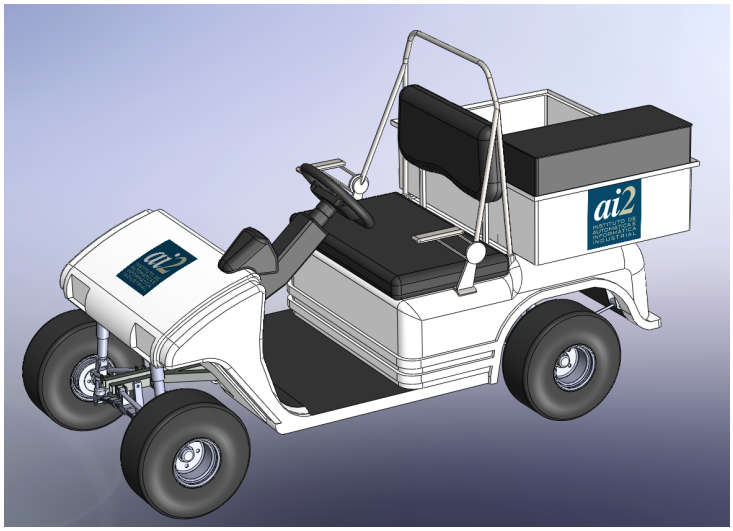

Figure 2.21: Virtual model in Solidworks side view

2.10 ADAMS/View

2.10.1 File import

By having the Parasolid ".x_t" model of the car it is possible to import the 3D model into ADAMS/View. The choice to import the model and not to build it directly in the software has been chosen to obtain a more realistic car model in terms of geometry and load distributions. ADAMS/View offers a design environment as well but, it takes a lot of time to draw the model and the possibility to create difficult geometries is limited. Once the 3D has been imported, it has been defined every material corresponding to the right part, in accordance with the 3D model. Then, it has been set the vehicle position in the space in accordance with the SAE definition. Finally, the acceleration of gravity has been set, always in accordance with SAE along the global $z - axis$.
The model needs to be reassembled with the proper constraints into ADAMS since the mating properties are not imported from Solidworks. The picture (2.22) shows the vehicle appearance after the importation from Solidworks.

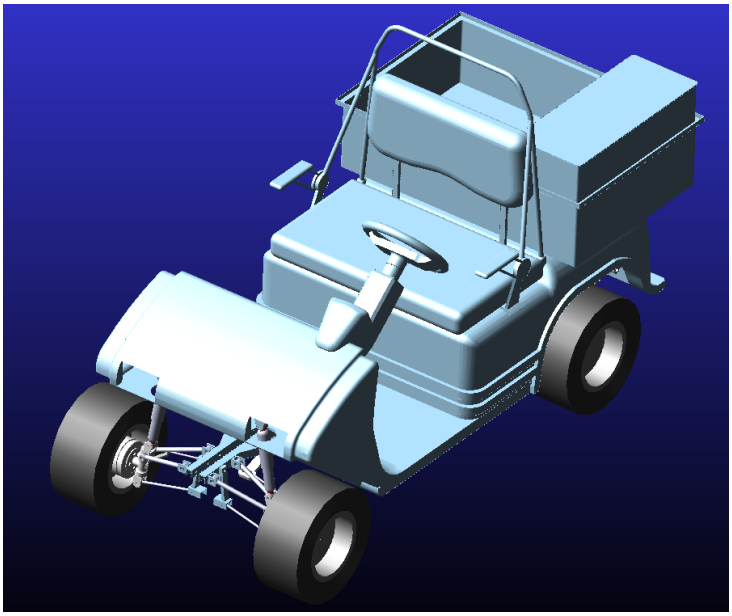

Figure 2.22: Assembled vehicle in ADAMS

2.10.2 Model Assembly

In order to apply the right constraints for the dynamic problem, it necessary to apply markers to define the kind of coupling. The markers have been put in every point of connection of the moving parts with the same direction of the global reference frame to easy manage the constraints application step.

Figure (2.23) shows the markers distribution on the car front-side.

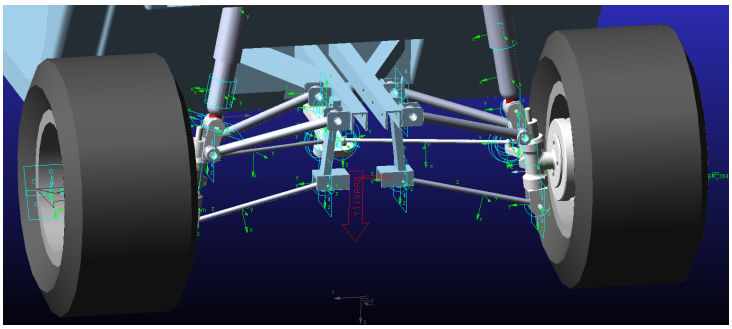

Figure 2.23: Front-side markers

Once all the markers have been applied, the joining have been applied to the elements to be connected.

Dampers

The relative motion between the upper and lower part of the dampers is modelled as a cylindrical joint which is a two degrees of freedom kinematic pair. The cylindrical joint provides a single axis sliding function as well as a single axis

rotation, providing a way for two rigid bodies to translate and rotate freely [31]. Figure (2.24) is an example of the assembly of the left front damper.

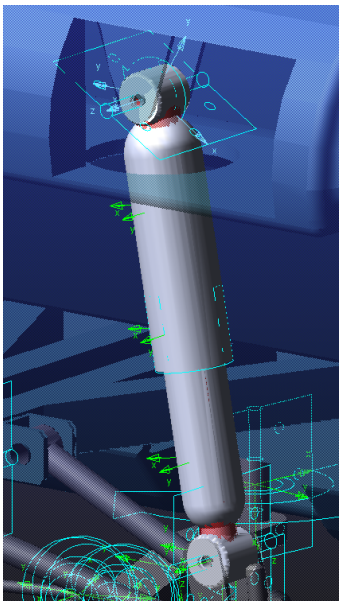

Figure 2.24: Damper assembly

Wheels

The four wheels are connected to the hub by means of revolute joint (2.25). The revolute joint is a one degree of freedom kinematic pair which provides a single axis rotation [32].

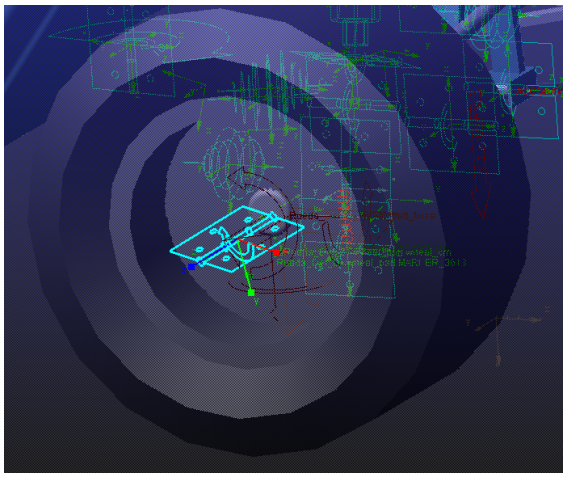

Figure 2.25: Wheel connection

Front upper arm

The front upper arm has been connected to the chassis and to the knuckle by means of a revolute joint [32].

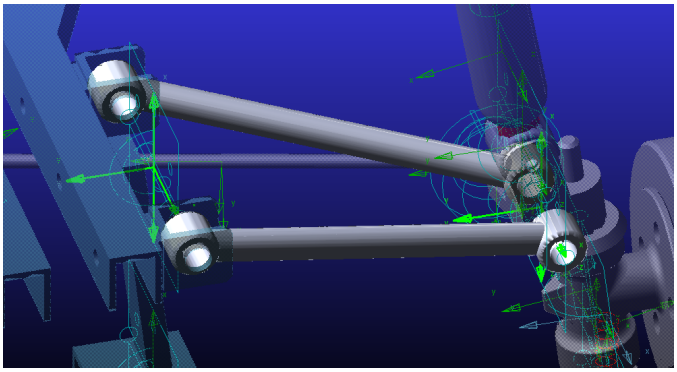

Figure 2.26: Upper arm

Front leaf spring

The front leaf spring has been connected as wheel by mean of two revolute joints for each rod, as shown in Figure (2.27).

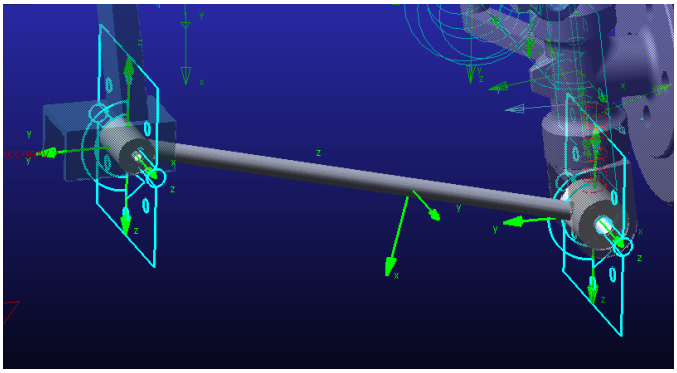

Figure 2.27: Front leaf connection

Direction system

The direction system is formed by a rotative actuator which provides the necessary rotation to define the vehicle direction. The motion is transferred to the wheels by means of a tie rod connected between the actuator and the knuckle, Figure (2.28). The extremities of the road are connected by means of two bushings which can be modelled into the model as a spherical joint. Each joint has three degrees of constraint as defined by the spherical joint [34].

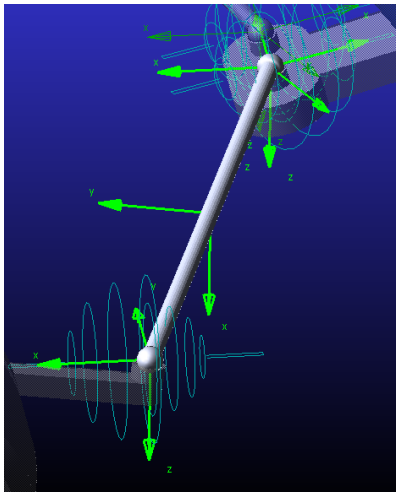

Figure 2.28: Direction system

Rear leaf spring

The rear leaf is connected by means of three revolute joint, two between the chassis and the suspension and one for the connection with the rigid axle, Figure (2.29).

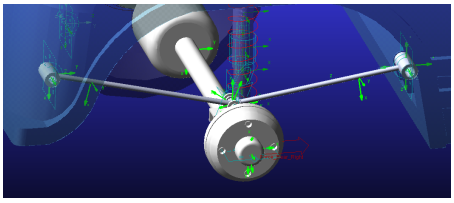

Figure 2.29: Rear suspension

Springs and dampers setting

After having assembled all the moving parts it is possible to set the stiffness and damping coefficients. the rear suspension has a damper and the spring equivalent to the leaf spring stiffens located in the same position, Figure (2.29).

The values of stiffens were previously calculated. These values are inserted into the program. The damping instead, was supposed to be equal to a certain value for the first calculation, its value was then improved and changed with a spline graph.

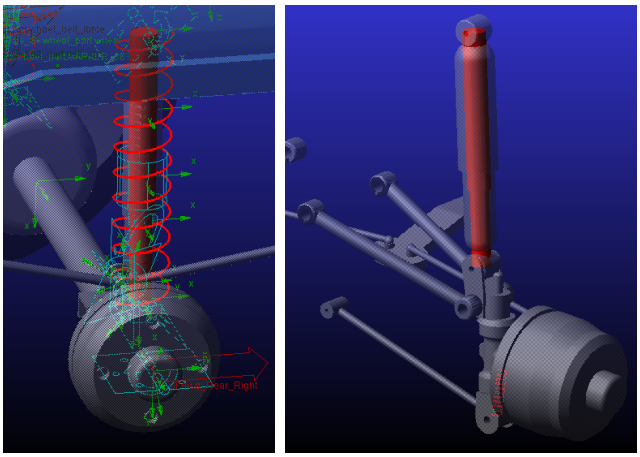

(a) Rear side **(b)** Front side

Figure 2.30: Front and rear suspension

2.10.3 Wheels and ground

The wheels have been inserted into the program by using the ADAMS/Tire add-on. The tire's property has been defined by using the so called "*Fiala's model*" [35].

The tires properties were previously taken by making practical experiments in order to obtain reasonable coefficients. While defining the tire properties, the program needs a definition of the road as well. The road has been defined from the ADAMS Database. The model selected is a conventional flat road with a given friction coefficient.

The ground has been set big enough to be able to perform all the trajectories required to be studied, Figure (2.31).

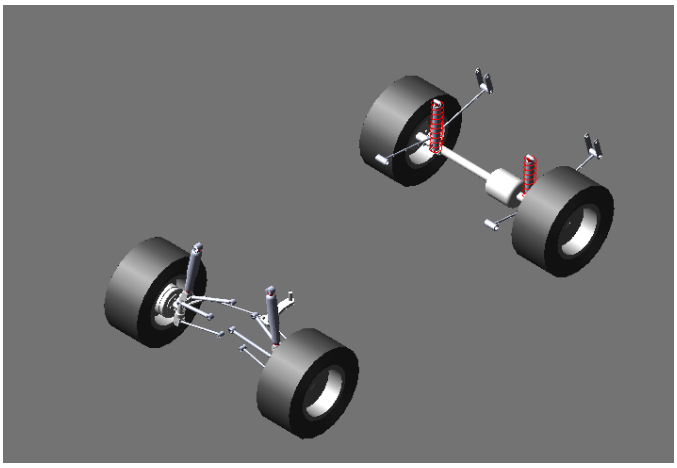

Figure 2.31: Wheels and ground

2.10.4 Stable position setting

Once the vehicle has been assembled it is necessary to verify if the height of the centre of gravity is respected. After the application of the constraints, the damping coefficient and the stiffness, the vehicle needs to be able to be stable without any force applied and stay in the same position in the space. The vertical load acting on each wheel needs to be checked, being equal to the measured one with the weight scale.

To do that, the model had been left free in the air, with a reasonable air gap and let it fall with the only effect of the acceleration of gravity, until the contact with the road. The height of center of mass and the load acting on each wheel are able to answer if the model can be able to correctly reproduce the reality in terms of loads on each wheel, suspension geometry and parameters.

The data obtained have been processed into Matlab. The results obtained are really close to the reality, exhibiting a good resemblance with the existing vehicle.

The height of the center of gravity was previously measured and resulted to be equal to $h = 500\ mm$.

The data obtained are shown in Figure (2.32). It is possible to notice a little variation of the height at the beginning due to the air-gap between the car and the ground. The model after a short settling time is able to maintain the stable position with the same features measured from the actual vehicle, implying that the suspension geometry measured, the stiffness value and the total load are coherent with the reality.

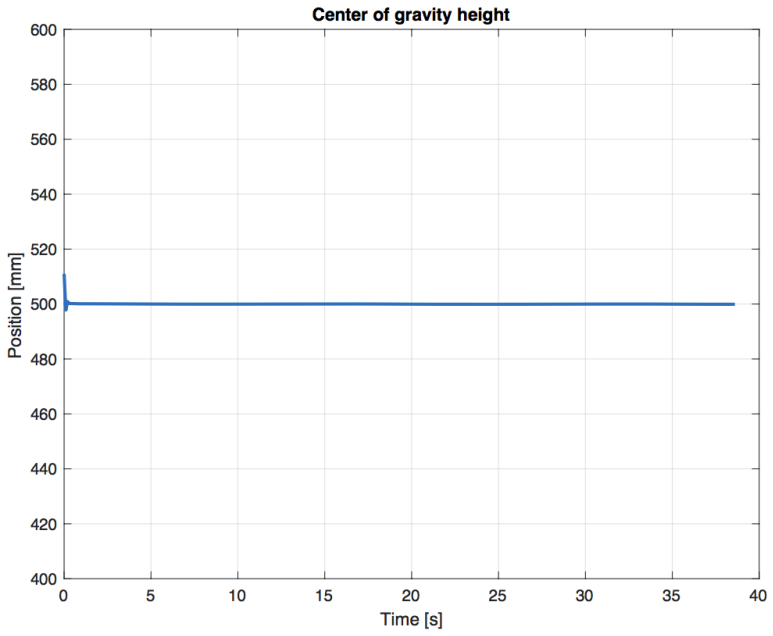

Figure 2.32: Center of gravity height

The load acting on each wheel needs to be equal to the measured one. The vertical force for the front and the rear wheel was equal to (2.8).

$$\begin{aligned} F_{Z_F} &= 1128\ N \\ F_{Z_R} &= 2256\ N \end{aligned} \tag{2.8}$$

while the front and rear distance from the center of gravity were respectively:

$$\begin{aligned} l_a &= 1100\ mm \\ l_b &= 550\ mm \end{aligned} \tag{2.9}$$

The vertical loads measured in ADAMS are shown in Figure (2.33). Here again, it is noticed a little variation of the loads at the origin of the graph. The reason is the impact of the tire with the road. After the transient, the vertical load acting on each tire holds a constant value, which is equal to the measured one. It is possible to state that the total load of the vehicle has been correctly distributed and the whole mass has been respected.

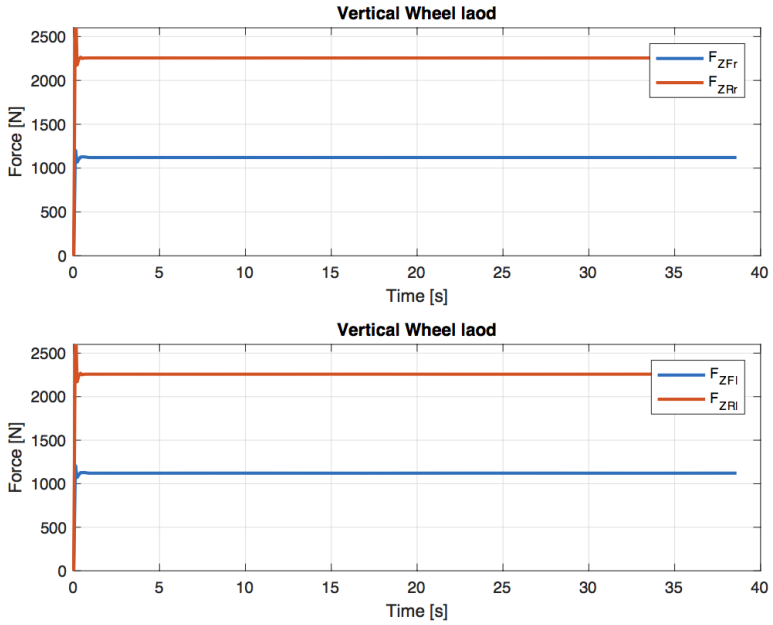

Figure 2.33: Vertical wheel load

Running the simulation, after some time, when the vehicle is completely settled and does not present any movement, a new configuration has been done. The new layout is saved and it is the starting point for all the further simulations. Figure (2.34) shows the stabilized configuration.

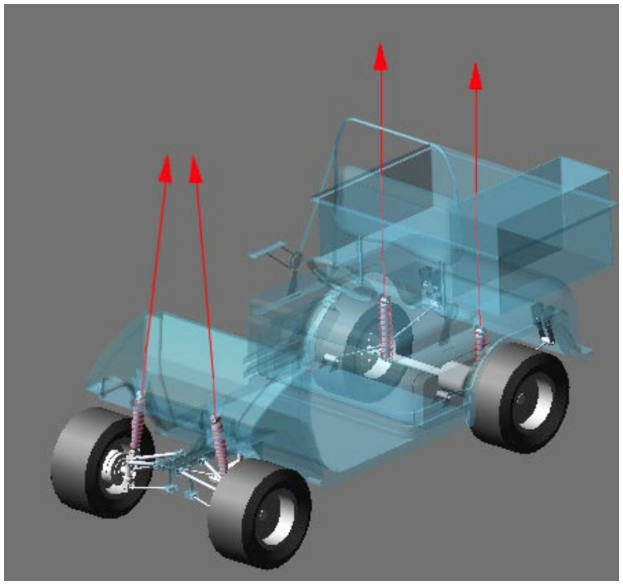

Figure 2.34: Stable configuration

2.10.5 Tire cornering stiffness

This section deals about the definition of the cornering stiffens of the tires mounted on the vehicle.

This is one of the most important parameters which define the dynamics of the vehicle. The producer doesn't give any information about the tire properties, the only information was known is the size. It should be necessary to test the tire parameters by using an appropriate test machine [19].

Due to the impossibility to perform this test, the vehicle has been tested in a circular path with a fixed radius of $4,40\ m$. The radius is quite small due to the impossibility to find a bigger area inside the university.

The vehicle is tested with the automatic mode, with the help of "ai2 [4]" technicians. Fixing steering angle and velocity with a remote control, the trajectory travelled is evaluated. Due to the tire deformation, the trajectory is not perfectly circular, even if the steering angle and velocity are fixed. This is due to the presence of the lateral slip of each tire.

The data obtained are shown in Table (2.12).

Table 2.12: Slip angle test data

Radius	[m]	4,4
Speed	[m/s]	5,28
Deviation	[m]	0,014

Figure 2.35: Circular path

The trajectory is obtained by making the vehicle accelerate from zero speed until the target speed, during a time of 2 seconds. During the acceleration the steering angle is passed gradually from zero to the steering angle. The set angle is able to make the vehicle perform a radius of $4,4$ m. The steering angle is represented in Figure (2.36) as a function of time, for the inner and outer wheel.

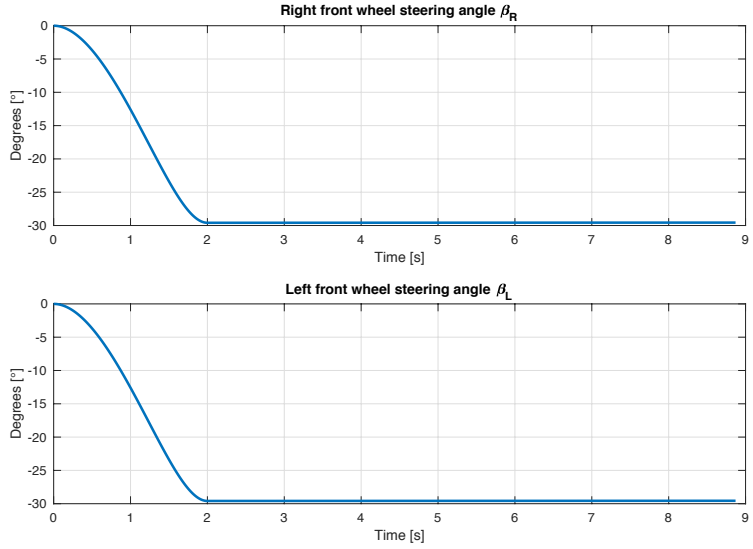

Figure 2.36: Front wheels street angle

The deviation of the vehicle after having run a circular trajectory is measured, the intention is to reproduce the same behaviour in ADAMS by changing the tire cornering stiffness. The test is done iterating many values of cornering stiffness. Once the values of deviation from the ideal trajectory equal the test path, the current value of cornering stiffness is achieved.

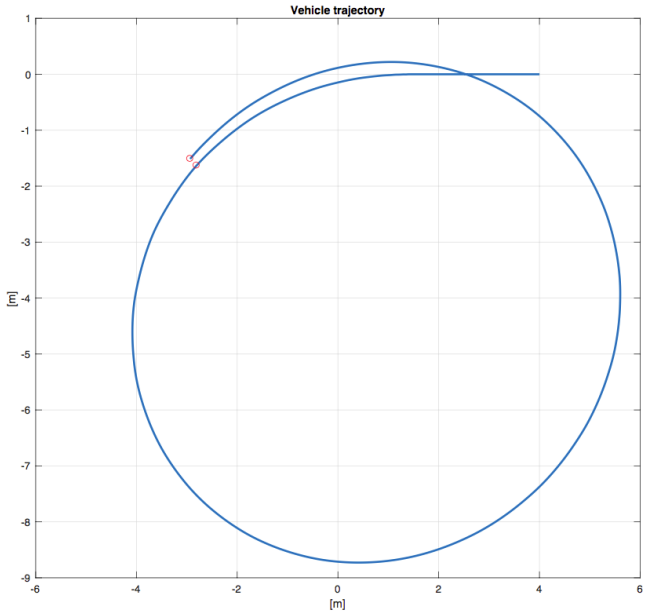

Figure 2.37: Straight line lateral forces

After many attempts in ADAMS the trajectory results to be equal to the real one, as shown in Figure (2.37). The red dots represent the point in which the steering angle is equal to the fixed value and the velocity is constant, in that point it is measured the deviation in the path, which is equal to $0,014\ m$ like in the practical case.

Chapter 3

Direct dynamics simulations

3.1 Introduction

In this chapter it is shown the procedure followed to perform the vehicle direct dynamics. At the beginning, it is defined which forces are applied to simulate the vehicle motion. Then, in order to verify the goodness of the model, it is checked the ability of the car to follow a rectilinear path with a null steering angle. The first interesting analysis consists of the analysis of circular trajectories. The test is done at different velocities and curvature radius in order to obtain data and information to study the vehicle behaviour. The results will be then compared to the data obtained from an inverse dynamics problem, shown in the following chapter. After having analysed a series of circular paths, the vehicle is tested for the so-called "Moose test", following the standard ISO procedure.

3.2 Forces and motions

3.2.1 Traction and braking

The vehicle is moved by means of a torque provided by an electric motor on both the rear wheels. To do that, a torque has been applied to the rear for both the wheels. At the beginning, the torque is applied using an Haversine step function [3]. The Haversine allows the vehicle to accelerate until to the desired target speed with a smooth variation. A speed control is implemented into the program to maintain the vehicle at a constant speed.

The brakes are designed as a torque applied to each wheel, with opposite direction with respect to the traction torque. The torque is defined with the program function builder.

3.2.2 Steering

The steering is controlled by a rotational joint motion in which a given displacement is applied through a function of time. In the same way, as done for the traction and braking, it has been used an Haversine function to reach a certain

level of steering, being able to run a circular trajectory. To test any other kind of trajectory, it has been implemented a spline function into a Matlab script and imported then into the motion function in ADAMS as a vector.

3.3 Measures

After having set forces and torques able to move and guide the vehicle, a list of functions has been implemented in order to evaluate all the necessary informations for the study of the model.

The data measured during the simulation are listed:

- Center of gravity height h, measured as the distance from the ground to the marker relative to the center of mass in case of unloaded vehicle
- Yaw rotation σ, rotation about the $z - axis$ of the vehicle
- Angular velocity $\dot{\sigma}$, angular speed about the $z - axis$ of the vehicle
- Angular acceleration $\ddot{\sigma}$, angular acceleration about the $z - axis$ of the vehicle
- Angular velocity of the wheels ω
- Absolute velocity of the vehicle V, velocity of the center of mass
- Longitudinal and lateral velocity of the center of mass, V_x and V_y
- Longitudinal, lateral and vertical force of each wheel, F_x, F_y and F_z, forces exchanged between the ground and the tire during the contact
- Steer angle of the front wheel δ, defined as the angle of direction of the left and right front wheel
- Vehicle sideslip β, defined as the angle formed between the longitudinal V_x and the lateral speed V_y of the vehicle, measured in the center of mass position as $\beta = atan(V_y/V_x)$
- Tire sideslip α, measured for each wheel and defined as the angle formed between the longitudinal V_x and the lateral speed V_y of each tire, $\alpha = atan(V_y/V_x)$

3.4 General test conditions

The test have been done up to the maximum target speed of the car which is 32 km/h.

Every test has been done with a fixed coefficients for dry asphalt. The data which have been used are listed in Table (3.1)

Table 3.1: Road friction coefficients

Static (Dry asphalt)	0,9
Dynamic (Dry asphalt)	0,75

3.5 Straight line test

After the definition of all the forces acting on the vehicle and the necessary measurements, a first test is performed. It consists of a simple test on a straight path. The objective is to verify if the results are coherent with the reality. The lateral forces acting on the vehicle are really close to a null value due to the null sideslip velocity. The only influence on the tire lateral forces should be the effect of camber and toe angle.

The test have been done with the following parameters:

- Steering angle: $0°$
- Velocity: $v = 6,6\ m/s\ \simeq\ 24\ km/h$
- Acceleration: $1\ m/s^2$

The initial velocity is null, after an initial acceleration the vehicle is maintained at a constant speed, as shown in Figure (3.1).

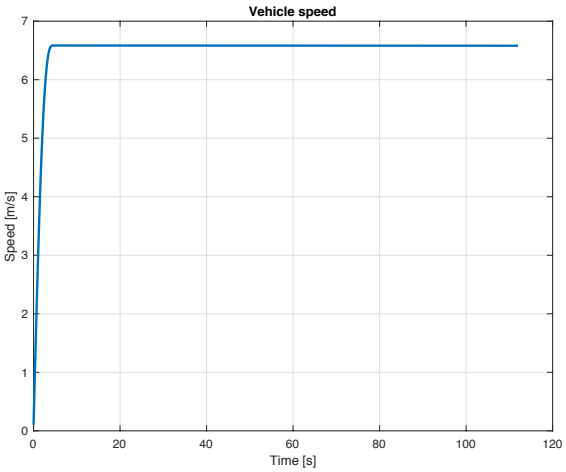

Figure 3.1: Straight line speed

Figure (3.2) shows the path followed by the center of mass of the car, which is a linear trajectory as expected.

The magnitude of the lateral forces is shown in Figure (3.3). They are almost null as expected, due to the absence of lateral slip.

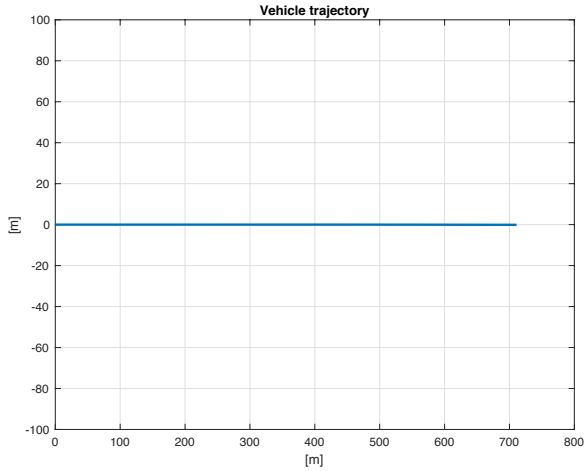

Figure 3.2: Straight line path

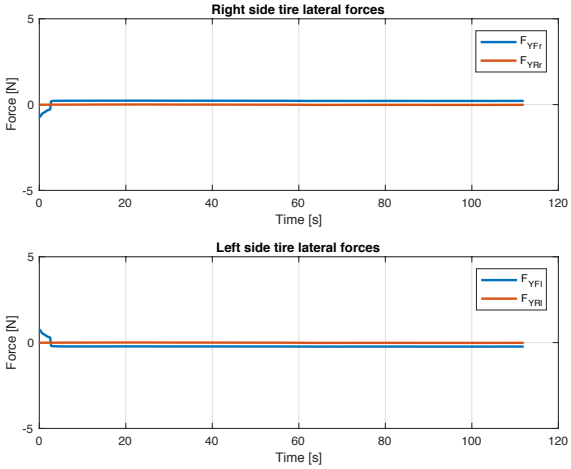

Figure 3.3: Lateral forces

It is noticed a really small lateral force ($\simeq \pm 0,2\ N$) for the front wheels. The presence is due to the camber/toe angle of the wheels. This force does not cause any despair since the two forces has different sign and they delete each other.

3.6 Skid past tests

3.6.1 Introduction

To study the cornering performance of the vehicle, a series of skid pad tests were conducted. A skid pad, is a test where the vehicle travel around on a circular track. The objective is to obtain how much the vehicle will sway or, how high velocity it can manage before turning over or skidding out the radius [20].

These tests have been conducted with the empty vehicle since, as already assumed, the study was done on a vehicle which is driving automatically, without any person onboard.

The skid past test has been performed with the guidance of the ISO 4138 : 1982 from the TC 22/SC 9 Road vehicles [14], which is a Steady-State Circular Test Procedure. According to ISO 4138 the standard skid pas is 40 m.

To get more perspective and to compare with the practical test, additional experiments were conducted with smaller radius and variable velocities.

3.6.2 Left turn, constant radius

The first skid pad test was based on the ISO standard test. The radius is set equal to 40 m, the steering angle that satisfies the radius can be calculated with equation number (3.1), which is the Ackerman angle equation [21]. This is a value for a perfect geometry of steer, it is necessary to check if the vehicle respects the Ackermann condition. In case the geometry does not respect the Ackermann condition, testing different angles of steer, the right angle to perform a given radius is found out. It has to be taken into account as well, that an higher speed provoke a bigger radius turn.

$$\delta = \left(\frac{l}{r}\right) = \left(\frac{1,650}{40}\right) = 0,04125\ rad \cong 2,4^{\circ} \tag{3.1}$$

The maximum velocity is set equal to 32 km/h since it is the maximum speed that the vehicle can have.

Test 1

The test parameters for the first analysis are listed,

- Steering angle: $\delta = 0,046\ rad \cong 2,64^{\circ}$
- Velocity: $v = 8,88\ m/s = 32\ km/h$

The absolute speed of the vehicle is shown in Figure (3.7). The vehicle starts from zero velocity, after an initial acceleration the vehicle raise the target speed and it goes into the curve. The steering system thanks to the Haversine function [3], changes gradually the direction of the two wheels, starting from zero to the angle

required to make the curve with the desired radius.

The trajectory followed by the vehicle is reported in Figure (3.4). The steering is able to make the vehicle perform a 40 m radius, Figure (3.5).

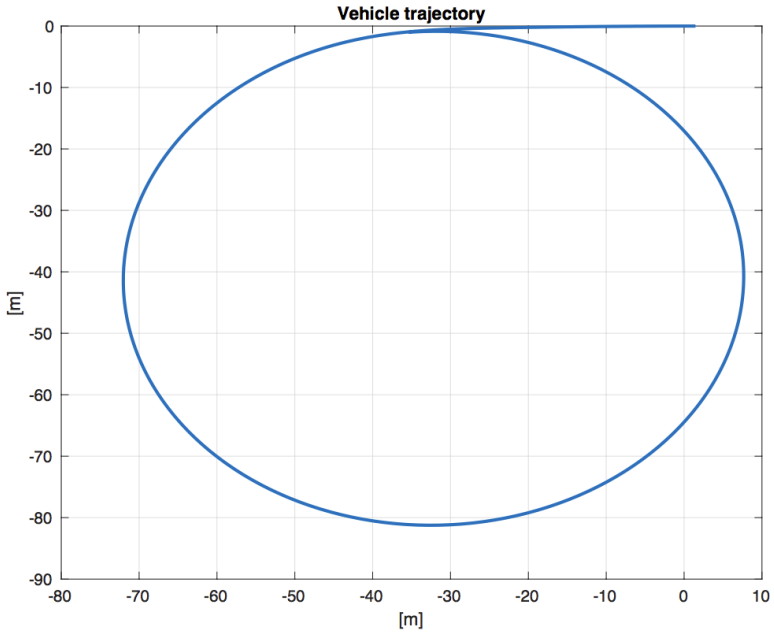

Figure 3.4: Circular path r=40m v=8,88 m/s

Figure (3.8) shows the vertical load acting on each tire. Due to the centrifugal force, the external wheels results to be more loaded. For this specific case, a left turn cause an increase of the vertical load on the right side tires.

The slip angles and the lateral forces acting on the vehicle are represented respectively in Figure (3.9) and Figure (3.10).

The inner wheel of the front axle due to the low vertical load which is acting on the tire and to the low slip angle, generates a really low lateral force. This effect is higher as far as the speed increases and as far as the radius of curvature is diminished.

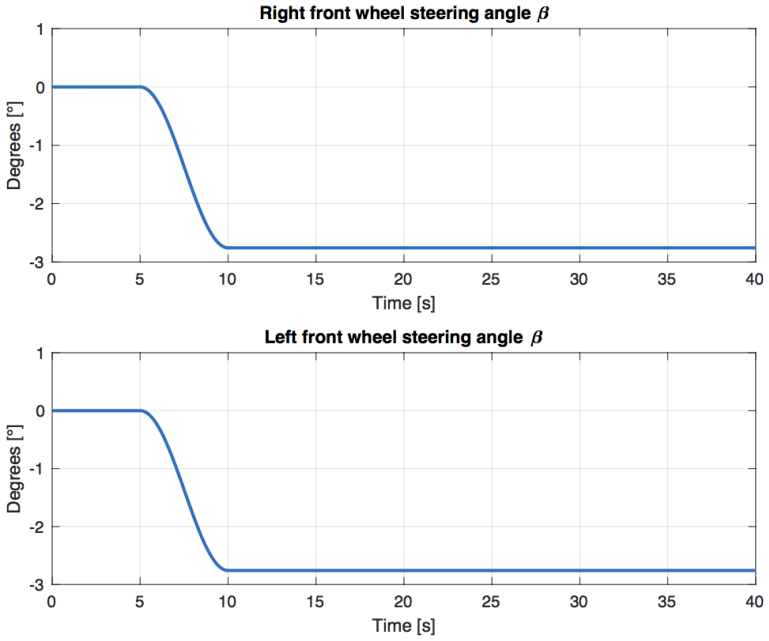

Figure 3.5: Wheels steering angle r=40m v=8,88 m/s

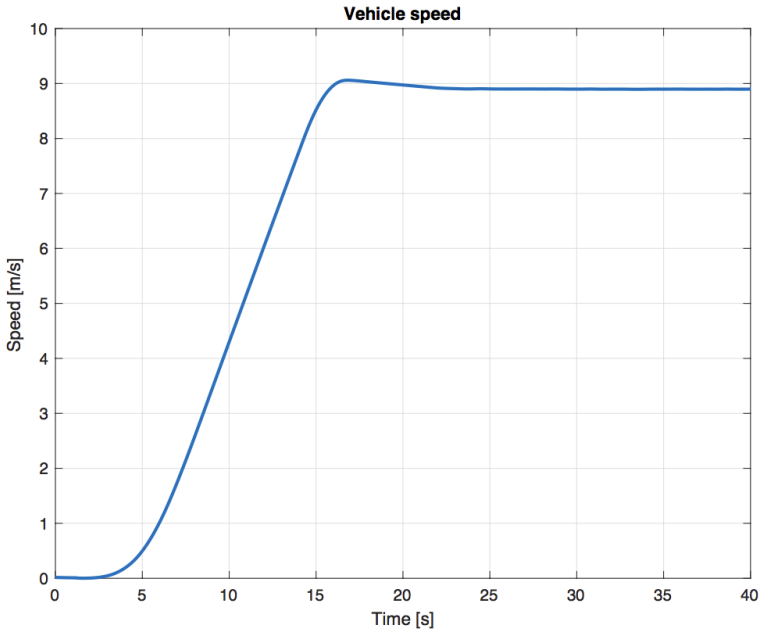

Figure 3.6: Speed profile

Figure 3.7: Overall vehicle speed r=40m v=8,88 m/s

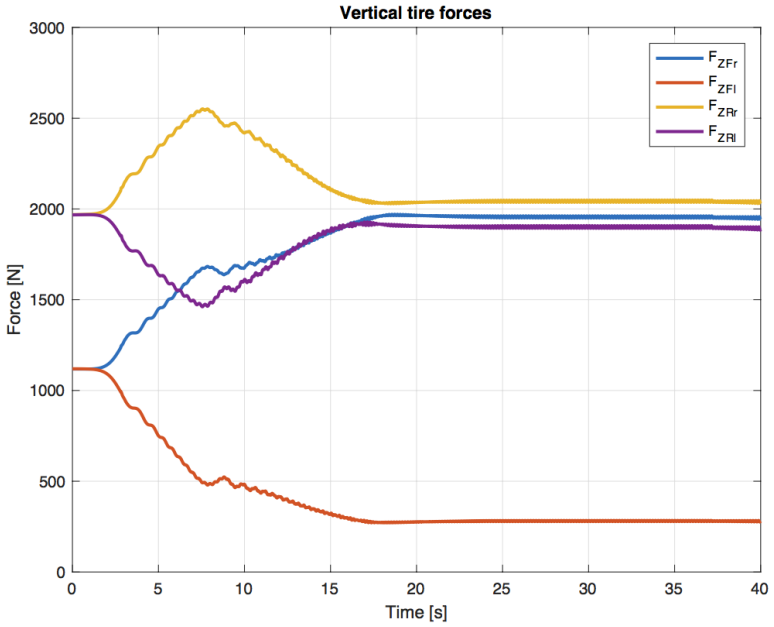

Figure 3.8: Vertical Forces r=40m v=8,88 m/s

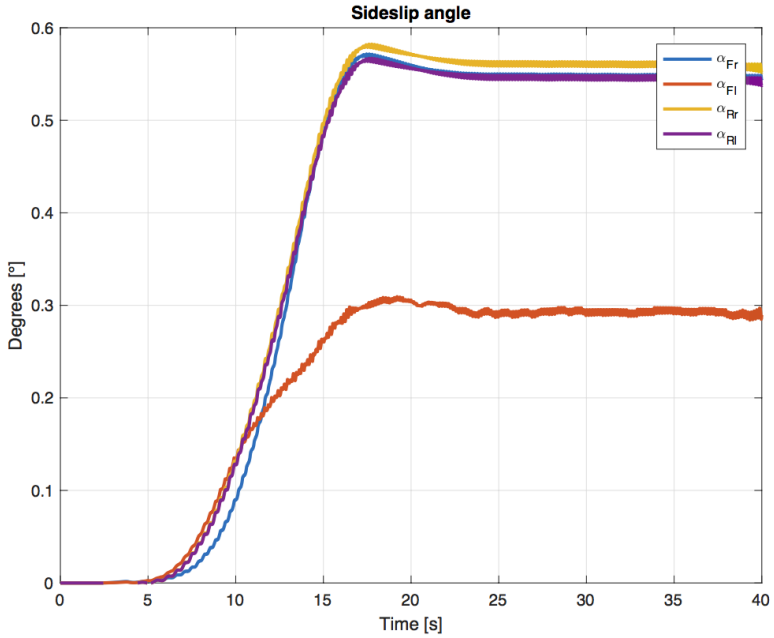

Figure 3.9: Slip angle r=40 m v=8,88 m/s

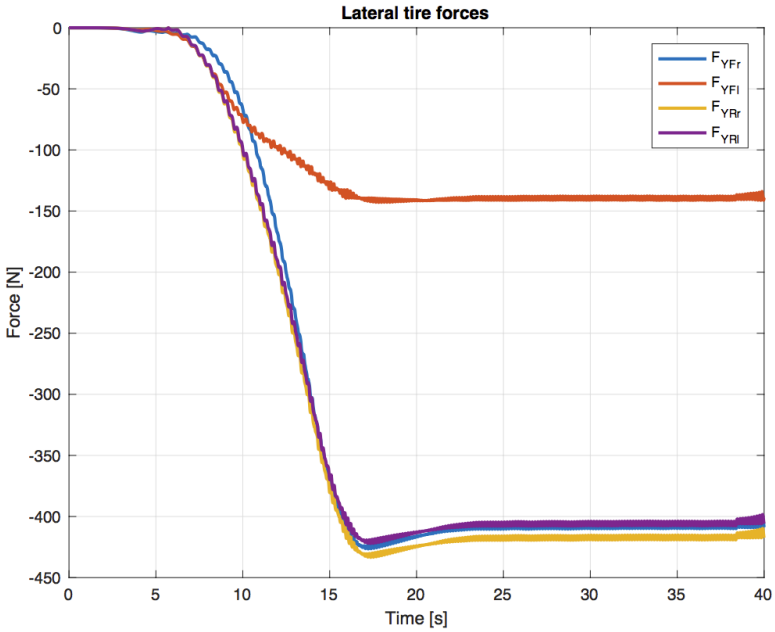

Figure 3.10: Lateral forces r=40 m v=8,88 m/s

Test 2

- Steering angle: $\delta = 0,044\ rad \simeq 2,55°$
- Velocity: $v = 5,28\ m/s = 19\ km/h$

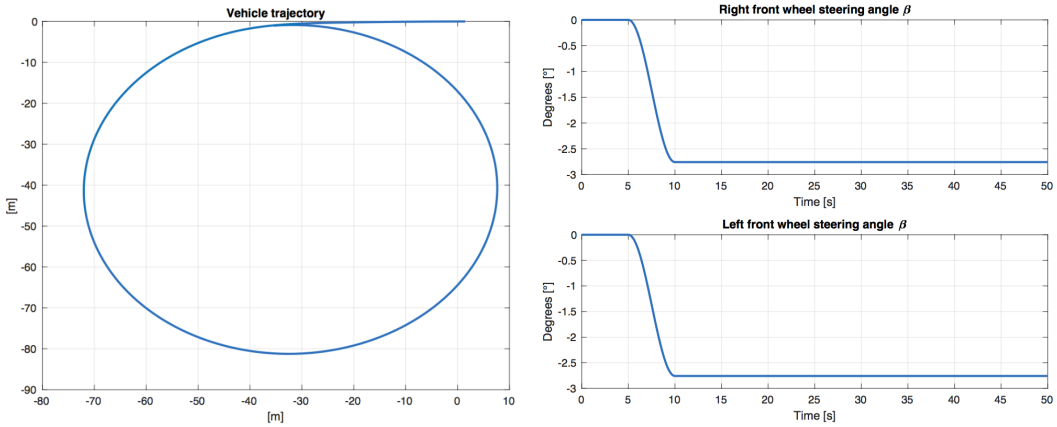

(a) Circular profile **(b)** Direction angles

Figure 3.11: Test condition r=40 m v=5,28 m/s

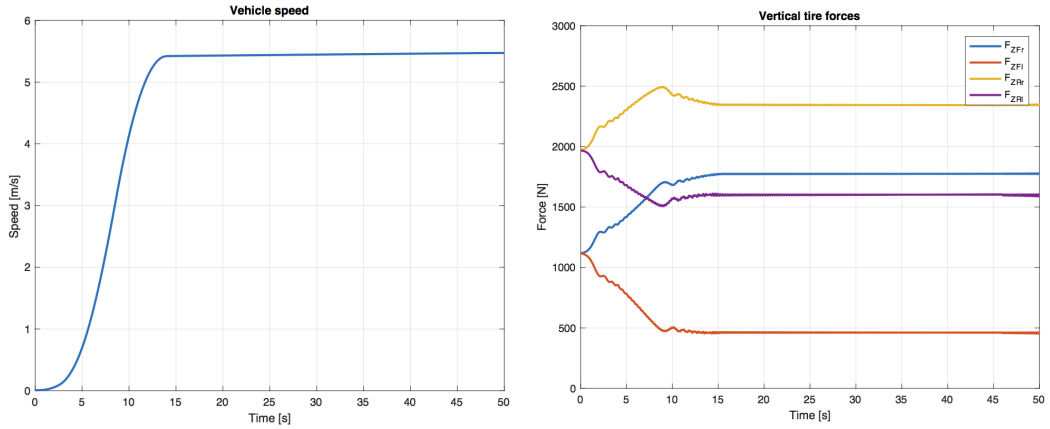

(a) Vehicle speed **(b)** Vertical forces

Figure 3.12: Test condition r=40 m v=5,28 m/s

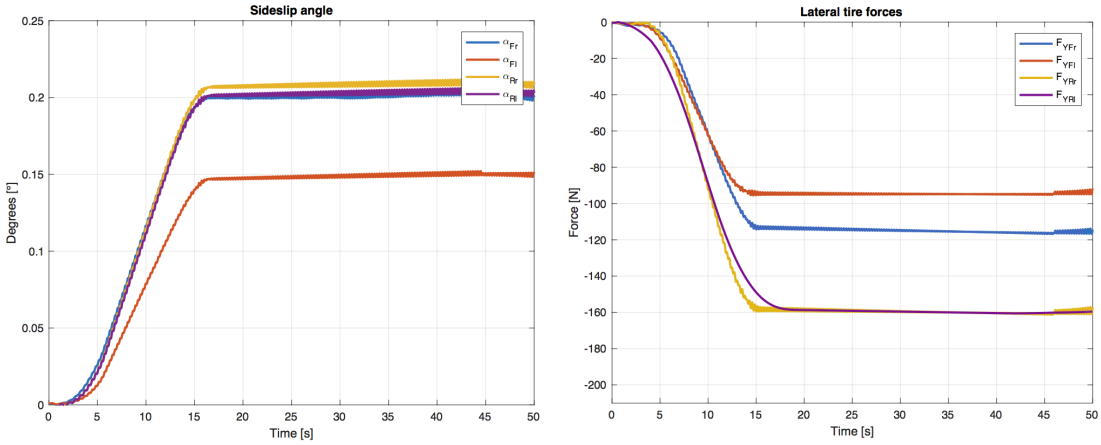

(a) Sideslip angles **(b)** Lateral forces

Figure 3.13: Test condition r=40 m v=5,28 m/s

Test 3

- Steering angle: $\delta = 0,046\ rad \simeq 2,63°$
- Velocity: $v = 2,22\ m/s = 8\ km/h$

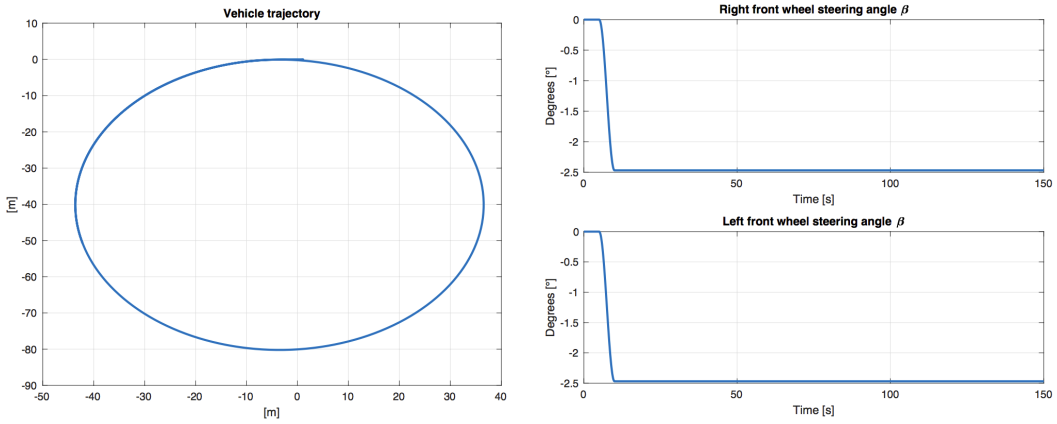

(a) Circular profile **(b)** Direction angles

Figure 3.14: Test condition r=40 m v=2,22 m/s

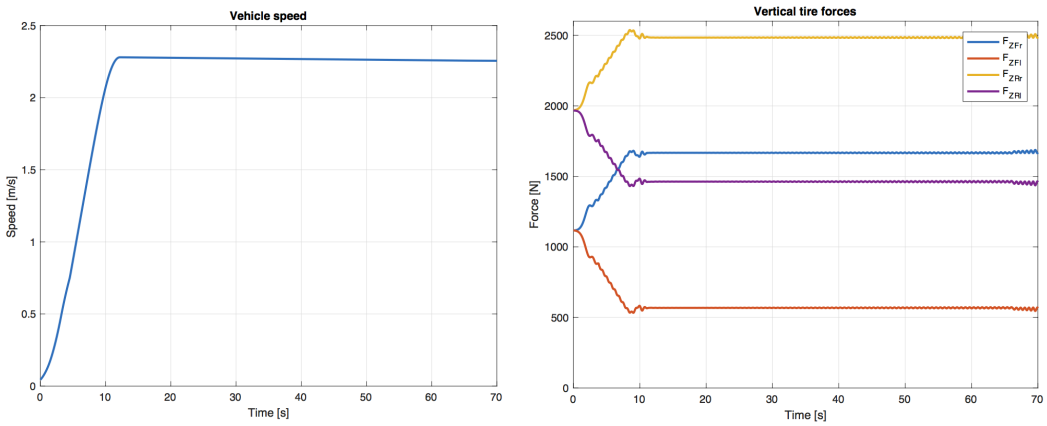

(a) Vehicle speed **(b)** Vertical forces

Figure 3.15: Test condition r=40 m v=2,22 m/s

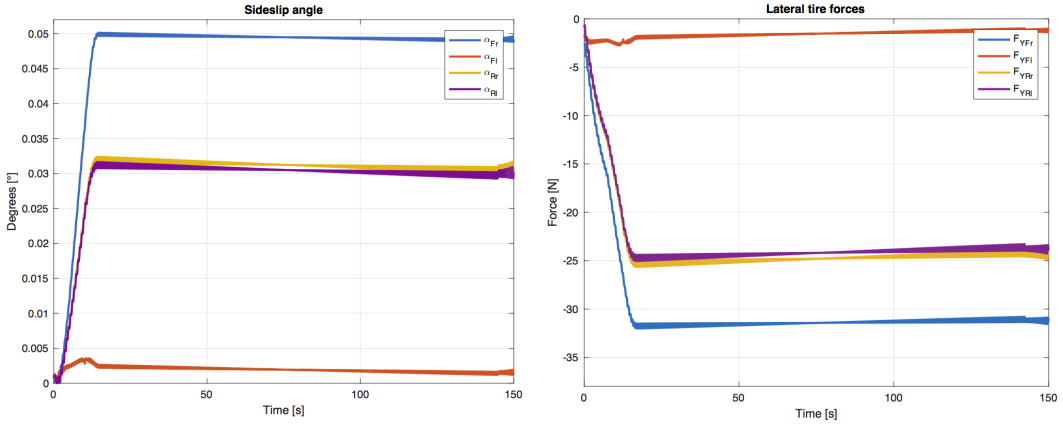

(a) Sideslip angles **(b)** Lateral forces

Figure 3.16: Test condition r=40 m v=2,22 m/s

3.6.3 Left turn, constant speed

10 m radius

- Steering angle: $\delta = 0,1855\ rad \simeq 10,63°$
- Velocity: $v = 5\ m/s = 18\ km/h$

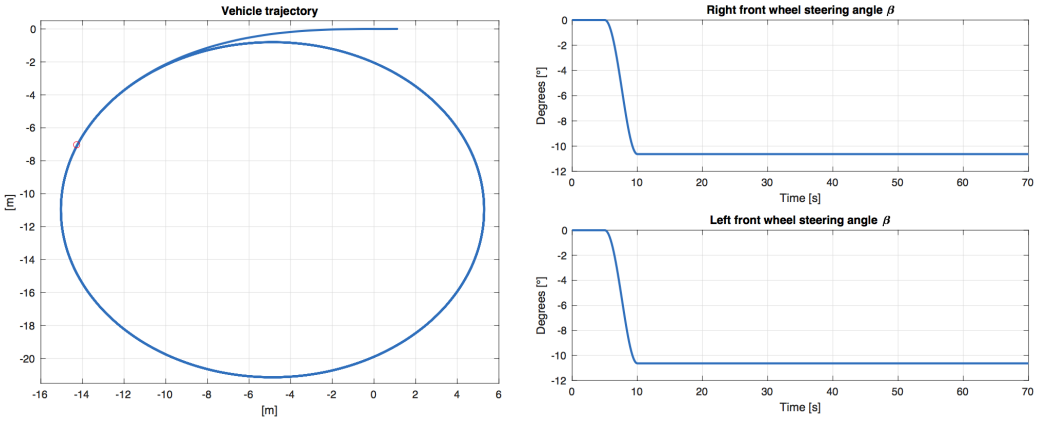

(a) Circular profile **(b)** Direction angles

Figure 3.17: Test condition r=10 m v=5 m/s

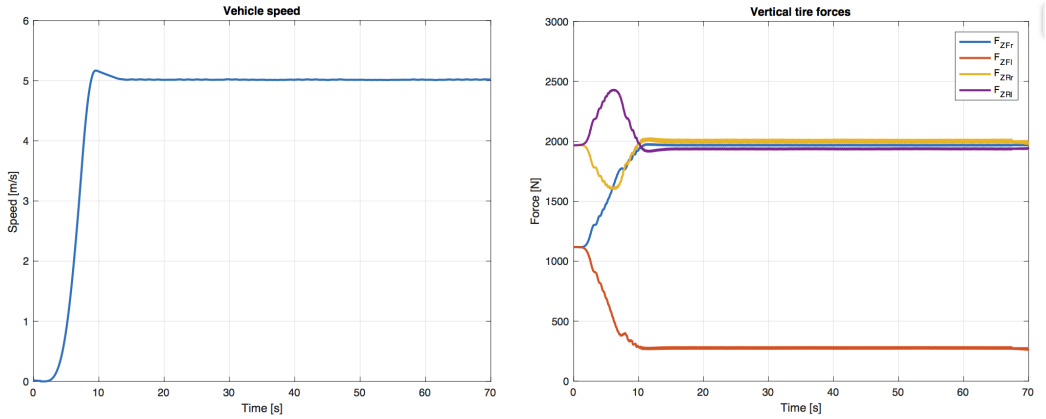

(a) Vehicle speed **(b)** Vertical forces

Figure 3.18: Test condition r=10 m v=5 m/s

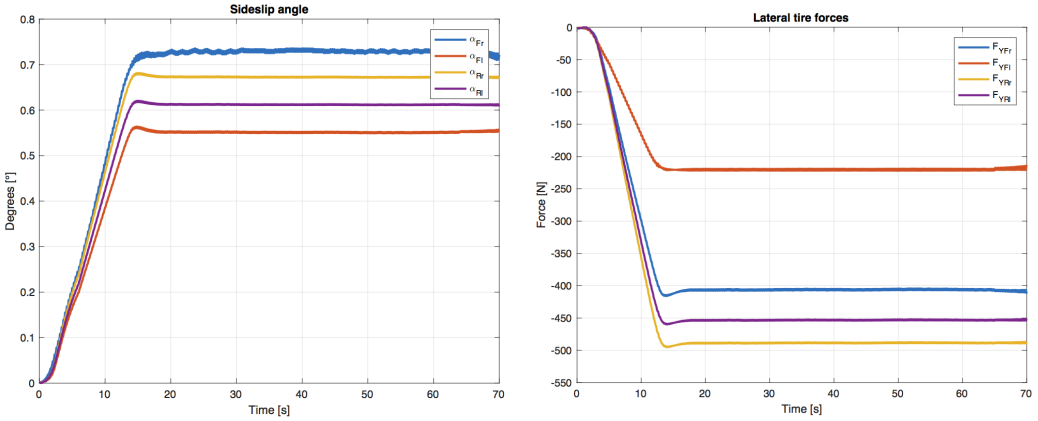

(a) Sideslip angles **(b)** Lateral forces

Figure 3.19: Test condition r=10 m v=5 m/s

8 m radius

- Steering angle: $\delta = 0,255\ rad \simeq 14,63°$
- Velocity: $v = 5\ m/s = 18\ km/h$

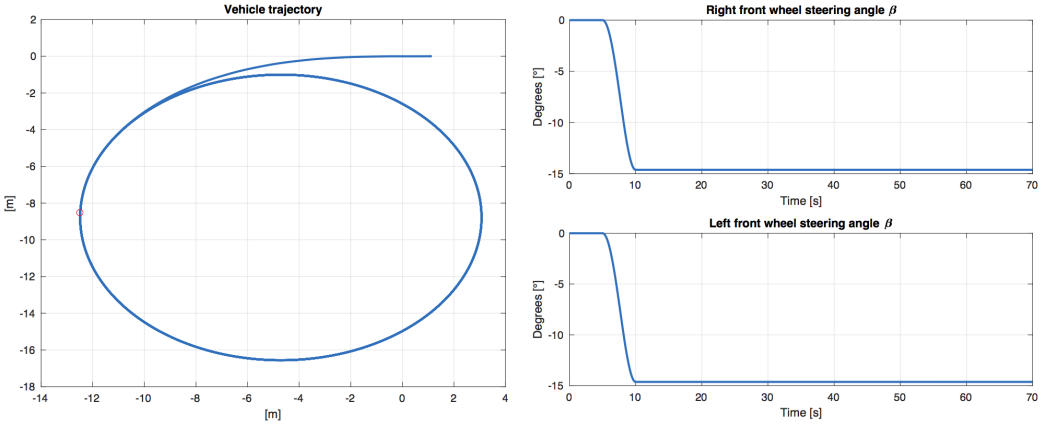

(a) Circular profile **(b)** Direction angles

Figure 3.20: Test condition r=8 m v=5 m/s

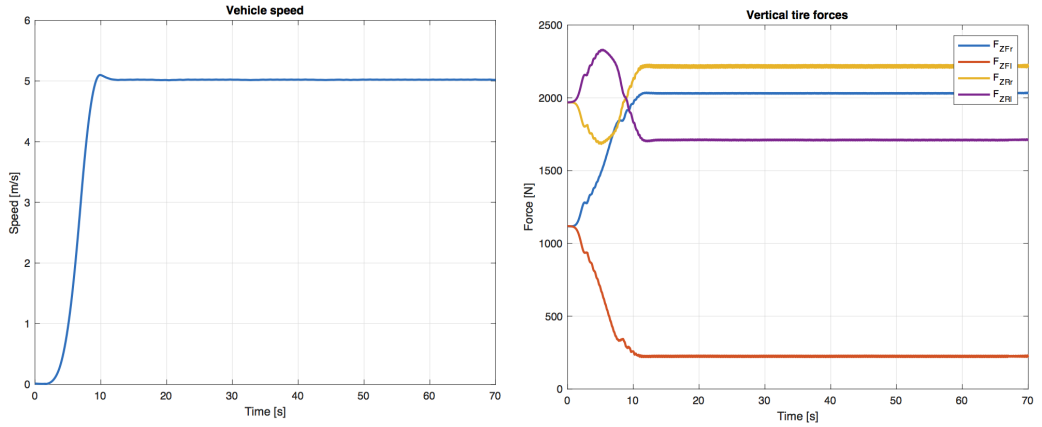

(a) Vehicle speed **(b)** Vertical forces

Figure 3.21: Test condition r=8 m v=5 m/s

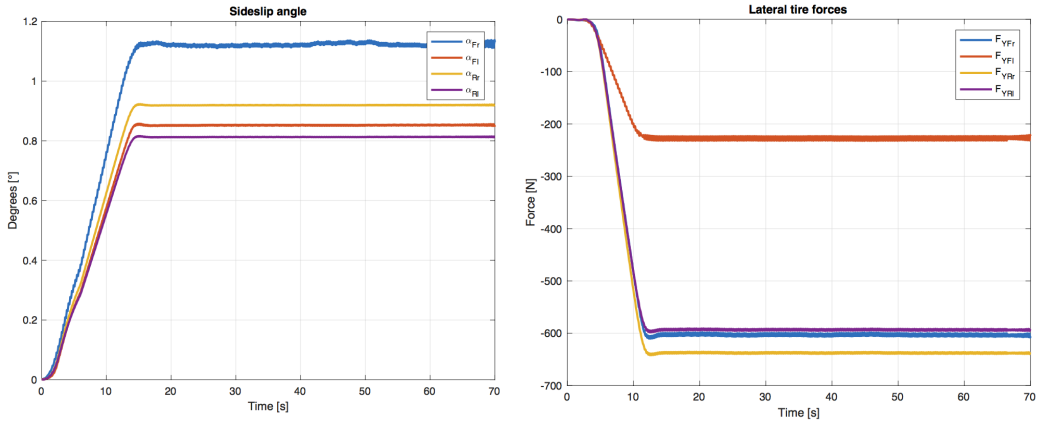

(a) Sideslip angles **(b)** Lateral forces

Figure 3.22: Test condition r=8 m v=5 m/s

7 m radius

- Steering angle: $\delta = 0,331\ rad \simeq 18,98°$
- Velocity: $v = 5\ m/s = 18\ km/h$

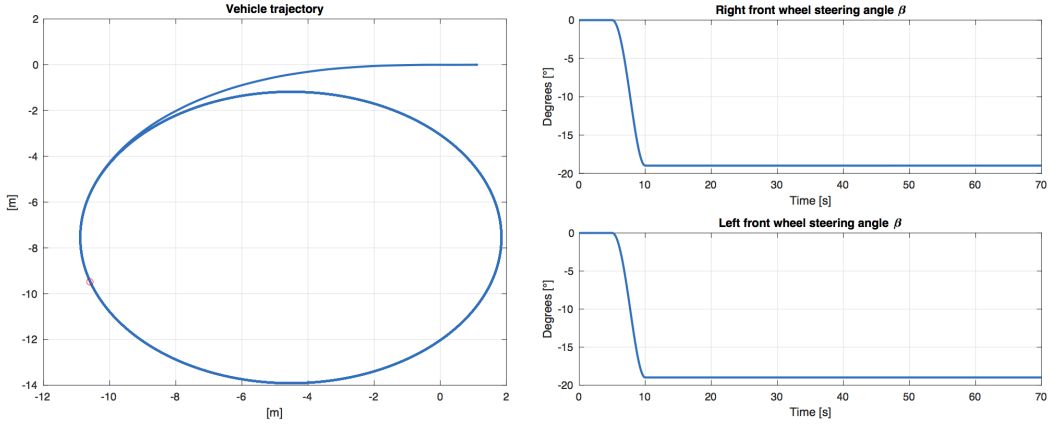

(a) Circular profile **(b)** Direction angles

Figure 3.23: Test condition r=7 m v=5 m/s

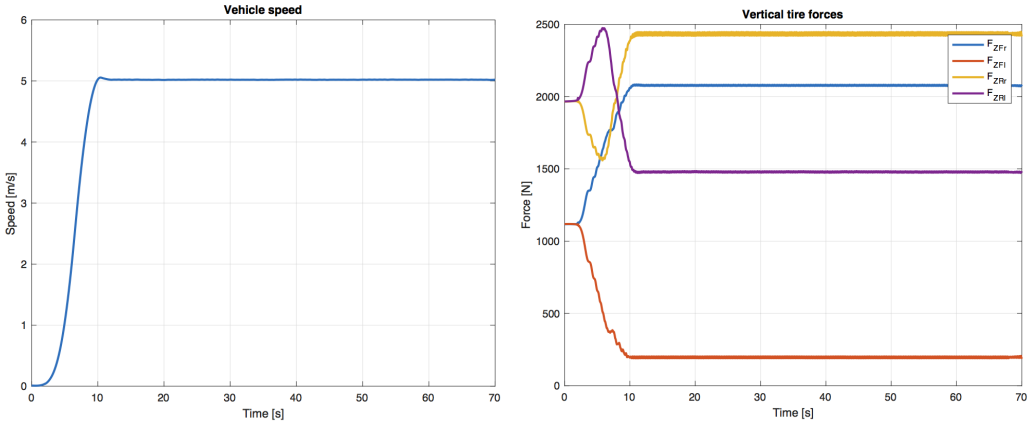

(a) Vehicle speed **(b)** Vertical forces

Figure 3.24: Test condition r=7 m v=5 m/s

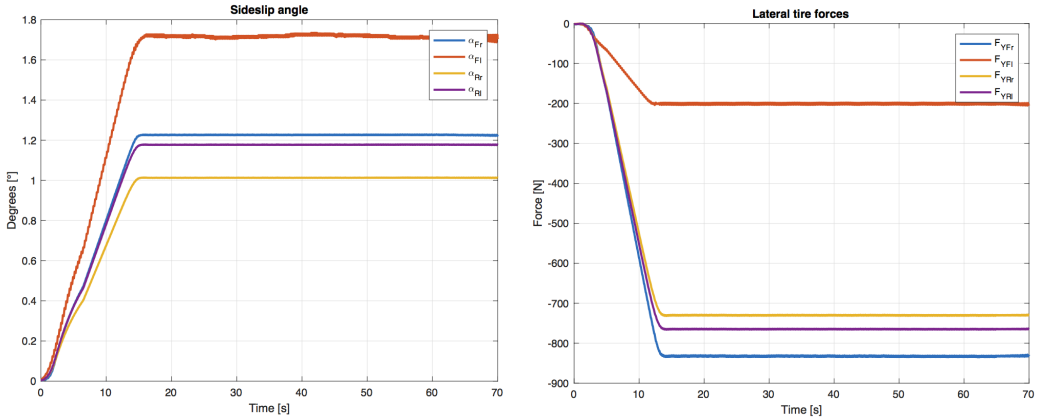

(a) Sideslip angles **(b)** Lateral forces

Figure 3.25: Test condition r=7 m v=5 m/s

3.7 Moose test

3.7.1 Introduction

The Moose test consists of a lane change manoeuvre. It is described by the international standard $ISO\ 3888-2$ [13], after a revision by the Association of German Automotive Industry (VDA) [9]. The moose test is used to evaluate the handling performance of a vehicle. There is a path to follow, which is described by three cones lanes, with a total length of 61 meters, where a double lane change is defined. The path needs to be performed at the vehicle maximum speed.

3.7.2 Test procedure

With reference to the normative, the track dimensions for the Moose test are defined in the Table (3.2).

Table 3.2: Moose test track dimensions

Section	Length of section	Section width
1	15,0 m	1,1 x vehicle width + 0,25 m
2	30,0 m	
3	25,0 m	1,2 x vehicle width + 0,25 m
4	25,0 m	
5	15,0 m	1,3 x vehicle width + 0,25 m

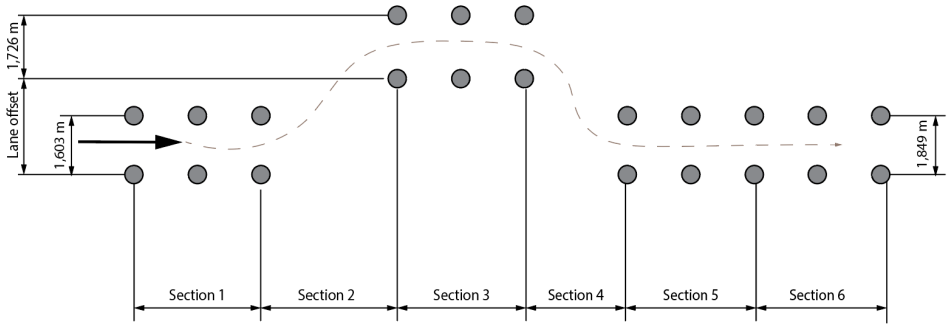

Figure 3.26: Moose test path

The vehicle width is measured as the width without considering the side mirrors. In this specific case, the width is equal to $1,230\ m$ and so, the section width results:

- $section1 = 1,1 \cdot 1,230 + 0,25 = 1,603\ m$
- $section2 = 1,2 \cdot 1,230 + 0,25 = 1,726\ m$
- $section3 = 1,3 \cdot 1,230 + 0,25 = 1,849\ m$

The time measurement starts in the entry line and it is stopped at the exit line of the cones.

After the entrance in the cones, the accelerator pedal is released and so the vehicle is moved only by its own inertia. The fact of the pedal release is due to the typical behaviour of the driver when is facing with an obstacle. The test is passed if no cones are hit.

The test starts with an initial speed of 60 km/h. The test is repeated many times until the car skids, hits cones, or spins around. Usually the failure occurs at about $70 - 80\ km/h$.

In this specific case, since the maximum speed is $v_{max} = 32\ km/h$, the test is performed at the maximum vehicle speed. The test should be passed to demonstrate the safety of itself. Furthermore, since the vehicle without acceleration would be stopped in few meters, it has been tested with an entering speed of 32 km/h and decreased with a constant deceleration until 28 km/h as shown in Figure (3.29).

When the test is performed many data can be acquired. Usually the most important ones are represented by:

- Longitudinal and transversal speed of the vehicle
- Longitudinal, transversal and yaw acceleration
- Vehicle slip angle
- Steering wheel
- Forces acting on the wheel
- Toe and camber angle
- Pitch, roll and yaw angles

3.7.3 Test results

The reproduction of a Moose test into ADAMS/View is quite complex since the software is not provided with trajectories available in the software libraries.

As consequence, the first task has been to reproduce a possible trajectory. It has been imposed a time dependent equation of motion to the steer. The trajectory is modelled using a series of Haversine functions [3].

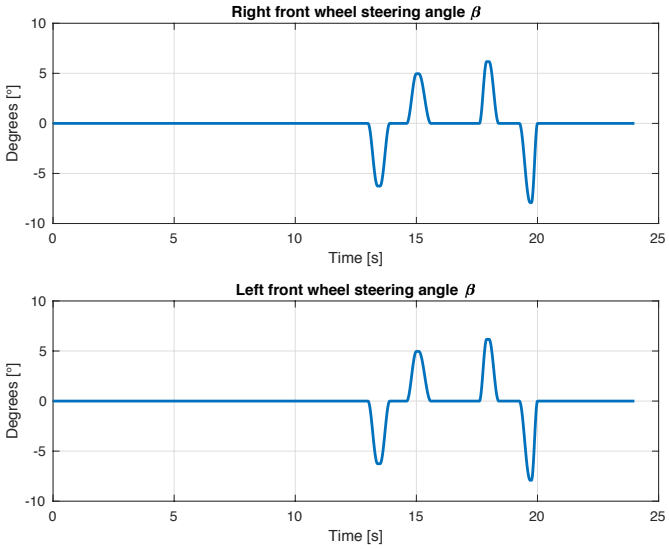

Figure 3.27: Moose test direction

The direction assumed by the front wheels is shown in Figure (3.27). The graph begins with a null angle which is the portion that the vehicle needs to accelerate from zero velocity until the maximum velocity, position in which the test starts. After having past the section one, shown in Figure (3.26), the vehicle makes a series

of curves which permits to avoid the contact with the cones. The trajectory chosen to perform the test is represented in Figure (3.28).

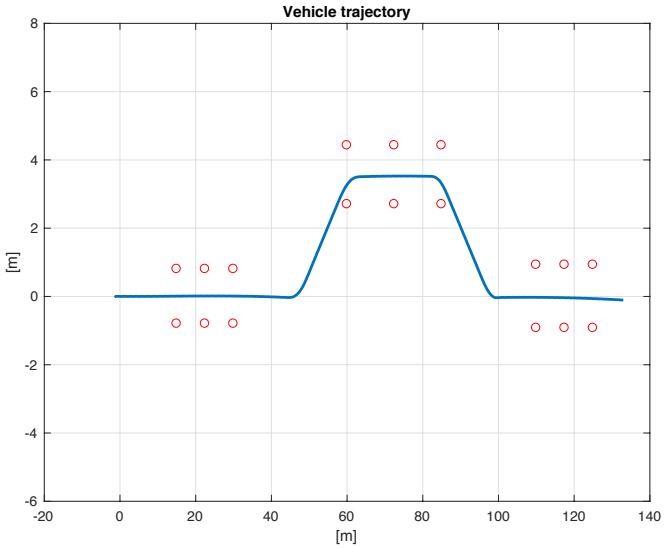

Figure 3.28: Moose test vehicle trajectory

The overall vehicle velocity is set from a maximum of 32 km/h until to a minimum of 28 km/h as shown in Figure (3.29).

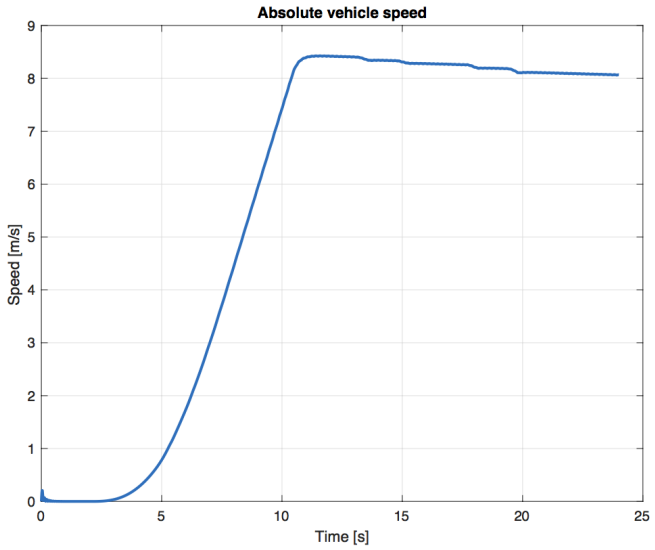

Figure 3.29: Vehicle speed delta

With the imposed trajectory, the resultant longitudinal and lateral velocity are shown in Figure (3.30a) and Figure (3.30b).

Considering the vertical forces acting on each wheel, due to the strong variation of direction, quite a great load transfer is expected. Figure (3.31) shows the trend

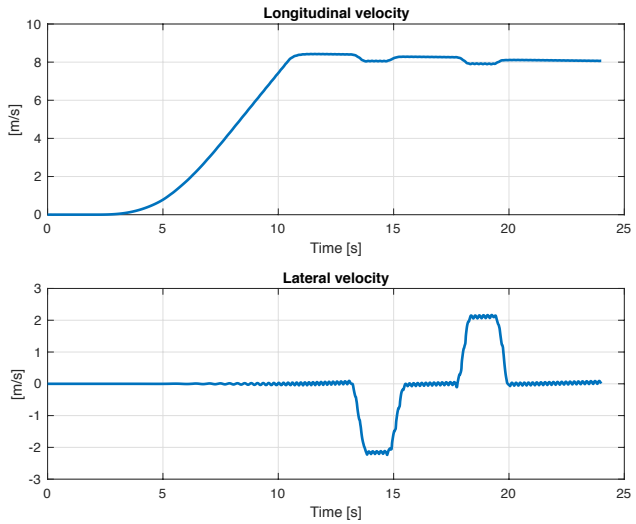

(a) longitudinal velocitiy

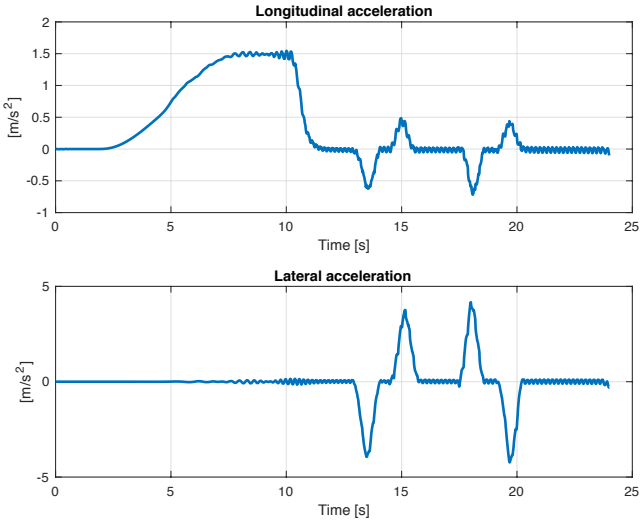

(b) acceleration

Figure 3.30: Velocity and acceleration profile

of the vertical forces during the test. At the beginning the vehicle is settled in the stable position and the load acting on each axle is equal for right and left side as expected.

During the acceleration, up to the maximum speed, a longitudinal transfer is present. When the vehicle enters the cones the effect of the longitudinal load transfer is less evident since the longitudinal speed is almost constant. The effect of the lateral load transfer is much evident, as clearly shown in the vertical load graph.

The resultant lateral forces are finally shown in Figure (3.33) while the sideslip angle for each tire are shown in figure (3.32). In conclusion, the vehicle is able to

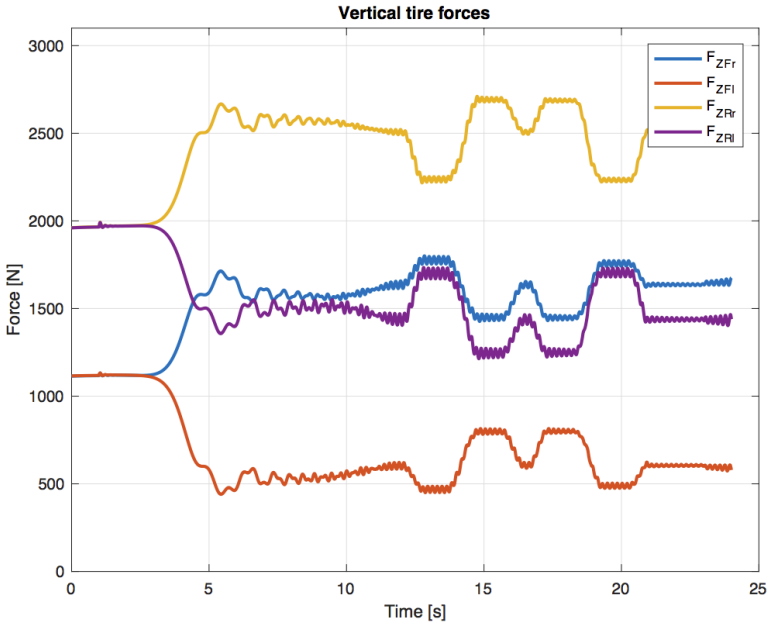

Figure 3.31: Moose test vertical tire forces

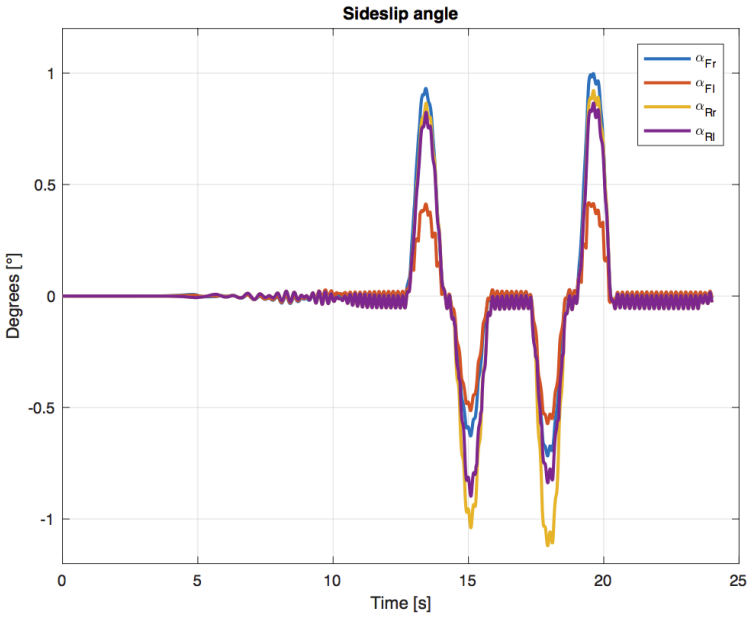

Figure 3.32: Sideslip angle

maintain its trajectory at the maximum speed and the set trajectory does not hit any cone, the test is considered to be passed.

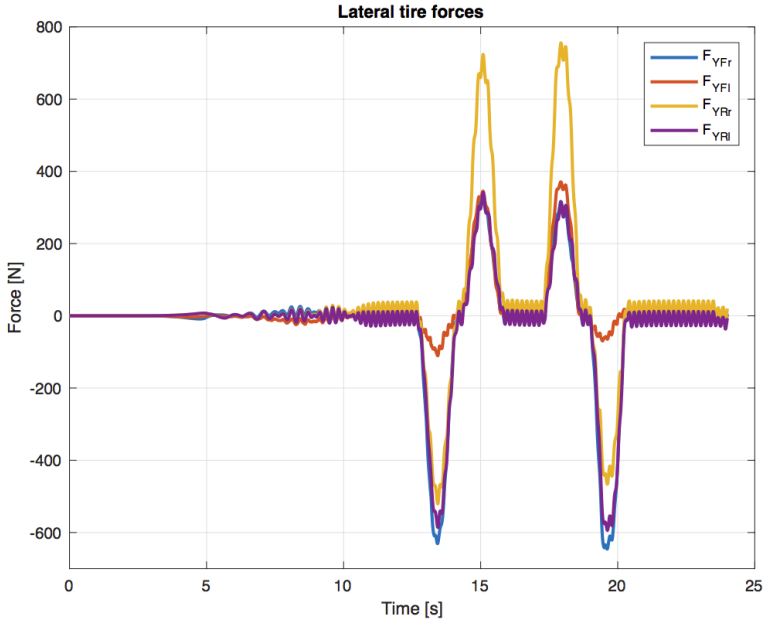

Figure 3.33: Lateral tire forces

Chapter 4

Inverse dynamics model

4.1 Introduction

After the creation of the direct dynamics into Adams/View, the objective is to compare the results to an inverse dynamics. the model is developed using quite a simple model into Matlab. The reason of the use of such a simple model is due to the fact that the target is to control the motion of the vehicle in an autonomous way, being able to generate and find the optimal trajectory on board in a real time.

The program needs to be fast and efficient at the same time, it has to take into account the vehicle dynamics constraints, a part of the ideal trajectory. To do that, a computer is iterating and calculating a series of paths in real time, they need to be obtained as fast as possible. It is exposed how the trajectory has been simulated and how the model has been developed.

4.2 Trajectory model

The local reference system has been set in the center of mass of the vehicle. The SAE reference has been taken into account.

The position of the robot is defined by the location of the origin of the local reference system, $p(x, y)$. Its configuration is defined by the position and orientation of the local reference system, $c(p, \vartheta)$.

A configuration is feasible if it respects the boundaries conditions coming from the vehicle limitation, such as maximum angle of the steer, maximum tire's adherence limit, etc. Since the system is discrete, the interval between two subsequent positions p_j and p_k is defined by the polynomials and denoted as ij:

$$\begin{aligned} &\forall t \in [0, t_j] \\ &x_G = a_x + b_x t + d_x t^2 + e_x t^3 \\ &y_G = a_y + b_y t + d_y t^2 + e_y t^3 \end{aligned} \tag{4.1}$$

t is the time variable associated with the motion of the vehicle.
The following conditions must be fulfilled:

$$\begin{cases} x_j(0) = x_j \\ y_j(0) = y_j \end{cases} \quad and \quad \begin{cases} x_j(t_j) = x_k \\ y_j(t_j) = y_k \end{cases} \tag{4.2}$$

Given a sequence of m positions of the car, $\{P = p1, p2, \ldots, pm\}$, a trajectory T is defined by a sequence of $m-1$ intervals between the position of P that satisfies:

- continuity in position

$$\begin{cases} x_j(0) = x_j \\ y_j(0) = y_j \end{cases} \quad and \quad \begin{cases} x_j(t_j) = x_{j+1} \\ y_j(t_j) = y_{j+1} \end{cases} \tag{4.3}$$

A set of $(4(m-1))$ equation is obtained.

- continuity in velocities

  The initial and final velocities of the trajectory must be zero,
  A set of four equation is obtained.

$$\begin{cases} \dot{x}_0(0) = 0 \\ \dot{y}_0(0) = 0 \end{cases} \quad and \quad \begin{cases} \dot{x}_{m-1}(t_m) = 0 \\ \dot{y}_{m-1}(t_m) = 0 \end{cases} \tag{4.4}$$

To maintain continuity in the trajectory, the initial velocity of each interval must be equal to the final velocity of the previous one,

$$\begin{cases} \dot{x}_j(0) = \dot{x}_{j-1}(t_j - 1) \\ \dot{y}_j(0) = \dot{y}_{j-1}(t_j - 1) \end{cases} \tag{4.5}$$

A set of $(2(m-2))$ equations is obtained.

- continuity in accelerations

$$\begin{cases} \ddot{x}_j(0) = \ddot{x}_{j-1}(t_j - 1) \\ \ddot{y}_j(0) = \ddot{y}_{j-1}(t_j - 1) \end{cases} \tag{4.6}$$

By knowing the trajectory times associated with different intervals, a linear system of $(8(m-1))$ equation is obtained and it is possible to obtain the coefficients of the polynomials (4.1), fully defining the trajectory.

4.2.1 Vehicle model

To perform an efficient onboard simulation of trajectories it is necessary to provide an efficient and simple model. The dynamic constraints have to be processed in real time by the onboard computer.

To do that, the so-called "Bicycle model" has been employed. The model implies a series of assumption which are now recalled.

The Bicycle model does not take into account the roll and pitch motions, the side-load transfer and the aerodynamic effects. The model works in the plane, with three degrees of freedom plus a restriction on the maximum steering angle, which corresponds to the maximum steering of the actual vehicle.

Then, the front and the rear wheels are simplified into one that exerts the force corresponding to the front and rear respectively. The steering angle corresponds to that of the single front wheel of the model.

Finally, the sideslip angles are considered to be small. For the studied case, these approximations can be accepted since the velocity is relatively small and the accelerations produced by the change of direction are always maintained quite small. The Bicycle model of the car is shown in the Figure (4.1).

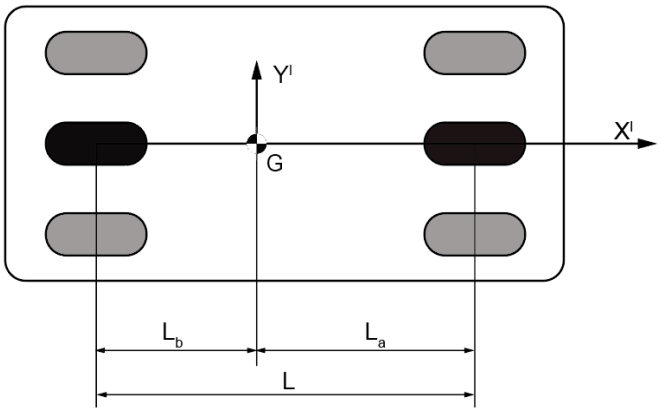

Figure 4.1: Bicycle model

4.2.2 Vehicle kinematics

The kinematics of the center of gravity of the vehicle on the trajectory is known. Taking into account the global reference system, the expressions (4.7) can be obtained and implemented in the Matlab program.

First of all, it is necessary to define the position of the center of gravity,

$$\begin{aligned} x_j &= a_{xj} + b_{xj}t + d_{xj}t^2 + e_{xj}t^3 \\ y_j &= a_{yj} + b_{yj}t + d_{yj}t^2 + e_{yj}t^3 \end{aligned} \tag{4.7}$$

Knowing the position of the center of mass with respect to the global reference, it is possible to compute a derivative with respect to the time, obtaining the velocity of the point taken into account,

$$\overrightarrow{V}_G = \dot{x}_G \overrightarrow{i} + \dot{y}_G \overrightarrow{j} \tag{4.8}$$

The magnitude of the velocity is expressed as follows,

$$|\overrightarrow{V}_G| = \sqrt{\dot{x}_G^2 + \dot{y}_G^2} \tag{4.9}$$

Once that the velocities are known, to completely define the position of the center of gravity, the angular position is obtained as,

$$\vartheta = \tan^{-1} \frac{\dot{y}_G}{\dot{x}_G} \tag{4.10}$$

The angular velocity is defined as,

$$\omega = \dot{\vartheta} + \dot{\beta} \tag{4.11}$$

Where, according to the Bicycle model assumptions, β is considered to be small and so, its derivative $\dot{\beta}$ is negligible. Consequently, the angular velocity is obtained as,

$$\omega = \frac{\dot{x}_G \ddot{y}_G - \dot{y}_G \ddot{x}_G}{\dot{x}_G^2 + \dot{y}_G^2} \tag{4.12}$$

Writing the equation with respect to the local reference system, the velocity of the rear axle is,

$$\overrightarrow{V_R^l} = \overrightarrow{V_G^l} + \overrightarrow{\omega} \wedge \overrightarrow{r_{GR}} \tag{4.13}$$

The equation (4.13) can be written in another form,

$$\overrightarrow{V_R^l} = |\overrightarrow{V_G}| \cos\beta \, \overrightarrow{l}_l + (|\overrightarrow{V_G}| \sin\beta - L_b\omega) \overrightarrow{j}_l \tag{4.14}$$

under the assumption of small sideslip angles (4.14) it is written in the following way,

$$\overrightarrow{V_R^l} \approx |\overrightarrow{V_G}| \, \overrightarrow{l}_l + (|\overrightarrow{V_G}| - L_b\omega) \overrightarrow{j}_l \tag{4.15}$$

The rear axle sideslip angle can be written taking into account the velocity components and express it as,

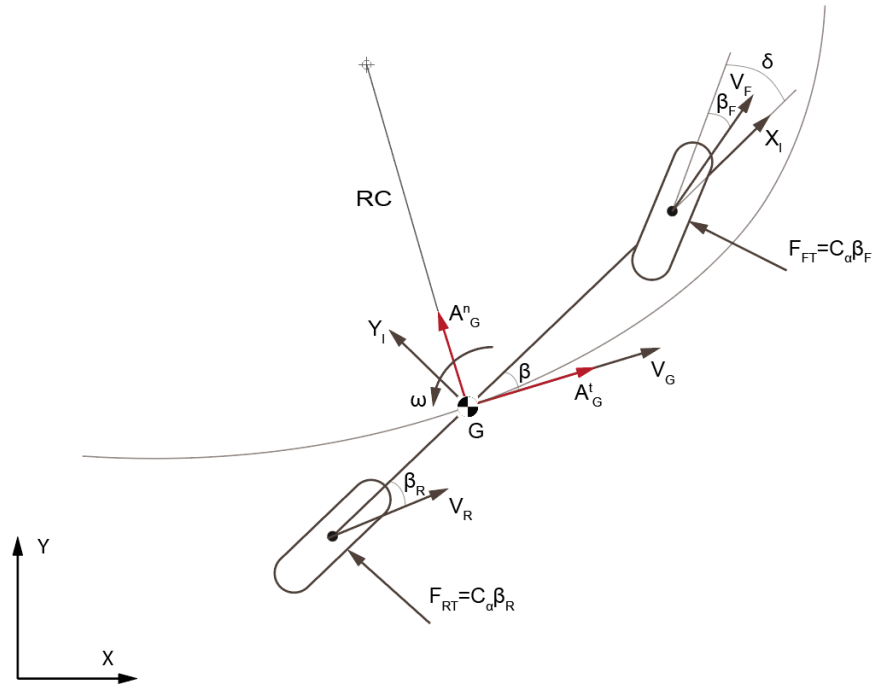

Figure 4.2: Kinematics and side slip angles

$$\beta_R = tan^{-1}\frac{(|V_G|\beta - l_b\omega)}{|\overrightarrow{V_G}|} \tag{4.16}$$

Always with the same assumption of small sideslip angles,

$$\beta_R \approx \beta - \frac{(\dot{x}_G\ddot{y}_G - \dot{y}_G\ddot{x}_G)L_b}{(\dot{x}_G^2 + \dot{y}_G^2)^{3/2}} \tag{4.17}$$

Similarly to the equation (4.17) and adding the "δ" steering angle the forward sideslip angles is defined as,

$$\beta_F \approx \delta - \beta - \frac{(\dot{x}_G\ddot{y}_G - \dot{y}_G\ddot{x}_G)L_b}{(\dot{x}_G^2 + \dot{y}_G^2)^{3/2}} \tag{4.18}$$

The normal acceleration for the trajectory in the center of gravity G is,

$$A_G^n = -\ddot{x_G}\sin\vartheta + \ddot{y_G}\cos\vartheta \tag{4.19}$$

and the tangential acceleration,

$$A_G^t = \ddot{x_G}\cos\vartheta + \ddot{y_G}\sin\vartheta \tag{4.20}$$

Writing the acceleration referring to the local reference system, linked to the vehicle, as shown in Figure (4.2), the lateral acceleration is expresses as,

$$A_G^{Y_l} = A_G^n \cos\beta - A_G^t \sin\beta \tag{4.21}$$

Under the assumption previously done, "β" is small, so the equation can be written as,

$$A_G^{Y_l} \approx A_G^n - A_G^t \beta \tag{4.22}$$

Considering the tire's lateral behaviour, under small sideslip hypothesis, the lateral force with respect to the slip angle have linear dependency, so the lateral force given by the rear and front tires is expressed with the equation,

$$\begin{aligned} F_{RT} &= -C_\alpha \beta_R \\ F_{FT} &= -C_\alpha \beta_F \end{aligned} \tag{4.23}$$

As studied in the theory, the minus is due to the opposite direction of the force with respect to the sideslip angle and the orientation, is normal to the rim.

Writing the Newton-Euler equations for the lateral force and moments, the following expression is obtained,

$$F_{RT} + F_{FT}\cos\delta = mA_G^{Y_l} \tag{4.24}$$

Substituting in the equation (4.24) the tire's lateral forces equation, it is possible to obtain,

$$-C_\alpha\beta_R - C_\alpha\beta_F\cos\delta = mA_G^{Y_l} \tag{4.25}$$

The equation of moments is,

$$F_{FT}\cos\delta L_a - F_{RT}L_b = I_z\dot{\omega} \tag{4.26}$$

Where, I_z is the moment of inertia about the $z-axis$, which is the axis perpendicular to the ground, passing through the car's center gravity. Writing in another way the formula (4.26),

$$C_\alpha(-L_\alpha\beta_F\cos\delta + L_b\beta_R) = I_z\dot{\omega} \tag{4.27}$$

It has been set a system of equations (4.24), (4.25), (4.26), (4.27) that, solving a non liner system, permits to obtain "δ", "β", "β_F", "β_R".

Chapter 5

Inverse dynamics results

5.1 Introduction

All the equations explained in the previous chapter have been implemented into a Matlab script. The objective is the creation of a program which, after the generation of a trajectory defined by the user, is able to say if the given trajectory is feasible and which forces are acting on the tires at each instant of time. Due to the simplicity of the model, it is expected a deviation of the results as far the speed increases and the steering angle increases. The results obtained from the program are then compared to the data coming from the ADAMS model.

5.2 Results

The program is potentially able to analyse any kind of trajectory. A series of fourth order polynomial equations have been used to build the trajectories. The script after having defined the position, velocity and acceleration of the vehicle, checks the feasibility of the path by checking the vehicle's boundaries. The vehicle boundaries have been set as the maximum steering angle δ, the maximum velocity V_{max} which correspond to the maximum speed the vehicle can reach and the maximum lateral force F_{max} that the wheel can exchange without slip. During each iteration, the program verifies if the boundaries are respected. At the end of the calculation, the output is the vehicle sideslip β, the tires sideslip angles β_F, β_R and the steering angle δ.

Table (5.1) recalls the data used for the simulation.

Table 5.1: Vehicle data

Wheelbase	[m]	1,65
Rear axle position b	[m]	0,55
Front axle position a	[m]	1,1
Moment of inertia I_{zz}	$[kg \cdot m^2]$	160
Mass	[kg]	690
Cornering stiffness C_α	$[N/°]$	800

5.2.1 Straight line trajectory

As first, the vehicle has been tested on a straight line trajectory. The reason for this test was to verify the goodness of the inverse dynamics model. The results need to be coherent with the reality. The steering angle δ is expected to be null as well as for the lateral force F_y on both tires.

The velocity is maintained constant and equal to $V = 8\ m/s$. The trajectory path is represented in Figure (5.1).

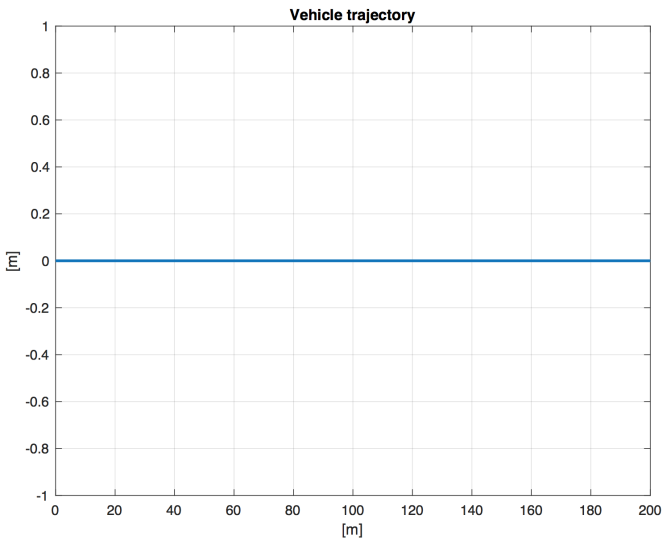

Figure 5.1: Vehicle trajectory

The angle of direction to make the linear trajectory is zero and it is shown in Figure (5.2a).

Since the Bicycle model does not take into account the influence of the toe angle and the camber angle, no lateral forces is created by this two factors. The only source of lateral force is given by the slip angle produced when the vehicle is travelling a curve.

The vehicle is travelling through a linear path, no lateral velocity is present. The vehicle and the tires have a null sideslip. Finally, the tire lateral forces as well results null, Figure (5.4a) and (5.4b).

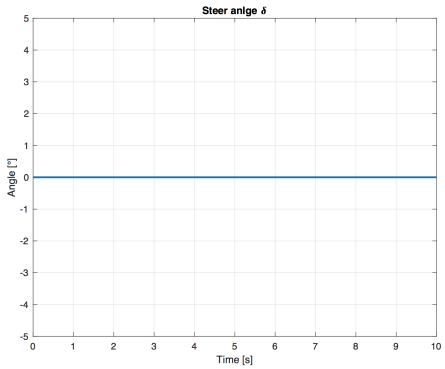

(a) Steering

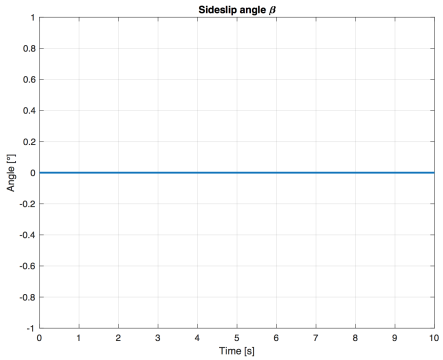

(b) Slip angle

Figure 5.2: Steering and Vehicle slip angle

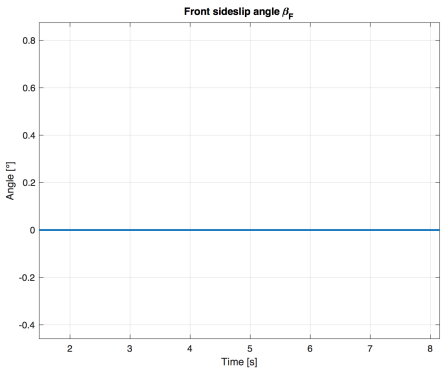

(a) Front tire

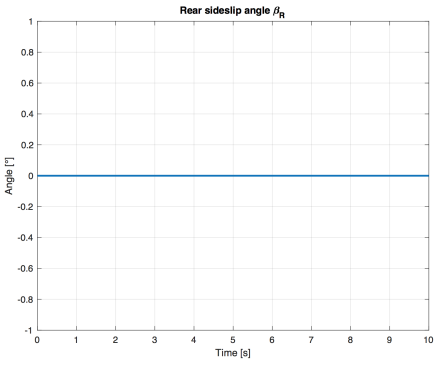

(b) Rear tire

Figure 5.3: Tire slip angles

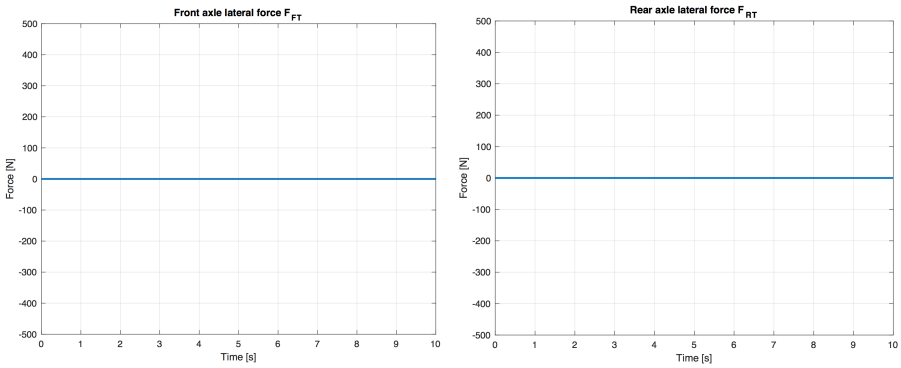

(a) Front axle **(b)** Rear axle

Figure 5.4: Lateral forces

5.3 Circular trajectory

The first trajectory tested consists of a 40 m radius circle. The speed is set equal to the maximum speed of the vehicle, $V_{max} = 32\ km/h$.

The trajectory path is shown in Figure (5.5).

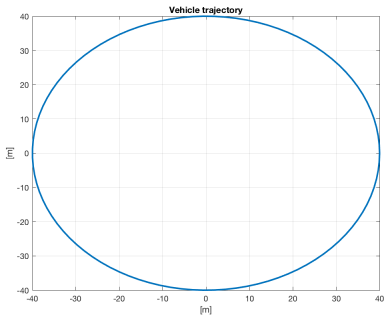

Figure 5.5: R=40m V=32 km/h trajectory

The steering angle able to travel the given trajectory is really close to the value calculated with ADAMS, as plotted in Figure (5.6).

The front and rear sideslip angles, figure (5.7), (5.8) results to be quite close as well to the ADAMS model, the front axle is not so close to the reality like the rear one. The reason is due to the presence of a quite big load transfer at the front axle, which is not taken into account in the Bicycle model.

The resultant lateral force results really close as well. Figure (5.9) (5.10), shows the force acting on the front and on the rear axle, thus the sum of the inner and outer wheel force.

As for the slip angles, the front axle is less accurate than the rear one, due to the lateral load transfer.

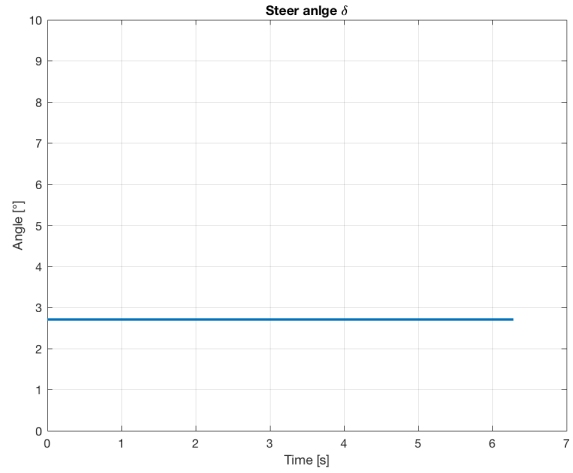

Figure 5.6: R=40m V=32km/h Delta

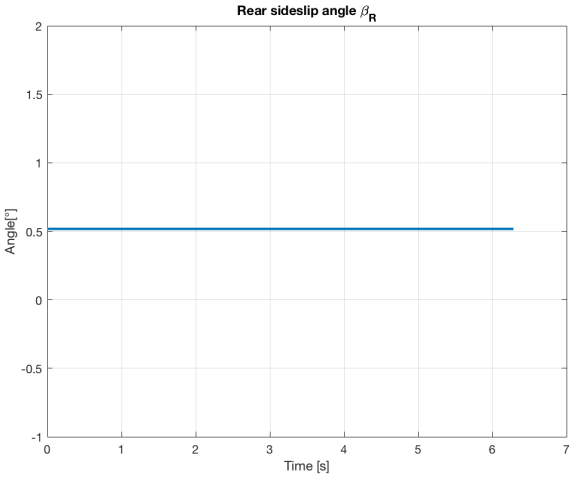

Figure 5.7: R=40m V=32km/h Inverse rear sideslip

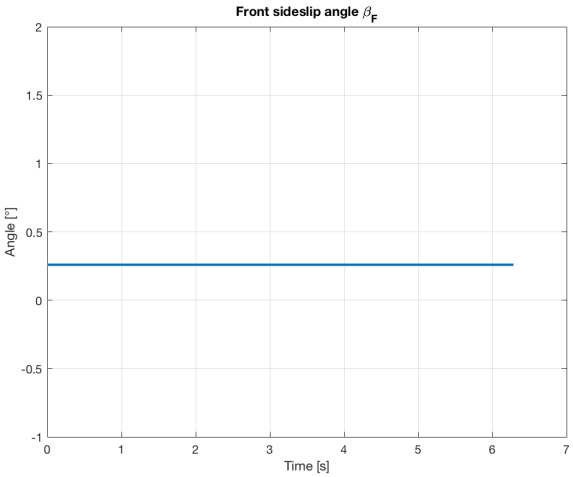

Figure 5.8: R=40m V=32 km/h Inverse front sideslip

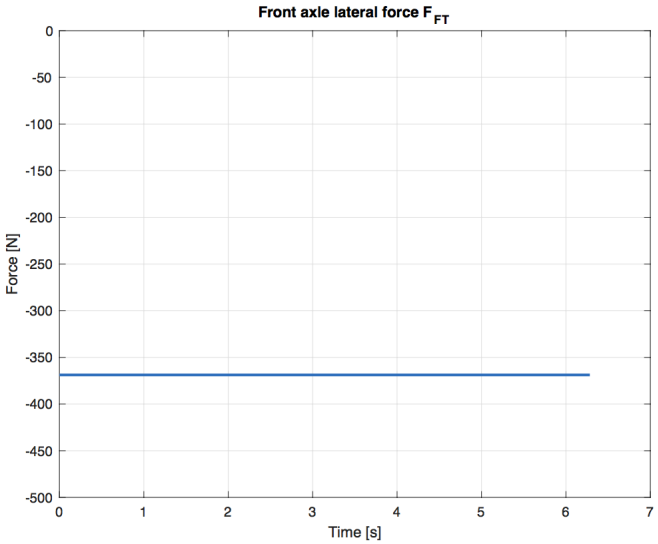

Figure 5.9: R=40m V=32km/h Front axle lateral force

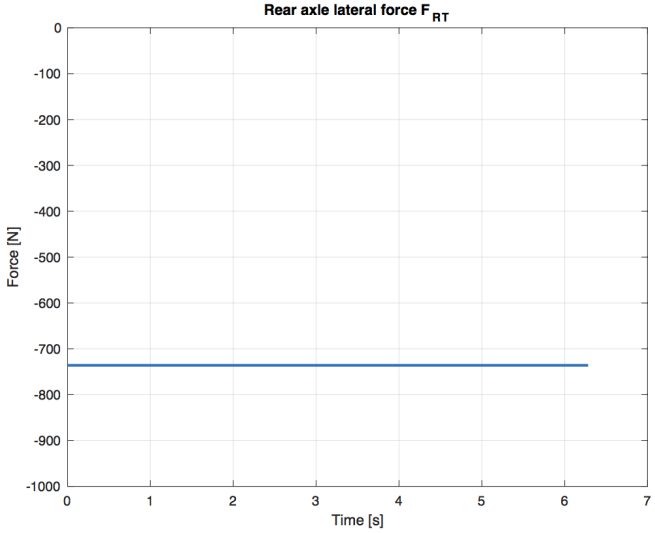

Figure 5.10: R=40m V=32km/h Rear axle lateral force

5.4 Moose test

A Moose test was performed, imposing a possible trajectory to travel without hit any cone. It has been evaluated the magnitude of velocities, accelerations, tire forces and sideslip angles resulting on the vehicle.

It is important to recall that the results obtained have to be analysed with care.A Bicycle model is not able to predict with precision the magnitude of the lateral forces and slip angles. The model does not take into account many factor in such a severe test.

The roll and pitch are not taken into account in the model, as well as the load transfer and the suspension system is not considered.

The trajectory is designed using a spline functions, Figure (5.11).

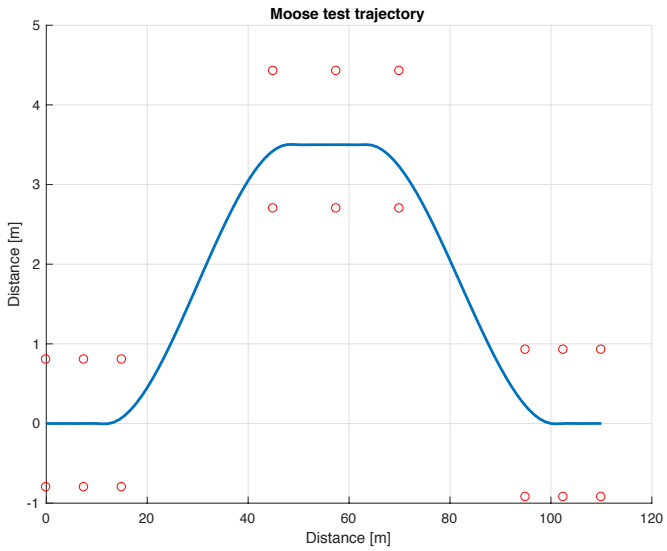

Figure 5.11: Moose test trajectory

The resultant speed of the test is set equal to 32 km/h. The longitudinal and lateral velocity of the vehicle during the test is shown in Figure (5.12) and the longitudinal and lateral acceleration in Figure (5.13)
Solving the non linear equation, the program output is represented by the front axle slip angle, the rear axle slip angle and the vehicle slip angles is represented. Data are shown in Figure (5.14), (5.15), (5.16).

Comparing the data obtained from the direct dynamics, it is possible to see that the general behaviour of the slip angle on the front and rear axle has the same trend. Obviously it is not possible to see the great change of behaviour between the external and internal wheels, especially in the case of the front axle.

The graphs referring to lateral forces acting on the front and rear axles are directly obtained from the slip angles. In fact, it was assumed a linear behaviour

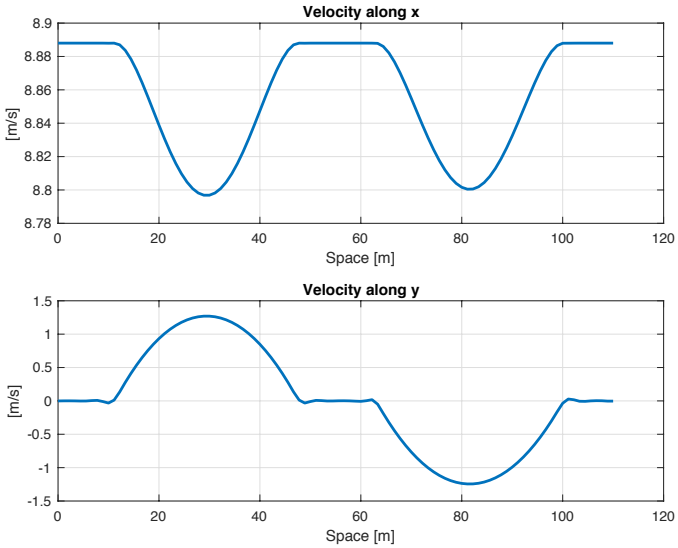

Figure 5.12: Longitudinal and lateral velocity

between the slip angle and the lateral force. The cornering stiffens used for the calculation is fixed to 800 $N/°$.

The lateral force is shown in Figure (5.17) and Figure (5.18) for the front ant rear respectively.

The force sign is coherent with the theory and with the direct dynamics.In fact, the lateral force has opposite sign with respect to the tire slip angle.

Comparing the order of magnitude of the resulting forces of the front axle and rear axle, the value is really close to the whole vehicle simulation. As said previously, as the lateral load transfer is not taken into account, it is impossible to see the loss of force on the internal front wheel, due to the geometry of the suspension and to the position of the center of gravity.

The last information obtained by the Bicycle model is represented by the angle of direction δ. The angle is really close to the previous test, but obviously not equal due to the simple model used and to the fact that the trajectory tested are not perfectly equal. Furthermore, the Bicycle model is not taking into account the direction geometry and the Ackerman error.

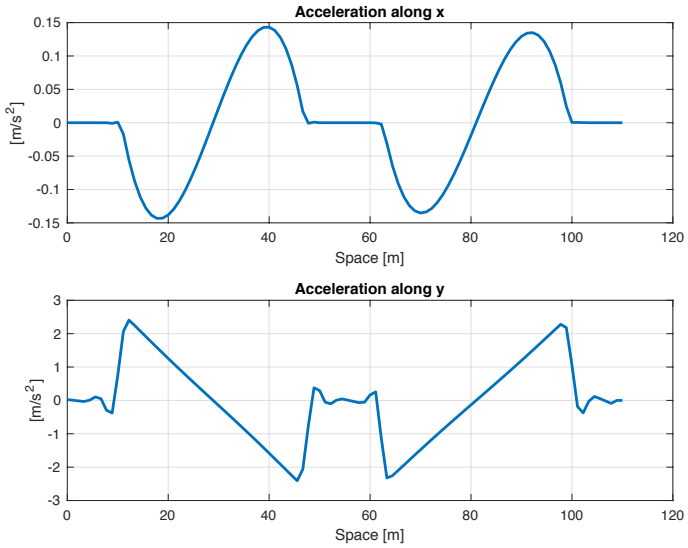

Figure 5.13: Longitudinal and lateral acceleration

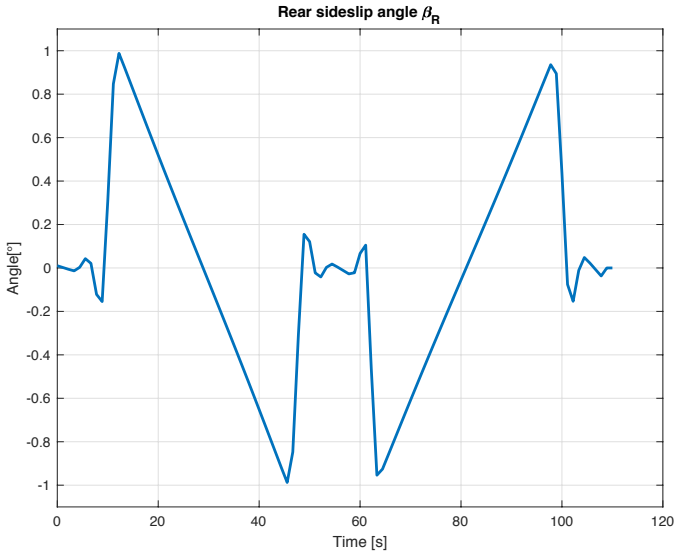

Figure 5.14: Rear axle side slip angle

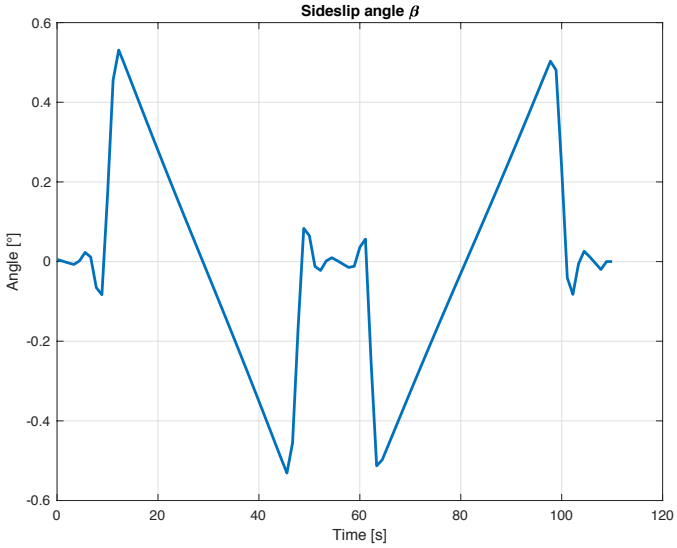

Figure 5.15: Vehicle side slip angle

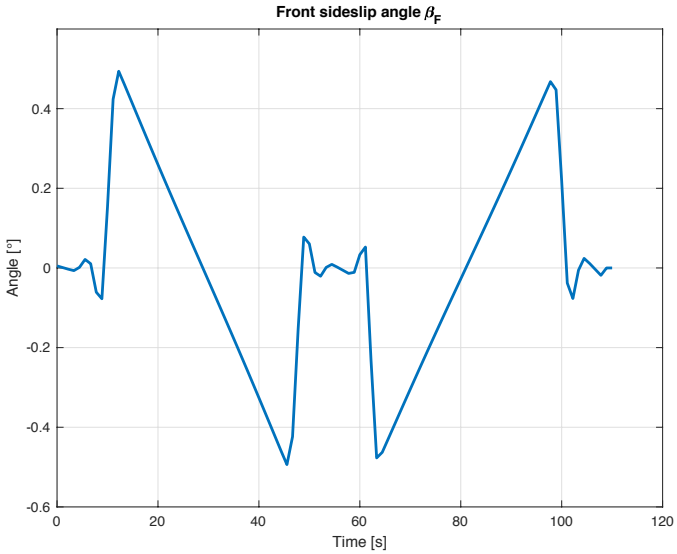

Figure 5.16: Front side slip angle

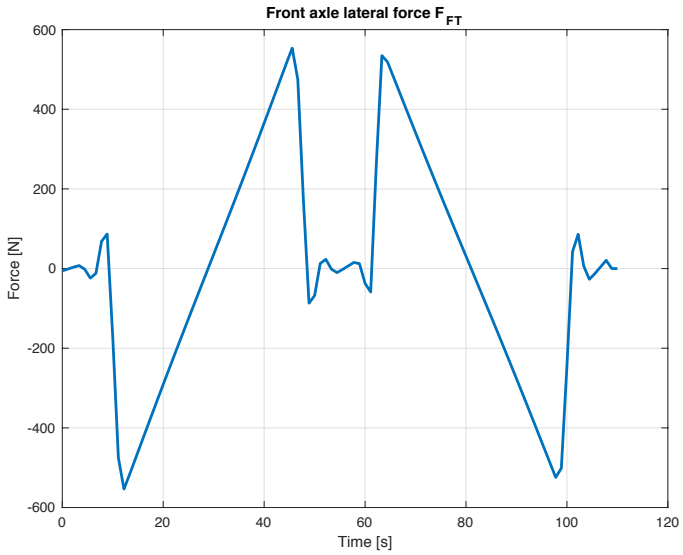

Figure 5.17: Front axle lateral force

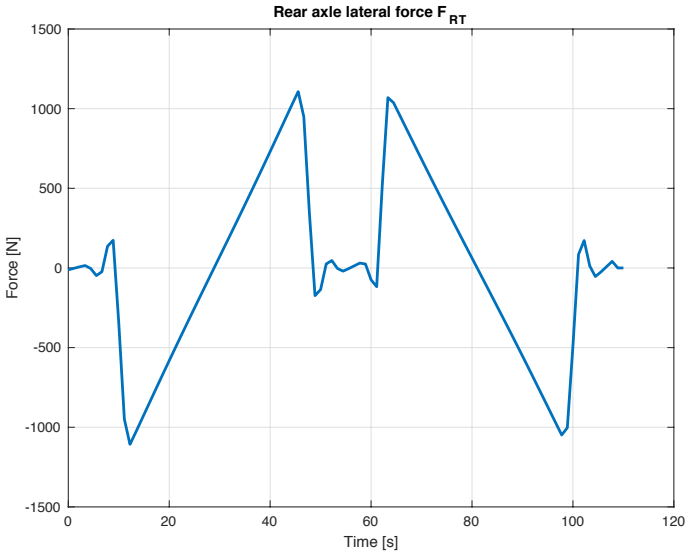

Figure 5.18: Rear axle slip angle

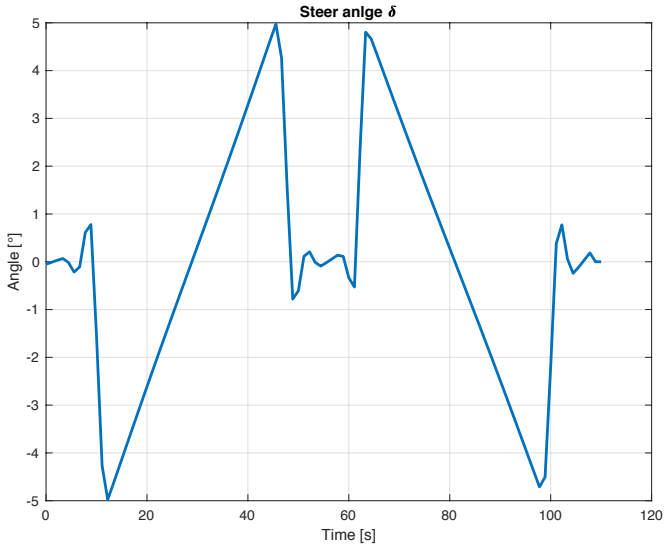

Figure 5.19: Steer angle

Chapter 6

Conclusions

6.1 Introduction

This Thesis work has proposed some basics of mathematics, analytical methods and models necessary to describe the behaviour of a vehicle, useful for any application. Starting from the information shown, the virtual model has been implemented and reproduced as close as possible to the reality. The objective has been to provide a vehicle model, to be used by colleagues to simulate the car. Imposing in the software any trajectory on a planar surface, the response of the vehicle is studied. The second part of the thesis aimed to develop an inverse dynamics model. This section illustrates a primitive model which should be implemented and optimized. The following pages make an analysis of the results and assumptions done for this work and focus the key points for a future work, aimed to improve this first one.

6.2 Conclusions

One of the objectives has been the development of a vehicle model able to predict its dynamics. The objective is to make a comparison with the trajectories developed with an easy model to see how much is the error for using such a simplified model. The virtual model used for the presents a series of assumptions. As instance, the tire model used, which is the Fiala's model, it is good as far the tire slip angle is small. Increasing the slip angle, the accuracy of the calculation is decreased. Another key issue in order to improve the model is related with the tire cornering stiffness. The coefficient has been calculated with an iteration in ADAMS, assuming that the geometry is perfectly equal to the real one, obtaining the same vehicle slip at the same test conditions. Obviously the test should be better done by testing the tire lateral stiffness with a proper machine. Then, The leaf spring stiffness, has been obtained by using empirical formulations and approximation of the geometry. The influence on the vehicle is less than the influence of the cornering stiffness but, it could be a key of improvement of the model as well. Finally, the dampers behaviour have been approximated with a spline function to commercial dampers installed in similar vehicles. The real value of damping of the studied vehicle were not calculated. The influence on the vehicle behaviour is quite small compared to other values but, it is again a matter of improvement of the model.

During the study of the vehicle motion, it has been noticed quite an instability of the calculation, the slip angles and the lateral forces are affected by an oscillation which not permits to read easily the magnitude of the forces acting. The results in average value are good. Without a proper signal processing, it results difficult to read the data in output. A propose for a future work would be to find the problem of this behaviour and try to improve the quality of the signals.

Considering the inverse dynamics, the trajectories have been implemented with fourth order polynomials, the time required to write a trajectory is quite high and done manually. The program should be able to calculate trajectories automatically, comparing a series of feasible trajectories and taking the optimal one. For this purpose only one has been taken into account, studying the forces acting on the tires. The model as well, works only for low velocities and low variation of direction. With higher velocities and curvature variations, the output data could be not real at all.

6.3 Future work

The suggestions for a future work are deduced from the conclusions written above. As first, it is suggested to improve the ADAMS model with the exact value of tire cornering stiffness. A a more precise tire model could be used, like for example the Pacejka model [23], introducing the coefficient calculated from a lateral tire slip test.

Into ADAMS it could be useful to develop a co-simulation with Matlab in real time. In this work, data from ADAMS where saved and processed after in Matlab, importing the vectors, with a big waste of time. The usage of a co-simulation between the two software would be interesting to develop new features, like advanced steering functions able to control for example an high speed turning, correcting the deviation in the trajectories induced by the lateral slip of the vehicle. It would be possible as well to control the traction of the engine with a controlled variation of speed, or control the braking during a trajectory.

The inverse dynamics model should be faster to calculate trajectories. In this work, the different paths are obtained by fixing some points and then computing each specific trajectory desired to be studied. With a proper script, it could be useful to give an initial point, a final point and eventually some obstacles as input. Using a trajectory optimization, the script should be able to find the optimal one. The calculation needs to be in accordance with the vehicle restrictions. Furthermore, a more sophisticated model than the Bicycle one could be taken into account. It would be useful to verify the difference of time effort in the calculation and the variation of the vehicle behaviour between the two cases.

Appendix A

Matlab scripts

A.1 Adams imported data

Listing A.1: Adams imported data

```
clear all
close all
clc


% ------------------------------------------------
% ADAMS/View simulation delta xxx rad -- xxx degrees
% Velocity: xxx mm/s _ xxx m/s _ xxx km/h
% ------------------------------------------------


load Alpha_Del_Dx;           % [degrees]
load Alpha_Del_Sx;           % [degrees]
load Alpha_Tras_Dx;      % [degrees]
load Alpha_Tras_Sx;      % [degrees]
load Fy_Del_Dx;          % [N]
load Fy_Del_Sx;            % [N]
load Fy_Tras_Dx;       % [N]
load Fy_Tras_Sx;       % [N]
load Fz_Del_Dx;        % [N]
load Fz_Del_Sx;        % [N]
load Fz_Tras_Dx;       % [N]
load Fz_Tras_Sx;       % [N]
load Posizione_X_mm;     % [mm]
load Posizione_Y_mm;     % [mm]
load time;               % [s]
load CM_speed_mm_s;      % [mm/s]
load Dir_Sx;             % [Degrees]
load Dir_Dx;             % [Degrees]

```

```
31
32 % ------------------------------------------------
33 % S.I. Transformations
34 % ------------------------------------------------
35
36
37 % Transformation from [mm/s] to [m/s]
38
39 for i=1:length(time)
40
41     CM_speed(i)=CM_speed_mm_s(i)/1000;       % [m/s]
42     Posizione_X(i)=Posizione_X_mm(i)/1000;   % [m]
43     Posizione_Y(i)=Posizione_Y_mm(i)/1000;   % [m]
44
45 end
46
47
48 % ------------------------------------------------
49 % Speed Profile
50 % ------------------------------------------------
51
52
53 figure ()
54
55 plot(time,CM_speed,'linewidth',2)
56
57 title('Vehicle speed')
58 grid on
59 xlabel('Time [s]')
60 ylabel('Speed [m/s]')
61
62
63 % ------------------------------------------------
64 % Trajectory Path
65 % ------------------------------------------------
66
67
68 figure ()
69
70 plot(Posizione_X,Posizione_Y,'linewidth',2)
71
72 hold on
73 title('Vehicle trajectory')
74 grid on
75 xlabel('[m]')
76 ylabel('[m]')
77
```

```
78
79 % ------------------------------------------------
80 % Radius calculation of the circle
81 % ------------------------------------------------
82
83
84 x_min=min(Posizione_X);
85 x_max=max(Posizione_X);
86
87 Rx=(x_max-x_min)/2;
88
89 y_min=min(Posizione_Y);
90 y_max=max(Posizione_Y);
91
92 R=(y_max-y_min)/2
93
94
95 % ------------------------------------------------
96 % Lateral Forces
97 % ------------------------------------------------
98
99
100 figure()
101
102
103 plot(time,Fy_Del_Dx,'linewidth',2)
104 hold on
105
106 plot(time,Fy_Del_Sx,'linewidth',2)
107 hold on
108
109 plot(time,Fy_Tras_Dx,'linewidth',2)
110 hold on
111
112 plot(time,Fy_Tras_Sx,'linewidth',2)
113 hold on
114
115 ylim([xxx xxx])
116 grid on
117 legend ('F_Y_F_r ','F_Y_F_l','F_Y_R_r','F_Y_R_l')
118 xlabel('Time [s]')
119 ylabel('Force [N]')
120 title('Lateral tire forces')
121
122
123 % ------------------------------------------------
124 % Vertical Forces
```

```
125 % ------------------------------------------------
126
127
128 figure()
129
130 plot(time,( Fz_Del_Dx),'linewidth',2)
131 hold on
132
133 plot(time,(Fz_Del_Sx),'linewidth',2)
134 hold on
135
136 plot(time,(Fz_Tras_Dx),'linewidth',2)
137 hold on
138
139 plot(time,(Fz_Tras_Sx),'linewidth',2)
140 hold on
141
142 ylim([xxx xxx])
143 grid on
144 legend ('F_Z_F_r ','F_Z_F_l','F_Z_R_r','F_Z_R_l')
145 xlabel('Time [s]')
146 ylabel('Force [N]')
147 title('Vertical tire forces')
148
149
150 % ------------------------------------------------
151 % Slip angle plots
152 % ------------------------------------------------
153
154
155 figure()
156
157 plot(time,Alpha_Del_Dx,'linewidth',2)
158 hold on
159
160 plot(time,Alpha_Del_Sx,'linewidth',2)
161 hold on
162
163 plot(time,Alpha_Tras_Dx,'linewidth',2)
164 hold on
165
166 plot(time,Alpha_Tras_Sx,'linewidth',2)
167 hold on
168
169 ylim([xxx xxx])
170 grid on
```

```
171 legend ('\alpha_F_r ','\alpha_F_l','\alpha_R_r','\
    alpha_R_l')
172 xlabel('Time [s]')
173 ylabel('Degrees [degrees]')
174 title('Sideslip angle')
```

A.2 Dampers graph

Listing A.2: Dampers graph

```
1  clear all
2  close all
3  clc
4
5
6  % ------------------------------------------------
7  % Adams Damper Front and Rear Plots
8  % ------------------------------------------------
9
10
11 x = [-20   -10   -5     -1   0   1    5   10   20] ;
12 y= [-500   -100   -20   -8   0   8   20   100   500] ;
13 n= x(1):0.25:x(length(x)) ;
14 y_axis=spline(x,y,n) ;
15
16 figure ()
17
18 plot(x,y,'or','linewidth',2)
19 hold on
20 plot (n,y_axis,'linewidth',2)
21 xlabel('Velocity [mm/s]')
22 ylabel('Force [N]')
23 grid on
24 title('Force vs Velocity')
```

A.3 Center of gravity calibration

Listing A.3: Dampers graph

```
1  clear all
2  close all
3  clc
4
5
6  % ------------------------------------------------
```

```
%   Center of gravity position test & Static laod
%   on tires
% -------------------------------------------------


% Datas imported from Adams

load CDG
load Fz_Rueda_Del_Dx
load Fz_Rueda_Del_Sx
load Fz_Rueda_Tras_Dx
load Fz_Rueda_Tras_Sx
load time


% -------------------------------------------------
% Plot Loads on the tires under static conditions
% -------------------------------------------------


figure()

% Vertical load front tire -- Right

subplot(2,1,1)
plot(time,( Fz_Rueda_Del_Dx),'linewidth',2)
hold on

% Vertical load rear tire -- Right

subplot(2,1,1)
plot(time,(Fz_Rueda_Tras_Dx),'linewidth',2)
hold on
ylim([0 2600])

xlabel('Time [s]')
ylabel('Force [N]')

grid on
legend('F_Z_F_r','F_Z_R_r')
title ('Vertical Wheel laod')

% Vertical load front tire -- Left

subplot(2,1,2)
plot(time,(Fz_Rueda_Del_Sx),'linewidth',2)
hold on
```

```
54
55 % Vertical load rear tire -- Right
56
57 subplot(2,1,2)
58 plot(time,(Fz_Rueda_Tras_Sx),'linewidth',2)
59 hold on
60 ylim([0 2600])
61 grid on
62
63 legend ('F_Z_F_l','F_Z_R_l')
64 xlabel('Time [s]')
65 ylabel('Force [N]')
66 title ('Vertical Wheel laod')
67
68
69 % ------------------------------------------------
70 % Plot Center of gravity height
71 % ------------------------------------------------
72
73
74 figure()
75 plot(time,CDG,'linewidth',2)
76 ylim([400 600])
77 grid on
78 xlabel('Time [s]')
79 ylabel('Position [mm]')
80 title ('Center of gravity height')
```

A.4 Inverse dynamic

Listing A.4: Dampers graph

```
1  clear all
2  close all
3  clc
4
5
6  global m;
7  global hh;
8  global Lb;
9  global La;
10 global Iz;
11 global omega_punto;
12 global a_g_norm;
13 global a_g_trans;
14 global i;
```

```
15 global C_t;
16
17
18 % ------------------------------------------------
19 % Inverse dynamic problem
20 % ------------------------------------------------
21
22
23 % Global constant
24
25
26     g=9.81 ; %[m/s^2]
27
28
29 % Vehicle data
30
31
32     m=690;      % [Kg]
33     L=1.65;     % [m]
34
35
36 % Distance from center of gravity to rear axle
37
38
39     Lb=0.55; ; % [m]
40
41
42 %  Distance from the center of gravity to the front axle
43
44
45     La=1.1;     % [m]
46
47
48 % Moment of Inertia ot the car
49
50     Iz=160;    % [Kg/m^2]
51
52
53
54 % Tire lateral stiffness
55
56
57     C_t=45836; %[N/rad]
58     mu_t=0.1;  %COEFICIENT OF FRICTION
59     mu_r=0.1;  %COEFFICIENT LOSSES DUE TO MOTION
60
61
```

```
% Time of the trajectory


    t=linspace (0,5,1000);


% Circular trajectory


    r=40 ;  % [m]

syms x1 x2 x3 x4 y1 y2 y3 y4

eqn1 = x1 == 0  ;
eqn2 = y1 == -r  ;
eqn3 = x2+x3+x4 == r  ;
eqn4 = y2+y3+y4 == r  ;
eqn5 = 2*x2+4*x3+8*x4 == 0;
eqn6 = 2*y2+4*y3+8*y4 == 2*r;
eqn7 = 3*x2+9*x3+27*x4 == -r ;
eqn8 = 3*y2+9*y3+27*y4 == r ;

[A, B] = equationsToMatrix ([eqn1, eqn2, eqn3, eqn4,
   eqn5, eqn6, eqn7, eqn8],[x1, x2, x3, x4, y1, y2, y3,
   y4]);

Soluzione_polinomiale=linsolve(A,B) ;


% Polynomial coefficients


a_x=B(1);
b_x=B(2) ;
d_x=B(3) ;
e_x=B(4) ;

a_y=B(5) ;
b_y=B(6) ;
d_y=B(7) ;
e_y=B(8) ;


% position of CM


        for i=1:length(t)
```

```
107
108  x_xg(i)=a_x+b_x*t(i)+d_x*t(i)^2+e_x*t(i)^3;
109  y_yg(i)=a_y+b_y*t(i)+d_y*t(i)^2+e_y*t(i)^3;
110
111         end
112
113
114 % ------------------------------------------------
115 % Velocities  and acceleration of the center of
116 % gravity (Global reference)
117 % ------------------------------------------------
118
119
120 for i=1:length(t)
121
122 % First derivative of the position
123
124 v_xg(i)=b_x + 2*d_x*t(i) + 3*e_x*t(i)^2  ;
125 v_yg(i)=b_y + 2*d_y*t(i) + 3*e_y*t(i)^2  ;
126
127 end   % CM Velocities
128
129 for i=1:length(t)
130
131     V_g_abs(i)=sqrt(v_xg(i)^2+v_yg(i)^2);
132
133 end   % CM Absolute velocity
134
135 for i=1:length(t)
136
137  a_xg(i)= 2*d_x + 6*e_x * t(i)  ;
138  a_yg(i)= 2*d_y + 6*e_y * t(i)  ;
139
140 end   % Accelerations
141
142 for i=1:length(t)
143
144 a3_xg(i)=   6*e_x   ;
145 a3_yg(i)=   6*e_y   ;
146
147 end   % Third derivative of acceleration
148
149
150 % ------------------------------------------------
151 % Trajectory plot
152 % ------------------------------------------------
153
```

```
154
155 figure ()
156 plot (x_xg,y_yg,'linewidth',2)
157 title('Trajectory')
158 xlabel('[m]')
159 ylabel('[m]')
160 grid on
161 title('Vehicle trajectory')
162
163
164 % ------------------------------------------------------
165 % Velocities Plots
166 % ------------------------------------------------------
167
168
169 figure()
170 subplot(2,1,1)
171 plot(t,v_xg)
172 title('Velocity along x')
173
174 subplot(2,1,2)
175 plot(t,v_yg)
176 title('Velocity along y')
177
178
179 figure()
180
181 subplot(2,1,1)
182 plot(t,a_xg)
183 title('Acceleration along x')
184
185 subplot(2,1,2)
186 plot(t,a_yg)
187 title('Acceleration along y')
188
189
190  % eq. (5) Orientation of the velocity of the center of
        gravity
191  % eq. (6) Angular velocity of the car
192
193 for i=1:length(t)
194
195         theta(i)=atan(v_yg(i)/v_xg(i)); % (5)
196
197 end % Theta
198
199
```

```
200 for i=1:length(t)
201
202         omega(i)=((v_xg(i)*a_yg(i))-(v_yg(i)*a_xg(i)))
              /((v_xg(i))^2+(v_yg(i))^2);     % (6)
203
204 end % Omega
205
206
207 for i=length(t)
208 omega_punto(i)=((v_xg(i)*a3_yg(i) + a_xg(i)*a_yg(i) -
    a_yg(i)*a_xg(i)+ v_xg(i)*a3_xg(i))*((v_xg(i))^2+(v_yg
    (i))^2))-((v_xg(i)*a_yg(i)-v_yg(i)*a_xg(i))*(2*v_xg(i
    )*a_xg(i)+2*v_yg(i)*a_yg(i)))/((v_xg(i))^2+(v_yg(i))
    ^2)^2;
209
210  end  % omega punto
211
212
213  omega_punto(i)=omega_punto(i-1);
214
215
216 figure()
217 plot(t,omega_punto)
218 title(' omega^\cdotprimo')
219
220
221 % ---------------------------------------------------
222 % Normal acceleration for the trajectory in G : (11)
223 % Global
224 % ---------------------------------------------------
225
226
227 for i=1:length(t)
228
229     a_g_norm(i)=-a_xg(i)*sin(theta(i))+a_yg(i)*cos(theta
        (i));
230
231 end
232
233
234 % ---------------------------------------------------
235 % Tangential acceleration for the trajectory in G : (12)
236 % Global
237 % ---------------------------------------------------
238
239
240 for i=1:length(t)
```

```
241
242     a_g_trans(i)=a_xg(i)*cos(theta(i))+a_yg(i)*sin(theta
           (i));
243
244 end
245
246
247 % ------------------------------------------------
248 % Setting Newton-Euler equations
249 % ------------------------------------------------
250
251
252 for i=1:length(t)
253
254     hh(i)=((v_xg(i)*a_yg(i))-(v_yg(i)*a_xg(i)))/((v_xg(i
           )^2+v_yg(i)^2)^(3/2));
255
256 end
257
258
259 for i=1:length(t)
260
261 fun = @root2d;
262 x0=[0,0,0,0];
263 %options = optimoptions('fmincon')
264 x = fsolve(fun,x0);
265
266 beta_rear(i)=x(1);
267 beta(i)=x(2);
268 beta_front(i)=x(3);
269 delta(i)=x(4);
270
271 end
272
273
274 % ------------------------------------------------
275 % Lateral force calculation
276 % ------------------------------------------------
277
278
279 for i=1:length(t)
280
281      Frt(i)=-C_t*beta_rear(i)    ;
282      Fft(i)=-C_t*beta_front(i)   ;
283
284 end
285
```

```
286
287 % ------------------------------------------------
288 % Steering angle plot and transformation in Degrees
289 % ------------------------------------------------
290
291
292 delta=rad2deg(delta);
293
294 figure()
295 plot(t,delta,'linewidth',2)
296 title('Steer anlge \delta')
297 grid on
298 xlabel('Time [s]')
299 ylabel('Angle [Degrees]')
300 ylim([0 10])
301
302
303 % ------------------------------------------------
304 % Rear axle lateral force plot
305 % ------------------------------------------------
306
307
308 figure()
309 plot(t,abs(Frt),'linewidth',2)
310 title('Rear axle lateral force F_R_T')
311 grid on
312 xlabel('Time [s]')
313 ylabel('Force [N]')
314 ylim([0 1000])
315
316
317 % ------------------------------------------------
318 % Front axle lateral force plot
319 % ------------------------------------------------
320
321
322 figure()
323 plot(t,abs(Fft),'linewidth',2)
324 title('Front axle lateral force F_F_T')
325 grid on
326 xlabel('Time [s]')
327 ylabel('Force [N]')
328 ylim([0 500])
329
330
331 % ------------------------------------------------
332 % Sideslip angle plot and transformation in Degrees
```

```
333 % ------------------------------------------------
334
335
336 beta=rad2deg(beta);
337
338 figure
339 plot(t,beta,'linewidth',2)
340 title('Sideslip angle \beta')
341 grid on
342 xlabel('Time [s]')
343 ylabel('Angle [Degrees]')
344 ylim([0 3])
345
346
347 % ------------------------------------------------
348 % Front Sideslip angle plot and transformation in
    Degrees
349 % ------------------------------------------------
350
351
352 beta_front=rad2deg(beta_front);
353
354 figure
355 plot(t,beta_front,'linewidth',2)
356 title('Front sideslip angle \beta_F')
357 grid on
358 xlabel('Time [s]')
359 ylabel('Angle [Degrees]')
360 ylim([-1 2])
361
362
363 % ------------------------------------------------
364 % Front Sideslip angle plot and transformation in
    Degrees
365 % ------------------------------------------------
366
367
368 beta_rear=rad2deg(beta_rear);
369
370
371 figure
372 plot(t,beta_rear,'linewidth',2)
373 title('Rear sideslip angle \beta_R')
374 grid on
375 xlabel('Time [s]')
376 ylabel('Angle[Degrees]')
377 ylim([-1 2])
```

A.5 Inverse dynamic equation solver function

Listing A.5: Dampers graph

```
function F=root2d(x)


global m;
global hh;
global Lb;
global La;
global Iz;
global omega_punto;
global a_g_norm;
global a_g_trans;
global i;
global C_t;


F(1)=x(1)-x(2)+hh(i)*Lb;
F(2)=x(2)+x(3)-x(4)+hh(i)*La;
% % F(3)=-C_t*(x(1)+x(3)*(1-(x(4)^2)/2)+((x(4)^4)/24)-((x(4)^6)/720))-m*(a_g_norm(i)-a_g_trans(i)*x(2));
% % F(4)=C_t*(-La*(x(3)*(1-(x(4)^2)/2)+((x(4)^4)/24)-((x(4)^6)/720))+(Lb*x(1)))-(Iz*omega_punto(i));
F(3)=-C_t*x(1) + m*a_g_trans(i)*x(2) - C_t*x(3)*cos(x(4))-m*a_g_norm(i);
F(4)=C_t*Lb*x(1)-C_t*La*x(3)*cos(x(4))-Iz*omega_punto(i);


% % beta_rear(i)=x(1);
% % beta(i)=x(2);
% % beta_front(i)=x(3);
% % delta(i)=x(4);
```

A.6 Moose test program

Listing A.6: Dampers graph

```
clear all
close all
clc
```

```
4
5
6  global m;
7  global hh;
8  global Lb;
9  global La;
10 global Iz;
11 global omega_punto;
12 global a_g_norm;
13 global a_g_trans;
14 global i;
15 global C_t;
16
17
18 % ------------------------------------------------
19 % Inverse dynamic problem
20 % Moose Test
21 % ------------------------------------------------
22
23
24 % Global constant
25
26     g=9.81 ; %[m/s^2]
27
28 % Vehicle data
29
30     m=690;      % [Kg]
31     L=1.65;     % [m]
32
33 % Distance from center of gravity to rear axle
34
35     Lb=0.55;  % [m]
36
37 %  Distance from the center of gravity to the front axle
38
39     La=1.1;     % [m]
40
41 % Moment of Inertia ot the car
42
43     Iz=160;    % [Kg/m^2]
44
45 % Tire lateral stiffness
46
47     C_t=45836;
48     mu_t=0.1;    %COEFICIENT OF FRICTION
49     mu_r=0.1;    %COEFFICIENT LOSSES DUE TO MOTION
50
```

```
% Trajecrtory constant speed

Vehicle_speed=8.888;    %  [m/s] Test at the maximum
   speed of 32 km/h


% -------------------------------------------------
% Generation of the trajectory
% -------------------------------------------------


% position of CM

load Moose_POINTS.txt
load MOOSE_position_cones.txt

x_axis=linspace(0,110,100); %ISO length of the test (110
    m)

x_vector=Moose_POINTS(:,1);
y_vector=Moose_POINTS(:,2);

y_axis=spline(x_vector,y_vector,x_axis);

figure()

% -------------------------------------------------
% Plot of the ISO path and the supposed trajectory
% -------------------------------------------------

hold on
plot(x_axis,y_axis,'linewidth',2)
hold on
plot(MOOSE_position_cones(:,1),MOOSE_position_cones(:,2)
   ,'or')
xlabel('Distance [m]')
ylabel('Distance [m]')
grid on
title('Moose test trajectory')


% -------------------------------------------------
%  Calculation of the trajectory length
% -------------------------------------------------


deltaL=zeros(1,length(x_axis));
```

```
95
96  % Trajectory increment
97  for i=1:(length(x_axis)-1)
98
99      deltaL(i)=sqrt(((x_axis(i+1))-(x_axis(i)))^2+((
            y_axis(i+1))-(y_axis(i)))^2);
100     deltaL(length(x_axis))=deltaL(length(x_axis)-1);
101     deltaT(i)=deltaL(i)/Vehicle_speed;
102
103 end
104
105
106 % ------------------------------------------------
107 % Velocities  and acceleration of the center of gravity
        (Global reference)
108 % ------------------------------------------------
109
110
111 for i=1:(length(x_axis)-1)
112
113
114 Speed_direction(i)=atan((y_axis(i+1)-y_axis(i))/(x_axis(
        i+1)-x_axis(i)));
115
116 end   %Velocity versors
117
118 Speed_direction(length(x_axis))=Speed_direction(length(
        x_axis)-1);
119
120
121 for i=1:(length(x_axis))
122
123 v_xg(i)=      Vehicle_speed*cos(Speed_direction(i)) ;
124 v_yg(i)=      Vehicle_speed*sin(Speed_direction(i)) ;
125 end % Velocities of of CM
126
127
128 a_xg=zeros(1 , length(x_axis) );
129 a_yg=zeros(1 , length(x_axis) );
130
131
132 for i=1:(length(x_axis)-1);
133
134 a_xg(i)=      (v_xg(i+1)-v_xg(i))/deltaT(i);
135 a_yg(i)=      (v_yg(i+1)-v_yg(i))/deltaT(i);
136
137 a_xg(length(x_axis))=a_xg(length(x_axis)-1);
```

```
138 a_yg(length(x_axis))=a_yg(length(x_axis)-1);
139
140 end % Acceleration of of CM
141
142
143 a3_xg=zeros(1 , length(x_axis) );
144 a3_yg=zeros(1 , length(x_axis) );
145
146
147 for i=1:(length(x_axis)-1)
148
149 a3_xg(i)= (a_xg(i+1)-a_xg(i))/deltaT(i);
150 a3_yg(i)= (a_yg(i+1)-a_yg(i))/deltaT(i);
151
152 end   % Third derivative of acceleration
153
154 a3_xg(length(x_axis))=a_xg(length(x_axis)-1);
155 a3_yg(length(x_axis))=a_yg(length(x_axis)-1);
156
157
158 % ------------------------------------------------
159 % Velocities Plots
160 % ------------------------------------------------
161
162
163 figure()
164 subplot(2,1,1)
165 plot(x_axis,v_xg,'linewidth',2)
166 title('Velocity along x')
167 xlabel('Space [m]')
168 ylabel('[m/s]')
169 grid on
170
171
172 subplot(2,1,2)
173 plot(x_axis,v_yg,'linewidth',2)
174 title('Velocity along y')
175 grid on
176 xlabel('Space [m]')
177 ylabel('[m/s]')
178
179
180 % ------------------------------------------------
181 % Acceleration plots
182 % ------------------------------------------------
183
184
```

```
185 figure()
186
187 subplot(2,1,1)
188 plot(x_axis,a_xg,'linewidth',2)
189 title('Acceleration along x')
190 xlabel('Space [m]')
191 ylabel('[m/s^2]')
192 grid on
193
194 subplot(2,1,2)
195 plot(x_axis,a_yg,'linewidth',2)
196 title('Acceleration along y')
197
198 grid on
199 xlabel('Space [m]')
200 ylabel('[m/s^2]')
201
202
203 for i=1:length(x_axis)
204
205         theta(i)=atan(v_yg(i)/v_xg(i)); % (5)
206
207 end % Theta
208
209
210 for i=1:length(x_axis)
211
212         omega(i)=((v_xg(i)*a_yg(i))-(v_yg(i)*a_xg(i)))
              /((v_xg(i))^2+(v_yg(i))^2);     % (6)
213
214 end % Omega
215
216
217 for i=length(x_axis)
218 omega_punto(i)=((v_xg(i)*a3_yg(i) + a_xg(i)*a_yg(i) -
    a_yg(i)*a_xg(i)+ v_xg(i)*a3_xg(i))*((v_xg(i))^2+(v_yg
    (i))^2))-((v_xg(i)*a_yg(i)-v_yg(i)*a_xg(i))*(2*v_xg(i
    )*a_xg(i)+2*v_yg(i)*a_yg(i)))/((v_xg(i))^2+(v_yg(i))
    ^2)^2;
219
220  end  % omega punto
221
222  omega_punto(i)=omega_punto(i-1);
223
224
225 figure()
226 plot(x_axis,omega_punto)
```

```
227 title(' omega^\cdotprimo')
228
229
230 % ------------------------------------------------
231 % Normal acceleration for the trajectory in G : (11)
          --Global
232 % ------------------------------------------------
233
234
235 for i=1:length(x_axis)
236
237     a_g_norm(i)=-a_xg(i)*sin(theta(i))+a_yg(i)*cos(theta
        (i));
238
239 end
240
241
242 % ------------------------------------------------
243 % Tangential acceleration for the trajectory in G : (12)
        --Global
244 % ------------------------------------------------
245
246
247 for i=1:length(x_axis)
248
249     a_g_trans(i)=a_xg(i)*cos(theta(i))+a_yg(i)*sin(theta
        (i));
250
251 end
252
253
254 % ------------------------------------------------
255 % Setting Newton-Euler equations to solve the problem
256 % ------------------------------------------------
257
258
259 for i=1:length(x_axis)
260      hh(i)=((v_xg(i)*a_yg(i))-(v_yg(i)*a_xg(i)))/((v_xg(
         i)^2+v_yg(i)^2)^(3/2));
261
262    % hh(i)=((v_xg(i)*cos(theta(i))*a_yg(i)*cos(theta(i))
       )-(v_yg(i)*cos(theta(i))*a_xg(i))*cos(theta(i)))
       /((v_xg(i)*cos(theta(i)))^2+(v_yg(i)*cos(theta(i))
       ^2)^(3/2));
263 end
264
265
```

```
266 for i=1:length(x_axis)
267
268 fun = @root2d;
269 x0=[0,0,0,0];
270 x = fsolve(fun,x0);
271
272 beta_rear(i)=x(1);
273 beta(i)=x(2);
274 beta_front(i)=x(3);
275 delta(i)=x(4);
276
277 end
278
279
280 % ------------------------------------------------
281 % Lateral force calculation
282 % ------------------------------------------------
283
284
285 for i=1:length(x_axis)
286
287      Frt(i)=-C_t*beta_rear(i)    ;
288      Fft(i)=-C_t*beta_front(i)   ;
289
290 end
291
292
293 % ------------------------------------------------
294 % Steering angle plot and transformation in Degrees
295 % ------------------------------------------------
296
297
298 delta=rad2deg(delta);
299
300 figure()
301 plot(x_axis,-delta,'linewidth',2)
302 title('Steer anlge \delta')
303 grid on
304 xlabel('Time [s]')
305 ylabel('Angle [Degrees]')
306 %ylim([-1 1])
307
308
309 % ------------------------------------------------
310 % Rear axle lateral force plot
311 % ------------------------------------------------
312
```

```
313
314 figure()
315 plot(x_axis,-(Frt),'linewidth',2)
316 title('Rear axle lateral force F_R_T')
317 grid on
318 xlabel('Time [s]')
319 ylabel('Force [N]')
320 %ylim([-600 700])
321
322
323 % ------------------------------------------------
324 % Front axle lateral force plot
325 % ------------------------------------------------
326
327
328 figure()
329 plot(x_axis,-(Fft),'linewidth',2)
330 title('Front axle lateral force F_F_T')
331 grid on
332 xlabel('Time [s]')
333 ylabel('Force [N]')
334 %ylim([-400 350])
335
336
337 % ------------------------------------------------
338 % Sideslip angle plot and transformation in Degrees
339 % ------------------------------------------------
340
341
342 beta=rad2deg(beta);
343
344 figure
345 plot(x_axis,-beta,'linewidth',2)
346 title('Sideslip angle \beta')
347 grid on
348 xlabel('Time [s]')
349 ylabel('Angle [Degrees]')
350 %ylim([-0.5 0.5])
351
352
353 % ------------------------------------------------
354 % Front Sideslip angle plot and transformation in
     Degrees
355 % ------------------------------------------------
356
357
358 beta_front=rad2deg(beta_front);
```

```
359
360 figure
361 plot(x_axis,-beta_front,'linewidth',2)
362 title('Front sideslip angle \beta_F')
363 grid on
364 xlabel('Time [s]')
365 ylabel('Angle [Degrees]')
366 ylim([-0.6 0.6])
367
368
369 % ------------------------------------------------
370 % Front Sideslip angle plot and transformation in
    Degrees
371 % ------------------------------------------------
372
373
374 beta_rear=rad2deg(beta_rear);
375
376 figure
377 plot(x_axis,-beta_rear,'linewidth',2)
378 title('Rear sideslip angle \beta_R')
379 grid on
380 xlabel('Time [s]')
381 ylabel('Angle[Degrees]')
382 ylim([-1.1 1.1])
```

A.7 Leaf spring calculation

Listing A.7: Leaf spring calculation

```
1  % ------------------------------------------------
2  % Stiffness calculations
3  % ------------------------------------------------
4
5
6  % ------------------------------------------------
7  % Front side
8  % ------------------------------------------------
9
10
11 n=4;
12 n1=1;
13 b=33; %[mm]
14 h=5;  %[mm]
15 l=327.20; %[mm]
16 E=206000;% [N/mm^2]
```

```
17
18 C_del=((2+(n1/n))*(E*n*b*h^3))/(6*l^3)
19
20 C_del_sol2=E*b*h^3/6/l^3
21
22
23 % ------------------------------------------------------
24 % Rear side
25 % ------------------------------------------------------
26
27
28 n=5;
29 E=5;
30 n1=1;
31 b=40; %[mm]
32 h=5;  %[mm]
33 l=335; %[mm]
34 E=206000;% [N/mm^2]
35
36 C_Tras=((2+(n1/n))*(E*n*b*h^3))/(6*l^3)
37 C_tras_sol2=E*b*h^3/6/l^3
```

Bibliography

[1] Masato Abe. *Vehicle handling dynamics: theory and application*. Butterworth-Heinemann, 2015.

[2] ADAMS. *Basic ADAMS Full Simulation Training Guide*. 2002. URL: https://paws.kettering.edu/~amazzei/student_guide.pdf (visited on 2017).

[3] *Adams/View Function Builder Manual. Run-Time Functions*. 2010.

[4] *ai2 Instituto de Automática e Informática Industrial*. 2017. URL: http://www.ai2.upv.es/es/index.php.

[5] Automotive Handbook Bosch. *Robert Bosch GmbH*. Tech. rep. ISBN 978-0-7680-1513-3, 2006.

[6] Ashwin Carvalho et al. "Predictive control of an autonomous ground vehicle using an iterative linearization approach". In: *Intelligent Transportation Systems-(ITSC), 2013 16th International IEEE Conference on*. IEEE. 2013, pp. 2335–2340.

[7] John C Dixon. *Suspension geometry and computation*. Wiley Online Library, 2009.

[8] Thomas D Gillespie. "Vehicle Dynamics". In: *Warren dale* (1997).

[9] VEHICO GmbH. *ISO Double Lane Change Test*. 2017. URL: http://www.vehico.com/index.php/en/applications/iso-lane-change-test (visited on 2017).

[10] Andrew Gray et al. "Semi-autonomous vehicle control for road departure and obstacle avoidance". In: *IFAC control of transportation systems* (2012), pp. 1–6.

[11] M. Guiggiani. *Dinamica del veicolo*. Città Studi Edizioni, 1998.

[12] SAE international. *Formula SAE rules*. 2017.

[13] *ISO 3888-2. Passenger cars – Test track for a severe lane-change manoeuvre*. 2011.

[14] *ISO 4138:1982. Road vehicles – Steady-state circular test procedure*. 2004.

[15] R.K. Jurgen. *Autonomous Vehicles for Safer Driving*. Electronic publications. Society of Automotive Engineers, 2013. ISBN: 9780768080391. URL: https://books.google.es/books?id=be4dnQAACAAJ.

[16] Donghyun Kim, Sungho Hwang, and Hyunsoo Kim. "Vehicle stability enhancement of four-wheel-drive hybrid electric vehicle using rear motor control". In: *IEEE Transactions on Vehicular Technology* 57.2 (2008), pp. 727–735.

[17] Gianpiero Mastinu and Manfred Ploechl. *Road and off-road vehicle system dynamics handbook*. CRC Press, 2014.

[18] *MATLAB*. 2013. URL: http://cimss.ssec.wisc.edu/wxwise/class/aos340/spr00/whatismatlab.htm (visited on 2017).

[19] Michelin. *tire model for dynamic vehicle analysis*. 2016. URL: http://www.michelin-engineering-and-services.com/eng/Test-and-Measurement/Tire (visited on 2017).

[20] William F Milliken, Douglas L Milliken, and Maurice Olley. *Chassis design: principles and analysis*. Vol. 400. Society of Automotive Engineers Warrendale, PA, 2002.

[21] William F Milliken, Douglas L Milliken, et al. *Race car vehicle dynamics*. Vol. 400. Society of Automotive Engineers Warrendale, 1995.

[22] Russell Lee Mueller. "Full vehicle dynamics model of a formula SAE racecar using ADAMS/Car". PhD thesis. Texas A&M University, 2005.

[23] Hans Pacejka. *Tire and vehicle dynamics*. Elsevier, 2005.

[24] Rajesh Rajamani. *Vehicle dynamics and control*. Springer Science & Business Media, 2011.

[25] Roberto Q. Riley. *Automobile Ride, Handling, and Suspension Design*. 2011. URL: https://www.rqriley.com/suspensn.htm (visited on 2017).

[26] Robotnik. *RBCAR*. 2016. URL: http://www.robotnik.es/web/wp-content/uploads/2015/09/RBCAR_Datasheet_2016_en.pdf (visited on 2017).

[27] *SAE J670 200801. Vehicle Dynamics Terminology*. 2008.

[28] Taehyun Shim and Chinar Ghike. "Understanding the limitations of different vehicle models for roll dynamics studies". In: *Vehicle system dynamics* 45.3 (2007), pp. 191–216.

[29] MSC Software. *MSC Software: Services Toolkit - Adams/Leafspring*. 2013. URL: http://www.mscsoftware.com/Submitted-Content/Resources/TK_Adams_Leafspring_LTR_w.pdf (visited on 2017).

[30] MSC Software. *Simulating Reality, Delivering Certainty*. 2013. URL: http://www.mscsoftware.com/page/msc-software (visited on 2017).

[31] Wikipedia. *Cylindrical joint*. 2015. URL: https://en.wikipedia.org/wiki/Cylindrical_joint (visited on 2017).

[32] Wikipedia. *Revolute joint*. 2015. URL: https://en.wikipedia.org/wiki/Revolute_joint (visited on 2017).

[33] Wikipedia. *SolidWorks*. 2017. URL: https://en.wikipedia.org/wiki/SolidWorks (visited on 2017).

[34] Wikipedia. *Spherical joint*. 2017. URL: https://en.wikipedia.org/wiki/Ball_joint (visited on 2017).

[35] Jo Yung Wong. *Theory of ground vehicles*. John Wiley & Sons, 2008.